Air Force Institute of Technology

AFIT Scholar

12-2006

Vacuum Chamber Construction and Contamination Study of a Micro Pulsed Plasma Thruster

Jacob H. Debevec

VACUUM CHAMBER CONSTRUCTION AND CONTAMINATION STUDY OF

A MICRO PULSED PLASMA THRUSTER

THESIS

Jacob H. Debevec, 2d Lt, USAF

AFIT/GAE/ENY/07-D01

**DEPARTMENT OF THE AIR FORCE
AIR UNIVERSITY**

AIR FORCE INSTITUTE OF TECHNOLOGY

Wright-Patterson Air Force Base, Ohio

VACUUM CHAMBER CONSTRUCTION AND CONTAMINATION STUDY OF

A MICRO PULSED PLASMA THRUSTER

THESIS

Presented to the Faculty

Department of Aeronautics & Astronautics

Graduate School of Engineering and Management

Air Force Institute of Technology

Air University

Air Education and Training Command

In Partial Fulfillment of the Requirements for the

Degree of Master of Science in Aeronautical Engineering

Jacob H. Debevec, BS

2d Lt, USAF

December 2006

AFIT/GAE/ENY/07-D01

VACUUM CHAMBER CONSTRUCTION AND CONTAMINATION STUDY OF

A MICRO PULSED PLASMA THRUSTER

Jacob H. Debevec, BS

2d Lt, USAF

Approved:

_____   _____
Richard Branam, Maj, USAF (Chairman)   Date

_____   _____
Nathan Titus, Lt Col, USAF (Member)   Date

_____   _____
Dr. Milton Franke, USAF (Member)   Date

AFIT/GAE/ENY/07-D01

Abstract

The micro pulsed plasma thruster (micro-PPT) is a simple and versatile electric thruster capable of performing multiple missions, from precise attitude control on standard satellites to primary propulsion for nanosatellites. In order to fill this role as both industry and government move toward utilizing smaller satellites, micro-PPTs first need to be thoroughly tested on the ground. This study examines the deposition profile and rate of particle emission from the thruster so that satellite designers understand any potential contamination issues with sensitive instruments and solar panels. Employing a newly assembled vacuum chamber system, four tests were completed with the micro-PPTs, and the results showed that particles discharge in all directions, with the surfaces directly facing the propellant tube collecting exponentially more particle deposition than surfaces at wider angles.

Acknowledgments

Throughout this thesis effort, numerous people have given me overwhelming help and support. My faculty advisor, Maj Richard Branam, guided me through each obstacle I encountered. The AFIT laboratory staff, especially Sean Miller, Barry Page, and Jay Anderson, always provided me with tools, experience, and expertise. Lt Dustin Warner walked me through basic vacuum practice, saving me many hours of work. Garrett Reed and Dr William Hargus, my sponsor from the AFRL Electric Propulsion Directorate, supplied the technical materials along with needed advice. I sincerely appreciate everyone's help and appreciate all of the time and effort spent on this project.

Jacob H. Debevec

Table of Contents

List of Figures

List of Tables

VACUUM CHAMBER CONSTRUCTION AND CONTAMINATION STUDY OF A MICRO PULSED PLASMA THRUSTER

I. Introduction

Background

The pulsed plasma thruster (PPT) is one of the simplest and most flexible electric thrusters, ideally suited for attitude control and precise spacecraft maneuvers. The Air Force and NASA, as well as many other companies, have great interest in developing constellations of smaller and cheaper satellites capable of performing the tasks of the larger, more expensive satellites currently in use. For example, large numbers of small satellites can improve performance by distributing functions among multiple satellites, reduce costs by increasing manufacturing and redundancy, and improve flexibility and upgradeability for industry or technologies whose needs are constantly shifting. As satellites move towards miniaturization, the PPT is a strong candidate for improving the propulsion systems due to its small impulse bit and high performance.

Micro pulsed plasma thrusters (micro-PPT) are designed for stationkeeping and as the primary propulsion system for microsatellites. They are similar to a standard PPT, except the micro-PPT eliminates some components, enabling it to be lighter and smaller. Although the standard PPT has been studied for decades and tested extensively, the micro-PPT is a relatively new thruster that warrants further study before entering widespread use. Specifically, the nature of the contaminants ejected from the thruster

1

need to be examined more thoroughly. If particulates from the thruster deposit on sensitive satellite components, instruments can be polluted and the solar panel performance may be degraded.

In order to perform the contamination study of the PPT, a vacuum chamber first needed to be constructed at the Air Force Institute of Technology (AFIT). Starting with a bell chamber and diffusion pump, all of the other necessary supplies were acquired and assembled, with the goal of building an automated system easy to use throughout this project and any similar experiments in the future.

Problem Statement

Satellites are equipped with many fine-tuned sensors and precisely calibrated instruments. A major issue in orbit is the contamination of these devices due to the ejected material from the propulsion system. As the thrusters fire, particles from the propellant can interfere with the instruments and degrade the performance of the satellite. In addition, future microsatellites may fly in close formations, where the thruster from one satellite points directly at another satellite, possibly causing contamination. The behavior of particles emitting from a standard PPT has previously been studied. However, the profile of the propellant particles and rate of deposition for micro-PPTs still needs to be examined in order to understand potential contamination effects.

Research Objectives

Within a vacuum chamber, the micro-PPT can be thoroughly tested for various lengths of time in order to study the deposition tendencies of the thruster. By studying the deposition as a function of angular and time dependence, a clear picture of the deposition formation can be developed. It is important to know whether deposition tendencies change as the thruster operates for extended periods of time and as the propellant recedes. For example, the particulates may get dispersed in different patterns as the propellant is used and the tip of the propellant ablates and changes shape. This deposition profile would aid in placing the PPTs on spacecraft so that the contamination effects are minimized.

Research Focus

The focus of the research is to develop a deposition profile of the PPT as a function of time and angle. Micro-PPTs, designed and built at the Air Force Research Lab at Edwards AFB, CA, are used in this study. This thruster operates with the same principles as a standard PPT, except the micro-PPT has fewer components and is therefore smaller – the entire thruster is no larger than the palm of a hand. Micro-PPTs have been studied at the research lab at Edwards AFB and other universities across the country, but the deposition profile remains an important unknown as the thruster is transitioned into a flight program.

Methodology

      The micro-PPT will be tested inside a bell jar vacuum chamber using witness plates spanning a wide range of angles, with the thruster operating for various lengths of time. Utilizing this matrix of test parameters, the PPT deposition profile can be developed as a function of each variable. The deposition can be measured with microscopes, such as a scanning electron microscope (SEM) available at AFIT, to determine the sizes of the particulates and the deposition pattern.

Assumptions/Limitations

      This study assumes that the vacuum chamber environment is similar to the space environment. Specifically, the pressure within the chamber must be similar to the pressure in orbit. Because these experiments investigate the deposition effects on witness plates, one must assume that almost all of the deposition material actually striking the witness plates remains on the plate surface for examination. This assumption is a concern because Teflon™ is known for its slippery qualities. For this study, the Teflon™ particles are assumed to possess a high enough velocity to stick to the aluminum surface of the witness plates. If a significant percentage of the deposition material does not remain on the witness plate surface, the study will underestimate the contamination effects of the PPT. In addition, the vacuum chamber cannot be contaminated with

4

foreign particles that can attach to the witness plates and lead to an overestimation of the deposition effects.

Another assumption for the thruster is axisymmetric emission of propellant particulates. Only the cross-sections parallel and perpendicular to the thrust plane will be examined in this study. If the particulate emission is axisymmetric, then the data obtained from these two planes will also describe the deposition for any other location at the same angle. This assumption can be tested by comparing the deposition levels for targets at the same angles, but different arms of the test stand.

Implications

The testing from this study will result in a detailed characterization of the deposition profile of the PPT. With this profile, the contamination effects from the PPT on delicate sensors, precisely tuned instruments, and solar panels will be better understood. Therefore, more care can be given to the placement of the PPT on a spacecraft to reduce contamination from the thruster.

Preview

The next two chapters focus on background information and experimental setup for the vacuum chamber, diffusion pump, and micro-PPTs. The last two chapters analyze

the results of the micro-PPT experiments and discuss possibilities for improvement and areas for further study.

II. Literature Review

Chapter Overview

The purpose of this chapter is to describe the process of vacuum chamber construction and diffusion pump operation, and to give an overview of micro-PPTs, including previous research related to this study.

Vacuum Chamber Construction

To simulate the space environment, a vacuum needs to be achieved inside a chamber by pumping out the air and thus lowering the pressure. Two vacuum pumps, a diffusion pump and a mechanical roughing pump, work together to evacuate the air particles and reach the desired pressure. Once the chamber is pumped down to vacuum levels, the thruster can be tested in an environment with a pressure similar to orbital conditions.

Building a vacuum chamber requires attention to every detail and precision in construction. Small leaks can cause large increases in pressure and prevent the chamber from reaching vacuum levels. Therefore, all of the bolts, nuts, o-rings, flanges, valves, and hoses must be carefully assembled so they fit together securely.

In a diffusion pump, a heater brings an oil reservoir up to its boiling point, as shown in Figure 1. The oil vapor travels upwards through the jet assembly and then accelerates downward through jet nozzles. The vapor acceleration can cause the particles to reach speeds of more than 335 meters per second (750 miles per hour). The high-

speed oil vapor collides with gas molecules while moving downward, thereby

compressing the gas continuously. When the vapor molecules hit the water-cooled walls

of the pump, the oil condenses back into a liquid. The fluid then reboils and cycles

through this process repeatedly. As the gas molecules become highly pressurized by the

high speed oil particles, the gas gets pumped out of the chamber through the attached

roughing pump. The diffusion pump must be used in tandem with a mechanical roughing

pump, because the diffusion pump cannot exhaust directly to atmosphere [1].
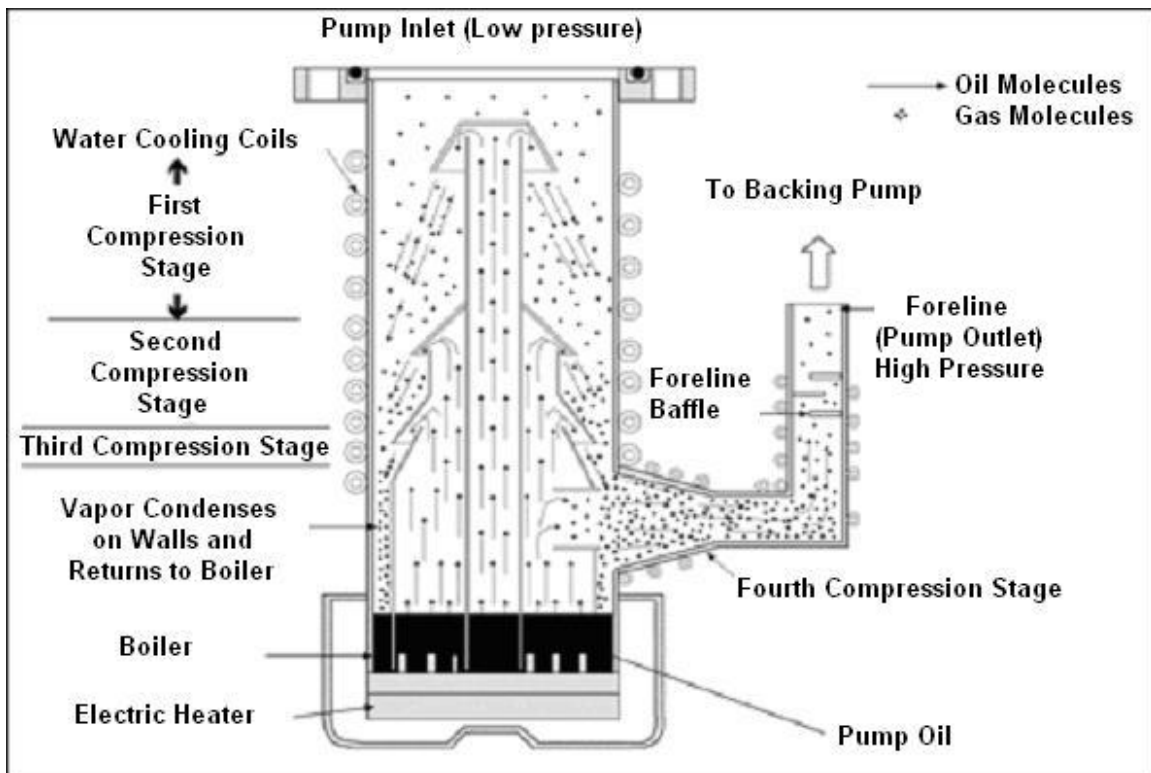
Figure 1 – Cross section of a typical oil diffusion pump [2].

PPT Overview

The operation of a standard PPT is shown in Figure 2 and explained below. The thruster contains two electrodes near the propellant placed in parallel with a capacitor. A power supply charges the capacitor to a high voltage, which is then discharged by a spark from an igniter. The power is typically supplied by a solar array when used in space. The discharge from the capacitor ablates and ionizes the surface of the propellant, creating plasma and a neutral vapor. The PPT uses an ablative solid propellant, usually Teflon™, to achieve high specific impulse with low energy requirements. The particles are accelerated out of the thruster at high velocities due to the Lorenz force resulting from the interaction of the magnetic field with the current flowing through the plasma. The plasma that discharges from the thruster has high velocity and low mass, which results in extremely low fuel consumption. A spring feeds new propellant forward to keep a consistent fuel supply as the propellant ablates and is ejected from the thruster. These pulse discharges can occur millions of times over the lifetime of the thruster, which can operate for hundreds of hours. For example, the Air Force's LES-6 communications satellite utilized four PPTs, producing approximately twelve million pulses over the thruster's lifetime [3].
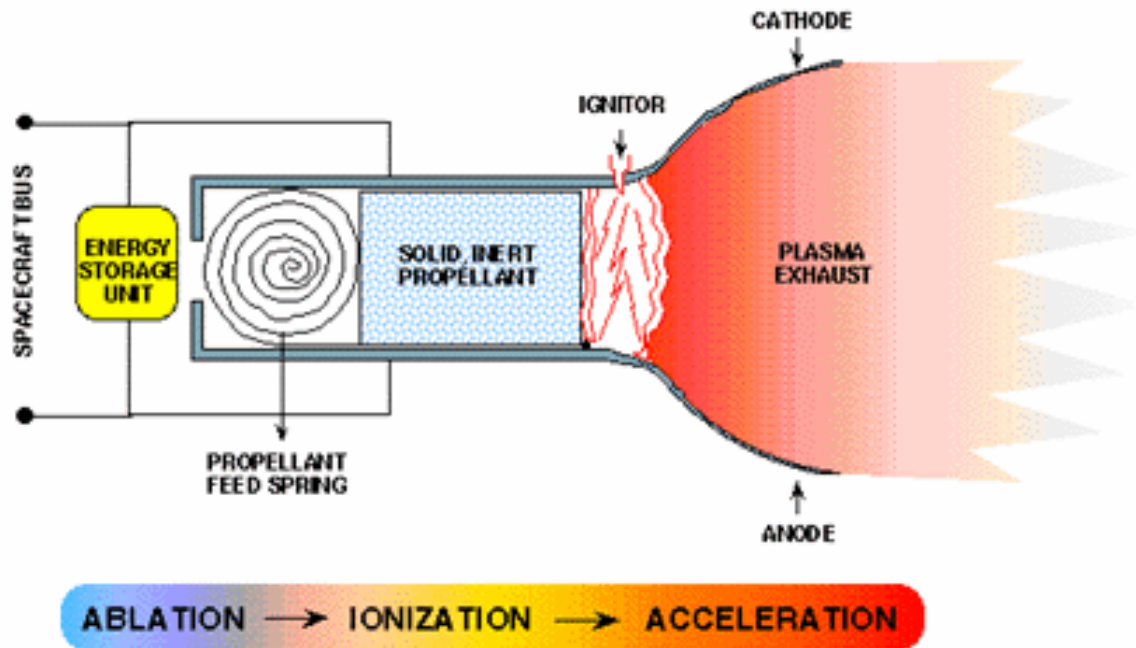
Figure 2 – PPT operation [4].

A micro-PPT, similar to the standard PPT, uses a surface discharge across the Teflon™ propellant surface to create and accelerate a plasma flow. However, the micro-PPT uses a self-igniting discharge, rather than a separate igniter and discharge unit from the thruster. The micro-PPT typically operates with three main components: a high voltage converter, a capacitor and the propellant tube. The high voltage converter takes a low voltage input, between 5 and 15 volts typically, and converts it to high voltage, usually between 2,000 and 8,000 volts. The high voltage is fed to the capacitor, which builds up the charge, then discharges. The charge is fed through the inner cathode and outer anode of the propellant tube, and the high voltage charge is applied directly to the

10

propellant. If the voltage is greater than the surface breakdown voltage, typically

between 2,000 V and 8,000 V, then the discharge self-ignites, and the current arcs across

the tip of the propellant. Each arc ablates a small amount of propellant and also ionizes a

small percentage of the ablated propellant. As the electrical current arcs across the face

of the propellant, a magnetic field is produced in a perpendicular vector. The current and

magnetic field produce a body force, called the Lorentz force, which produces the

majority of the thrust by accelerating the ionized propellant [5]. Equation (1) shows how

the Lorentz force is produced [6]:

$$F = q(E + v \times B) \tag{1}$$

where

> F is the force (newtons)
>
> E is the electric field (in volts per meter)
>
> B is the magnetic field (teslas)
>
> q is the electric charge of the particle (coulombs)
>
> v is the velocity of the particle (in meters per second)
>
> and $\times$ is the cross product.

To compare some of the characteristics of a standard PPT and a micro-PPT, the

PPT from the Earth Observing 1 (EO-1) spacecraft [7] is compared with the micro-PPTs

studied at the Air Force Research Lab (AFRL) [6]. The standard PPT from the EO-1

spacecraft has a mass of 4.95 kg, capacitance of 40 microfarads, specific impulse ranging

from 650 to 1400 seconds, maximum thrust of 854 micronewtons, and a lifetime of over

40 million pulses. The mission of the PPT on the EO-1 spacecraft is to control the

attitude of the satellite. The micro-PPTs studied at AFRL has a mass of approximately

100 grams, capacitance near 0.5 microfarads, specific impulse of approximately 300

seconds, thrust typically less than 20 micronewtons, and lifetimes lasting over one

million pulses. The micro-PPTs can be used for attitude control and stationkeeping of

100-kilogram-class satellites, or as the primary propulsion system for 25-kilogram-class

satellites.

The propellant module of a micro-PPT has a coaxial geometry that includes an

annular rod of Teflon™, an inner cathode, and an outer conductive shell that serves as the

anode. The schematic for this structure can be seen in Figure 3. Unlike the standard

PPT, where the propellant can be spring-fed forward as the propellant face ablates, the

mass and size of a micro-PPT dictate that a different approach must be used. One early

method was to machine micro-springs to operate in a similar manner as the standard PPT,

and another allowed the propellant to recede into the outer electrode. These techniques

were discarded in favor of the current design, where both the inner and outer electrodes

ablate and recede at the same rate as the propellant. By eliminating extra components,

the thruster is simplified and the size and weight can be reduced by many orders of

magnitude to meet the needs of microsatellites [8].
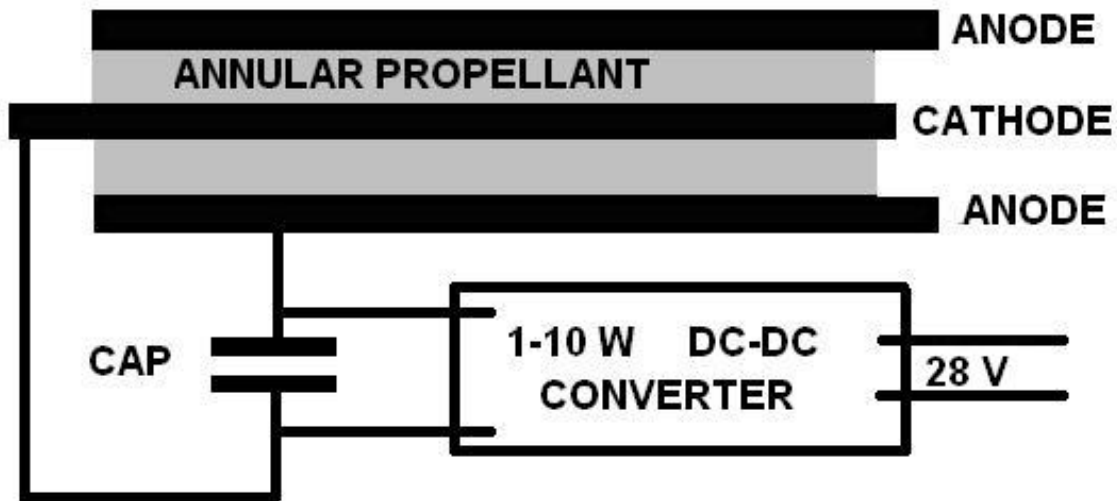
Figure 3 - Schematic of a micro-PPT [8]

PPTs have been used from the mid-1960s to the present. The Soviet Union was the first nation to use PPTs in 1964, but the United States soon followed in 1968. The main applications for PPTs have included attitude control, stationkeeping, and drag correction maneuvers for standard satellites, as well as the primary propulsion system for microsatellites. The most noteworthy and recent use of a PPT is in the EO-1 spacecraft (Figure 4), launched in 2000, where the PPT is being successfully used for precise pitch control and momentum management. No adverse interactions occurred between the PPT and the rest of the sensors on the spacecraft. This PPT was developed as part of a renewed effort in modernizing, simplifying, and improving the performance of the PPT [6].

NASA, along with the Air Force and several companies in the private sector, are interested in using PPTs more often in upcoming satellites, due to their simplicity, small size, and control capabilities. On January 17, 2007, the Air Force Academy's FalconSAT-3 is scheduled to launch with a micro-PPTs used for attitude control.
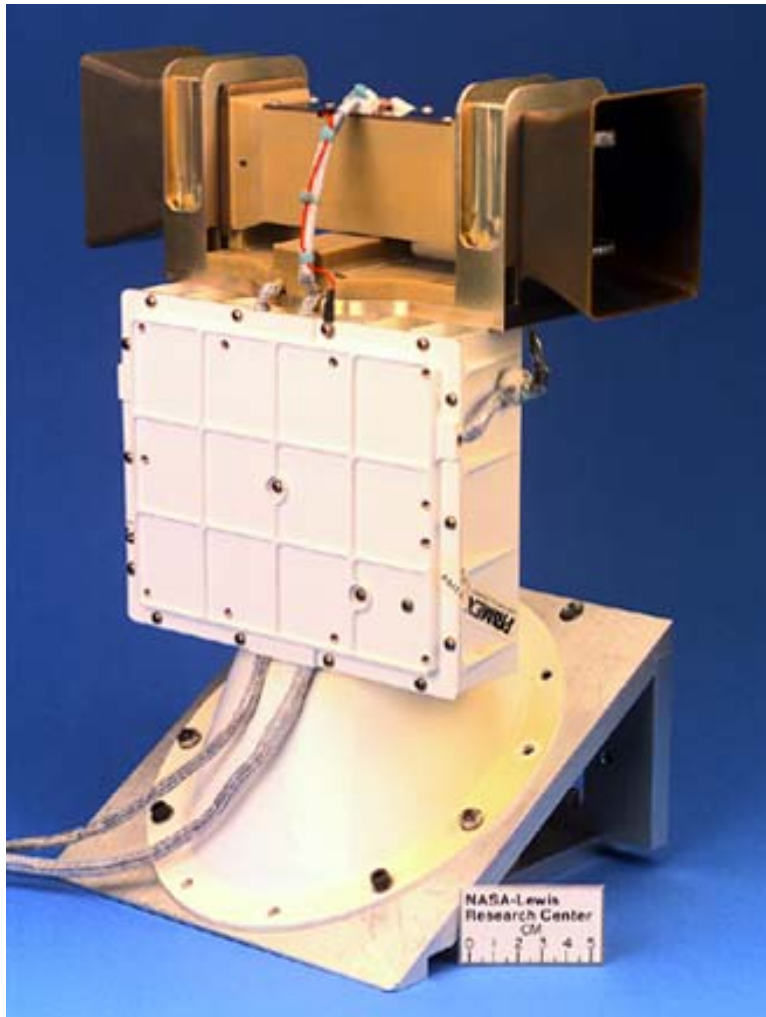
Figure 4 – Earth Observing 1 Pulsed Plasma Thruster [6].

Relevant Research

The Electric Propulsion Laboratory at Edwards AFB, CA has done extensive research with PPTs. Similar to this study, they have looked at the effects of particulates on PPT performance. A PPT was fired with an array of aluminum samples to collect the particulate deposits at various angles. Photos were taken of the PPT as it was fired to study the discharge and motion of the particulates (Figure 5). Using a scanning electron microscope (SEM), the amount of particulates was quantified and shown to be significant. Figure 6 shows an SEM image of the deposition on an aluminum witness plate [9].

In this analysis, the particles were counted and sorted by size. By assuming a spherical particle shape and the density of Teflon™, the mass of the ejected particles was calculated and compared with the remaining propellant mass. This analysis estimated that 30% of the propellant was consumed as particulates, thus largely contributing to PPT inefficiencies. If a significant portion of the propellant remains in the solid state, without becoming ionized and accelerating to high velocities, then that propellant does not contribute as much to the thrust. The other main component of PPT inefficiency is the result of incomplete ionization of the gaseous propellant. Up to 90% of the solid propellant remains neutral when changing to the gaseous state, and the inert gas travels at low velocities without contributing to the thrust. These inefficiencies give PPTs the distinction of being one of the least efficient electric propulsion systems, with thrust efficiencies usually less than 10% [9].

15
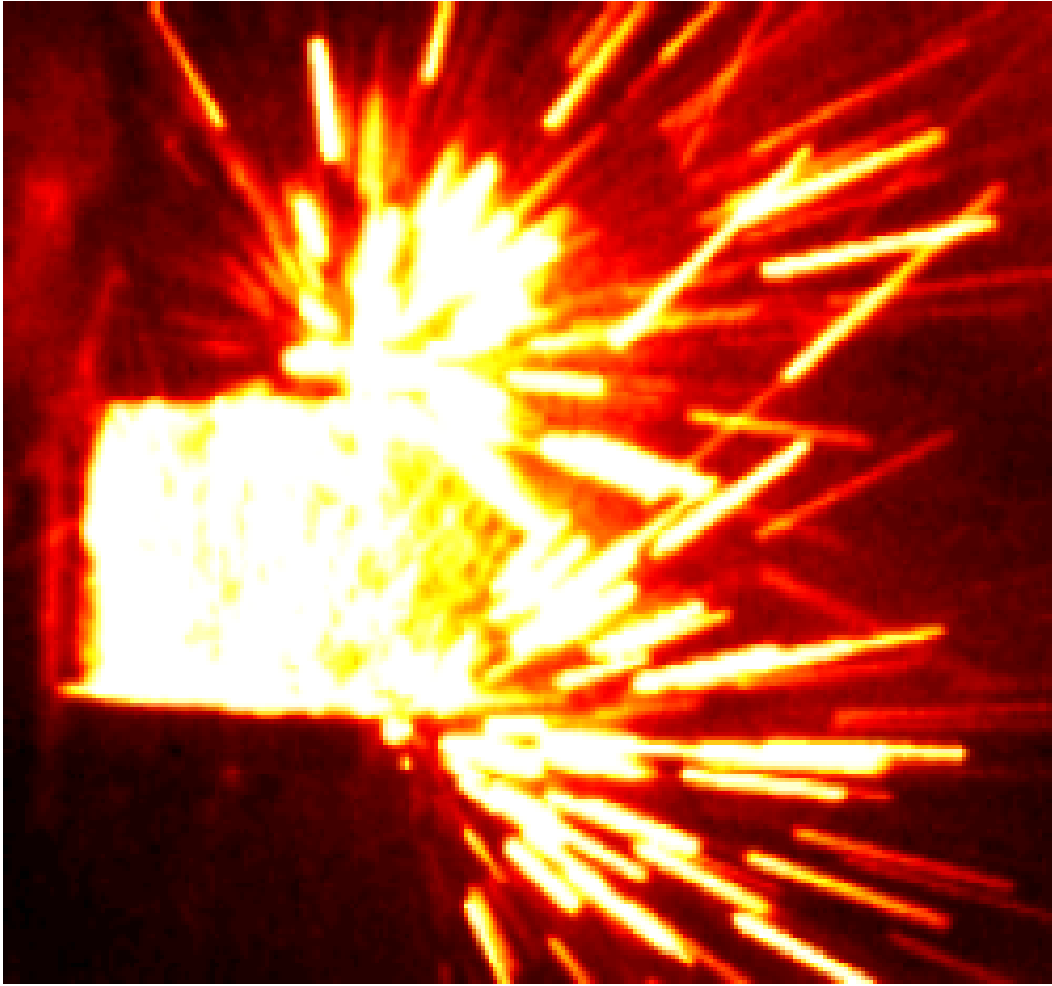
Figure 5 - PPT emission and particulate motion [9].
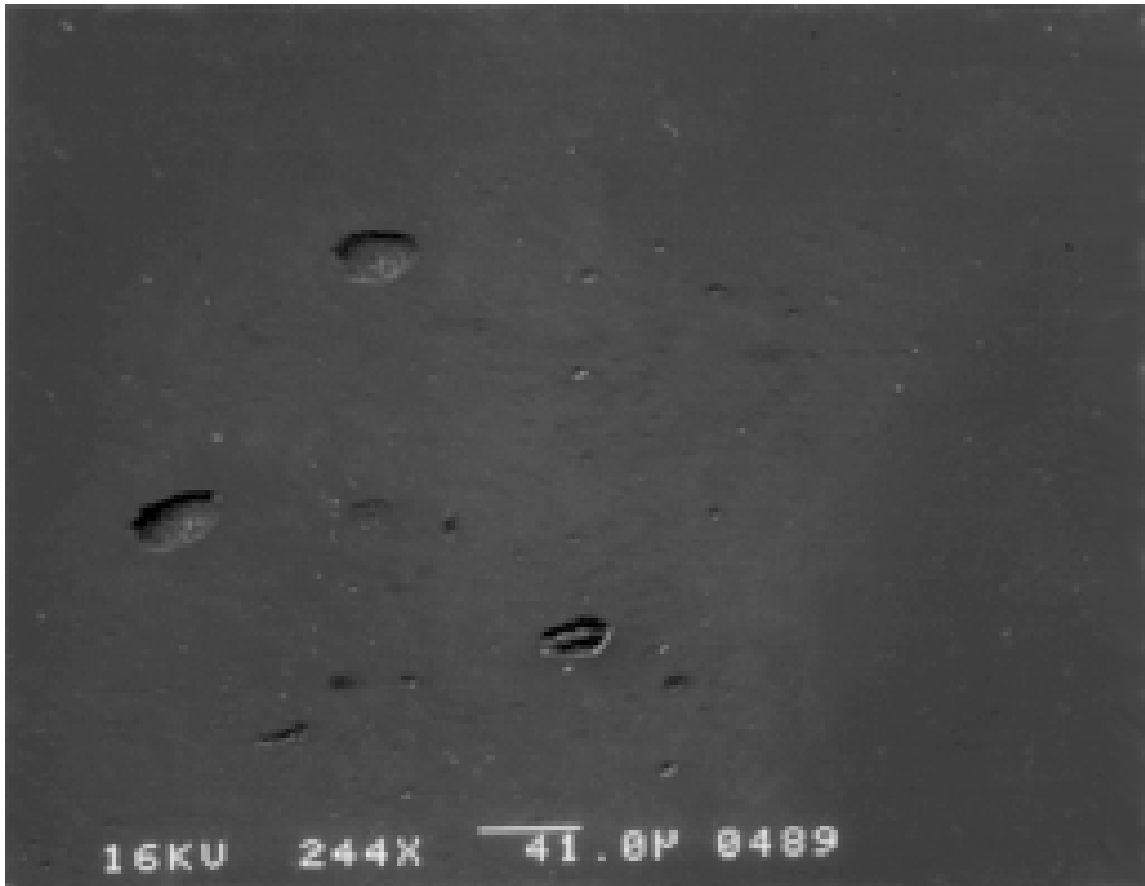
Figure 6 - SEM image of PPT particulate deposits [9].

Despite the poor thrust efficiency of PPTs, the high specific impulse compared to other electrical thrusters makes the PPT a good option for a variety of missions. The specific impulse of a PPT can range from less than 200 to more than 2,000 seconds. This is greater than the typical specific impulse, typically less than 450 seconds, for chemical rockets. In addition to the higher specific impulse, the simplicity of the PPT reduces the number of components and overall mass of the system. The specific impulses of other electric thrusters range from 150 and 700 seconds for a resistojet, 450 and 1,500 seconds

17

for an arcjet, 1,500 and 2,500 seconds for a Hall thruster, 2,000 and 6,000 seconds for an ion thruster, and 2,000 and 30,000 seconds for a magnetoplasmadynamic (MPD) thruster. Other electrical thrusters may have higher specific impulses, but once again, the simplicity of the PPT design can offer other advantages, such as reduced weight and lower chance of component failure.

Other studies at the AFRL Propulsion Directorate researched the effect of total capacitance, maximum charge voltage, and propellant diameter on propellant ablation with a micro-PPT. Each of these parameters was varied in order to find a configuration where the propellant and electrodes receded uniformly and charring was eliminated. These tests found that increasing the discharge energy avoids deposits on the propellant face. In order for the inner cathode to have sufficient energy to recede at the same rate as the propellant, the current density must be increased, either by decreasing the propellant diameter or increasing the discharge energy. If the cathode is not kept uniform with the propellant, electron field emission is decreased and the propellant breakdown voltage is increased past design constraints. Figure 7 shows a propellant face with minimal charring and a cathode that has receded at the same rate as the propellant. This same study also examined possible contamination issues of the micro-PPT by photographing the plume (see Figure 8). The plume was shown to be directed forward, unlike a standard PPT, where the particulates travel in all directions [8].
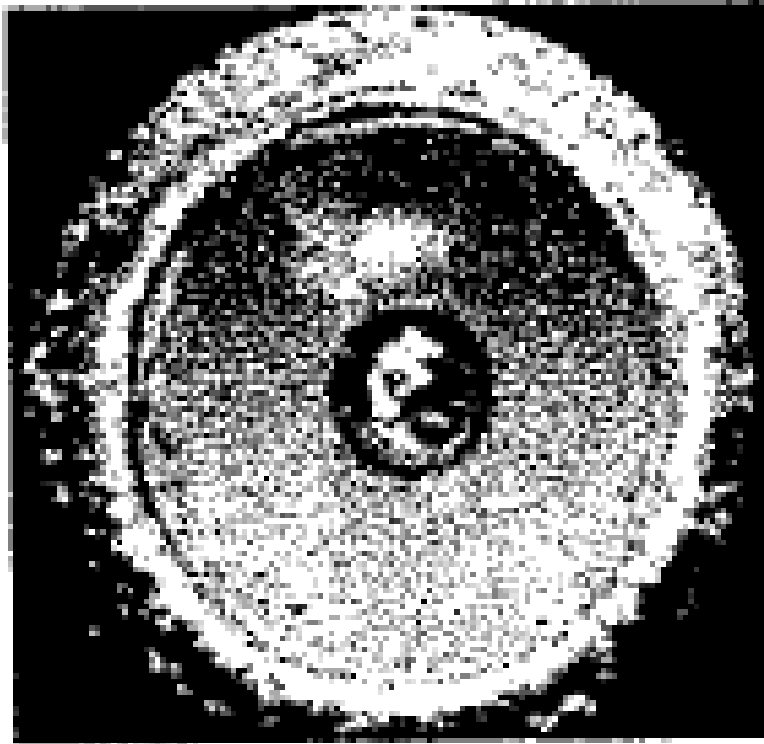
Figure 7 - Propellant and electrode ablation [8].
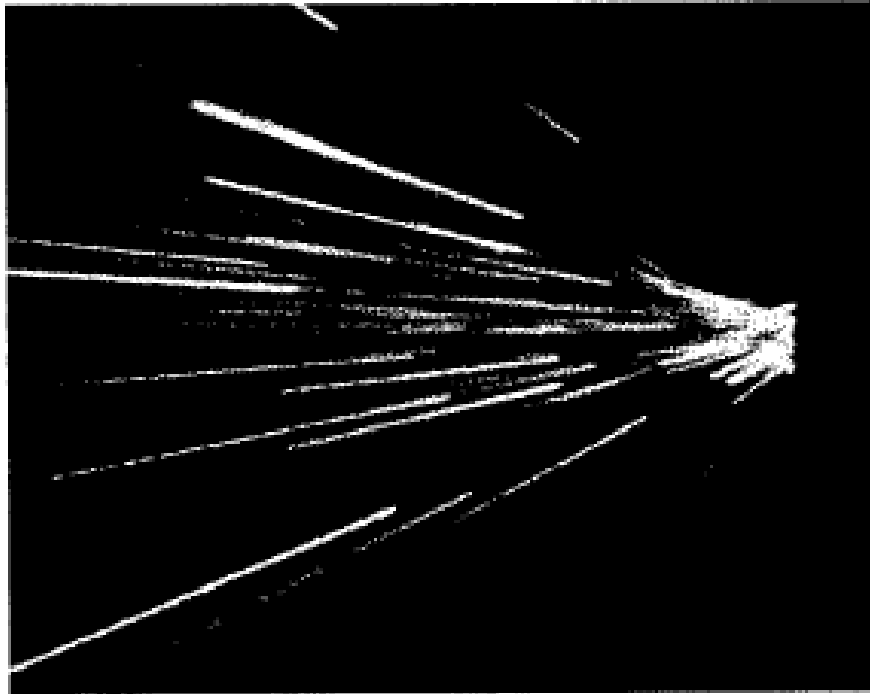
Figure 8 – Exhaust plume of a micro-PPT [8].

Thruster efficiency in the PPT was the focus of another study by AFRL. This study examined the effect of propellant temperature on efficiency and looked at performance factors that increased the propellant consumption rate. Long duration use, low propellant mass, and high PPT power levels all contributed to higher propellant temperature and increased propellant consumption, with no significant increase in thrust. When more propellant is used without increasing thrust, an undesirable inefficiency is present. This inefficiency suggests that lowering the propellant temperature can offset the higher propellant consumption rate and improve performance. The temperature can be lowered by using the thruster for shorter durations, increasing propellant mass, and lowering the PPT power levels [10].

In an extensive multi-year study performed at the University of Michigan, numerical approaches were used to model all aspects of a PPT, including Teflon ablation, plasma formation, electro-magnetic acceleration, plume expansion, and particulate transport. The numerical models helped understand the nature of the plasma plume of a PPT, where the particulates are charged, heated, and accelerated. The particulates can range in speed from zero to a few hundred meters per second, depending on size and point of formation. Also, the particulates can interact electrostatically with the surfaces around the thruster. Small particles may even decompose during the discharge pulse and contribute to the neutral plasma component. Some of this data, such as particle velocities, has been validated experimentally, but future work remains to combine and verify the computational methods with experimental results [11].

Another aspect of this study at the University of Michigan was modeling the near field plume of a micro-PPT. The numerical approach helped understand the electromagnetic acceleration and some potential contamination issues. The micro-PPT presents a different modeling challenge because there is no separation between the main plasma acceleration region and the plume expansion. Figure 9 shows a schematic of the plasma layer near the Teflon™ surface. The particles can have both positive and negative radial velocities, indicating that some particles may traveled back towards the thruster after being fired out of the propellant tip. The magnetic field causes many of the particles to travel at various angles as well [12].
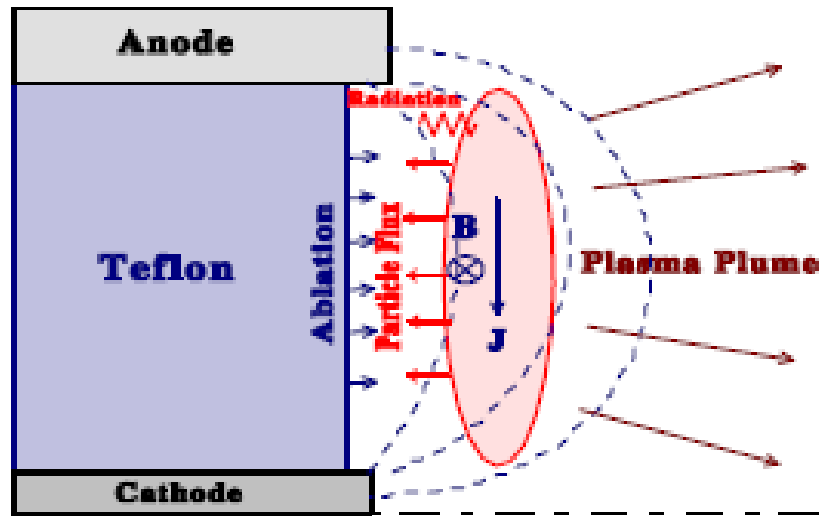
Figure 9 - Schematic of the near Teflon plasma layer [13].

Summary

PPTs have been studied for multiple decades, but the interest in micro-PPTs has only developed since the late 1990s. Extensive work has been performed in order to optimize various configurations and power requirements, but a few areas still remain to be studied before micro-PPTs are widely used on new satellites. A combination of theoretical, computational, and experimental projects have recently contributed to a broader understanding of PPT operation and behavior.

III. Methodology

Chapter Overview

The purpose of this chapter is to describe the experimental setup and test procedures of this study. The assembly and operation of the vacuum chamber and the construction of the micro-PPTs are discussed.

Test Setup

Before conducting any experiments with the PPT, the vacuum chamber first needed to be assembled. Initially, the laboratory at AFIT only owned a bell chamber and diffusion pump. All of the other parts and supplies needed to be acquired. Figure 10 shows a preliminary schematic of the vacuum chamber system, while Figure 11 shows the actual vacuum system in the laboratory. The valves, hose lines, pressure gauge, mechanical roughing pump, control relay, chamber feedthroughs, flange adapters, and oils needed to be attached to the diffusion pump-vacuum chamber assembly. The chamber is 30 inches high and 26 inches in diameter, and it contains 36 ports used for instrumentation or viewing. The diffusion pump is a Varian VHS-6 model, and the roughing pump is a Welch 1374 belt-drive model. A closer view of the diffusion pump and roughing pump can be seen in Figure 12.
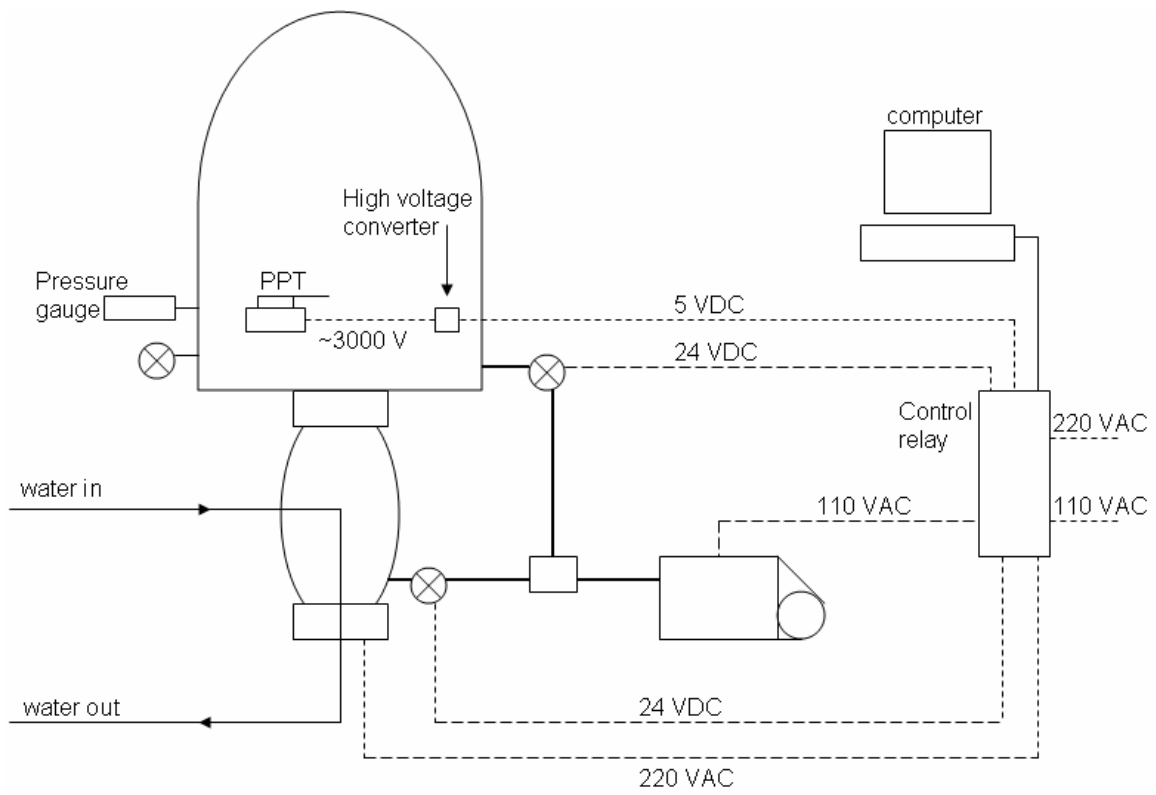
Figure 10 - Preliminary vacuum schematic
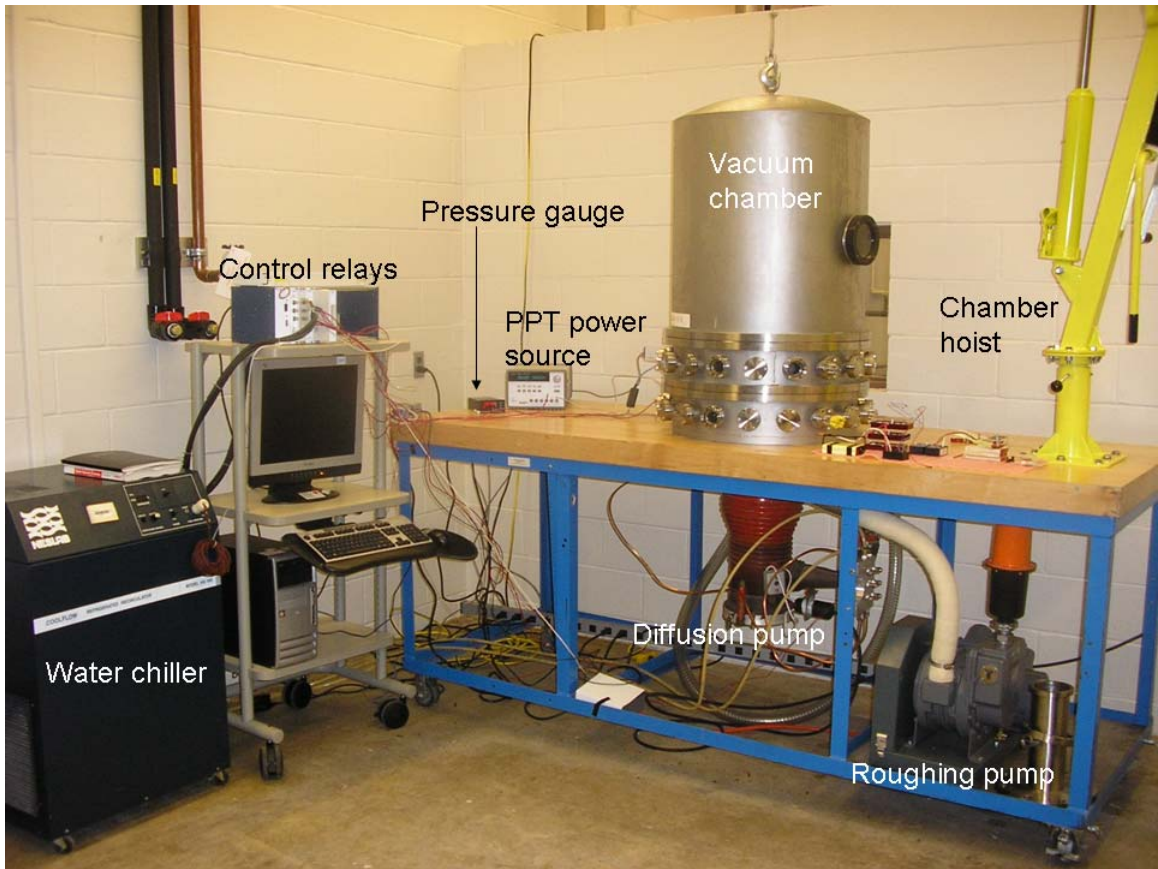
Figure 11 - Laboratory setup
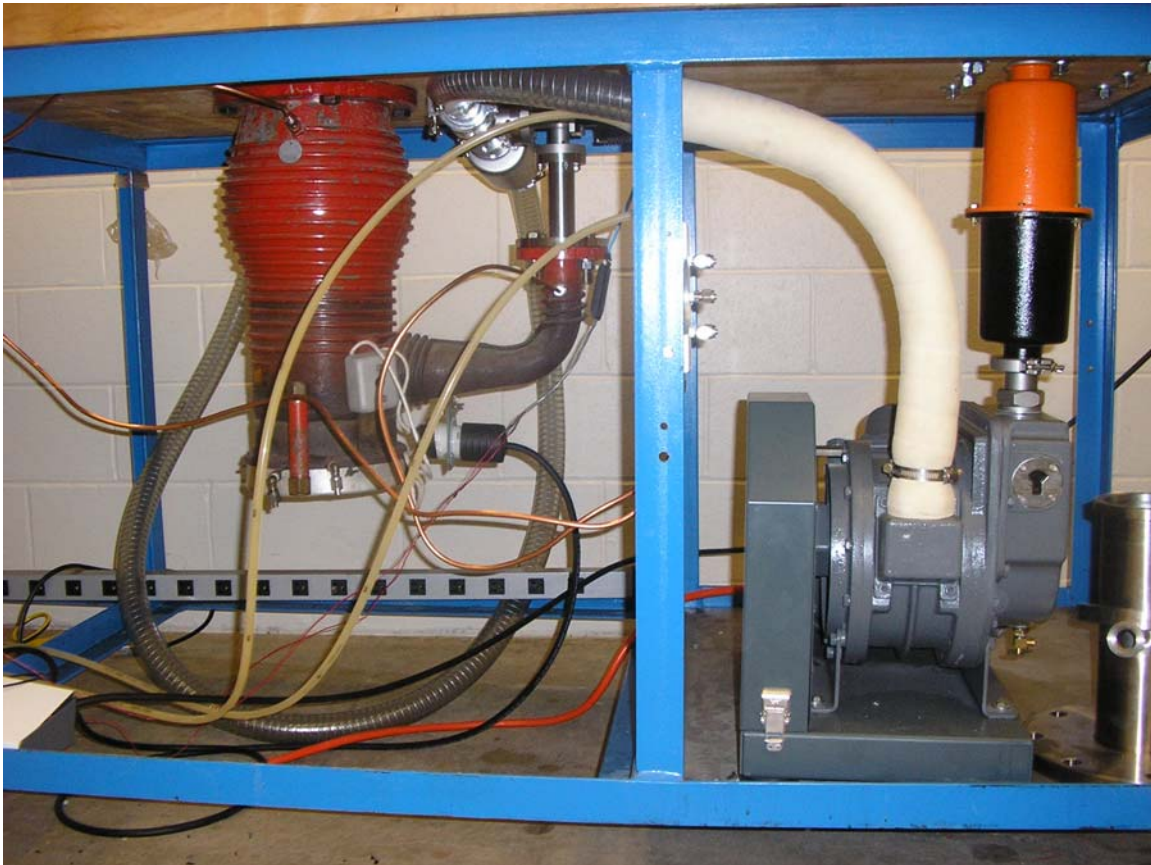
Figure 12 - Diffusion pump and roughing pump

The pumps and valves need to be turned on and off in a specified sequence to pump down the vacuum chamber. One of the goals of this study was to automate the pump down and venting processes using control relays and a computer. A software program was written to regulate when the control relays turn on and off, based on a user specified period of time or pressure level achieved.

When turning on the chamber and initiating the pump down process, only the roughing pump is operating and only the roughing pump valve is open, as shown in Figure 13. Once the chamber reaches a pressure of approximately 13 pascals (0.1 torr),

the diffusion pump can begin operation. At this point, both the roughing pump and the diffusion pump are running, the roughing valve is closed, and the diffusion pump valve is opened, as seen in Figure 14. The chamber operates at this state for the duration of the experiments. Figure 15 shows the chamber and valve configuration for venting the bell jar and bringing it back to atmospheric pressure.
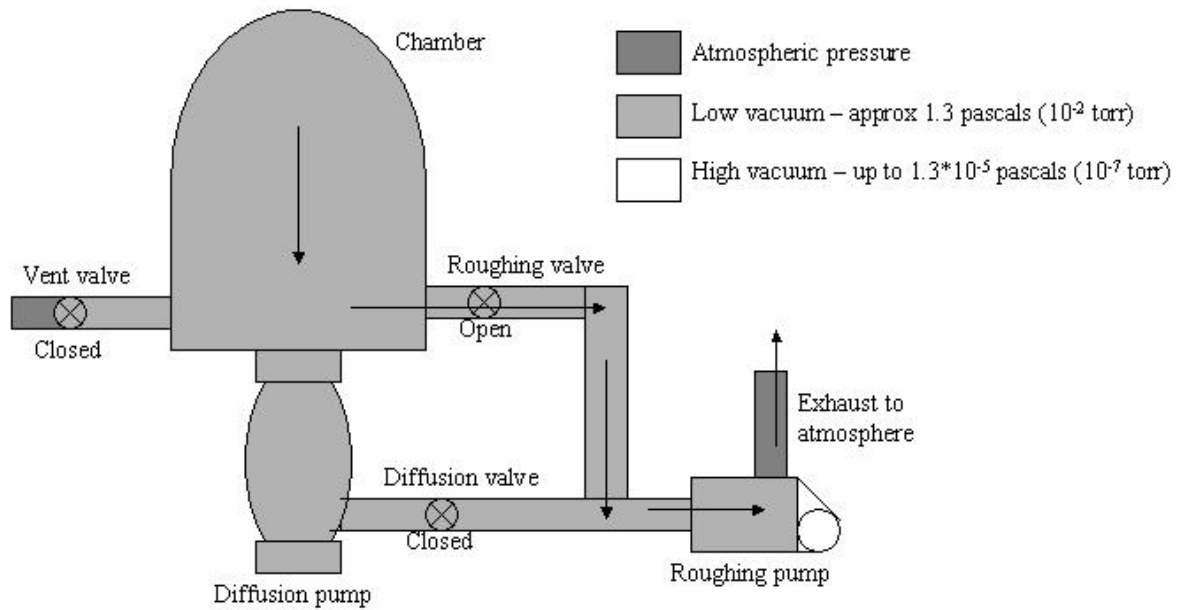
Figure 13 - Roughing down the chamber
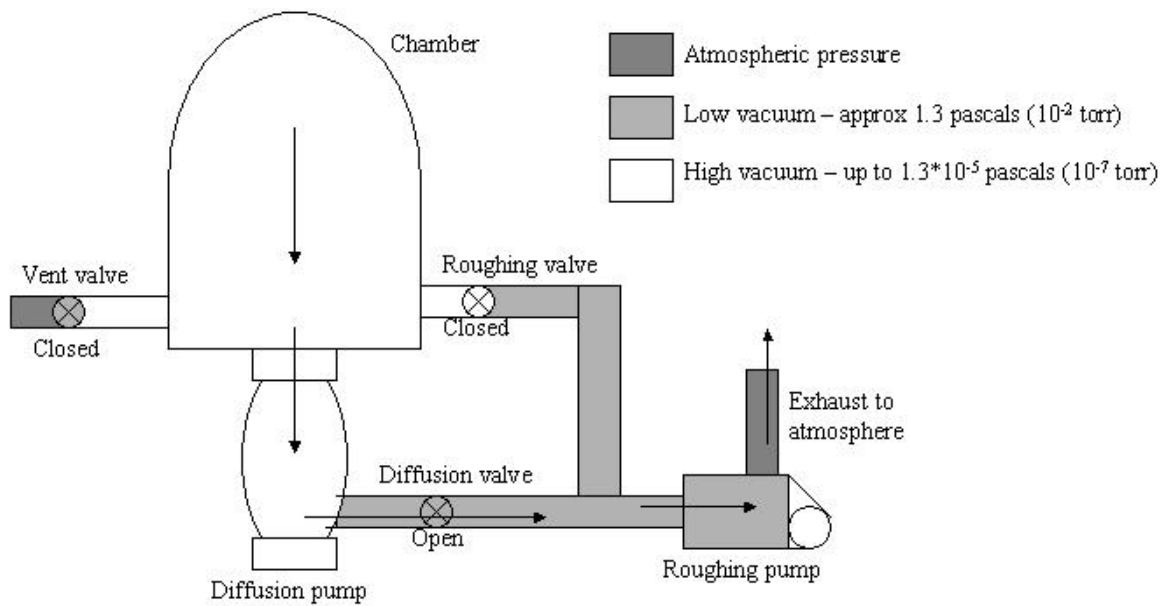
Figure 14 - Bringing the chamber to high vacuum
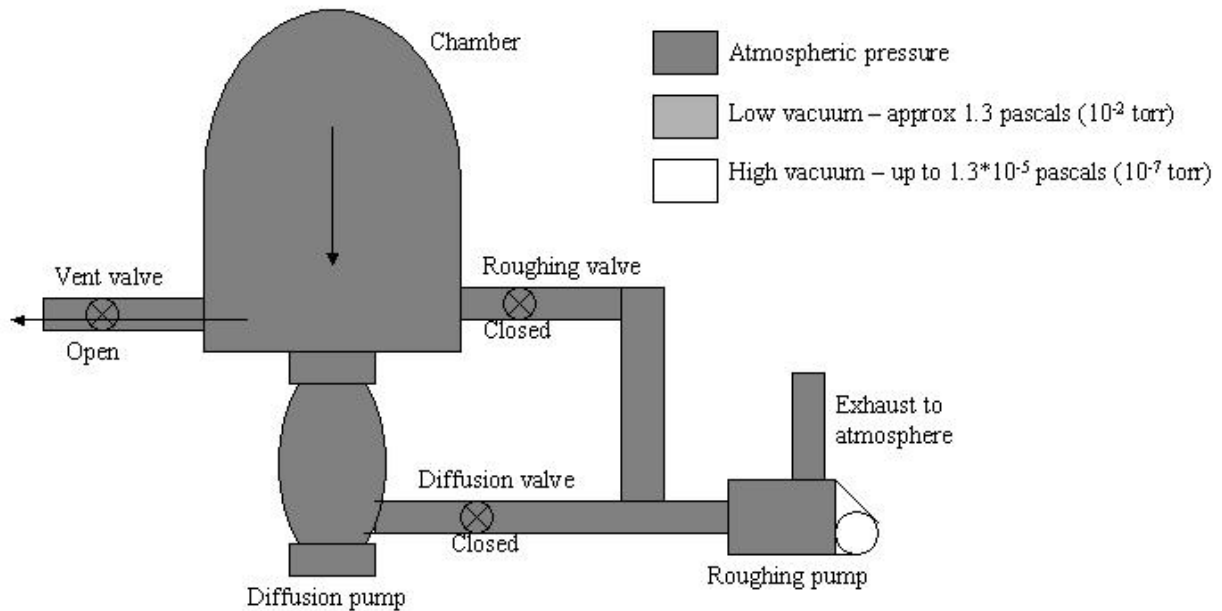
Figure 15 - Venting the chamber

The diffusion pumped needs to cool down before venting the chamber, or else the diffusion pump's oil vapor may enter the chamber and cover anything inside. In order to vent the chamber correctly, the diffusion pump is shut down for approximately ten minutes while the roughing pump continues to run. Then, the roughing pump is shut

down, and the roughing pump valve and diffusion pump valve are closed. After another ten minutes, the vent valve can be safely opened.

This entire sequence is automated with a data acquisition and control system. All three valves, the roughing pump, the diffusion pump, and the micro-PPT are each wired into a National Instruments relay unit. The data from the pressure sensor is fed directly into the laboratory computer. Using National Instruments LabVIEW software, the relays can be controlled, and the pump down procedure is completed by simply initiating a LabVIEW program. The program continuously reads the pressure level and triggers the relays accordingly.

When assembling a vacuum chamber, care must be given to constructing a leak-free system. All of the numerous connections must be properly sealed with o-rings, leak preventing grease, and multiple nuts and bolts. If a connection is improperly sealed, then the chamber will not be able to reach vacuum levels, and the experiment will not correctly simulate a space environment. Almost every vacuum system develops a leak during its construction, and the chamber assembled for this study was no exception. When the pumps were turned on, the pressure did not drop as far as it should, and even a hissing sound could be heard from certain locations around the chamber. A simple method to locate leaks that are not audible is to spray acetone around the connections and look for a sudden pressure rise due to acetone vaporization. The leaks were located, the o-rings were replaced, and the flanges retightened. After fixing the leaks, the diffusion pump and roughing pump can now bring the chamber down to high vacuum levels, reaching pressures as low as $2.0*10^{-5}$ pascals ($1.5*10^{-7}$ torr).

Achieving high vacuum conditions is necessary for this study, because atmospheric or near-atmospheric conditions cause oxidation on the PPT. If the PPT operates at pressure higher than 1.3 pascals (0.01 torr), the thruster is prone to uncontrolled arcing. In these conditions, the increased amount of air particles opens up alternate paths for the current to cross, causing arcing at other locations than the electrode tip.

An array of aluminum witness plates forms the shape of a half-sphere with a radius of two inches, spanning 180 degrees. Two arrays connect in a perpendicular cross that outline the frame the half-sphere. The tests use a total of thirteen witness plates. One plate is in the center of the array branches, and three plates are at the 30°, 60°, and 90° points of all four branches (Figure 16). The tip of the micro-PPT points towards the center of this array, such that the 90° targets of each array are above, below, and to each side of the PPT. This arrangement gives a complete deposition profile, assuming the particulate emission is axisymmetric.

Figure 16 - Configuration of deposition targets

The micro-PPTs were constructed at the Electric Propulsion Laboratory at Edwards AFB, CA. These thrusters contain three main components: a capacitor, high voltage power converter, and propellant tube (Figure 17). The capacitors are rated for 0.5 microfarads and between 3000 and 6000 volts. The high voltage converters take an input of less than 15 volts and output up to 12,000 volts. It is important to note that extreme care must be used when working with these dangerously high voltages. The propellant tube contains an inner wire electrode, enclosed in a tube of Teflon™, which in turn is enclosed in the outer capacitor, a copper tube.
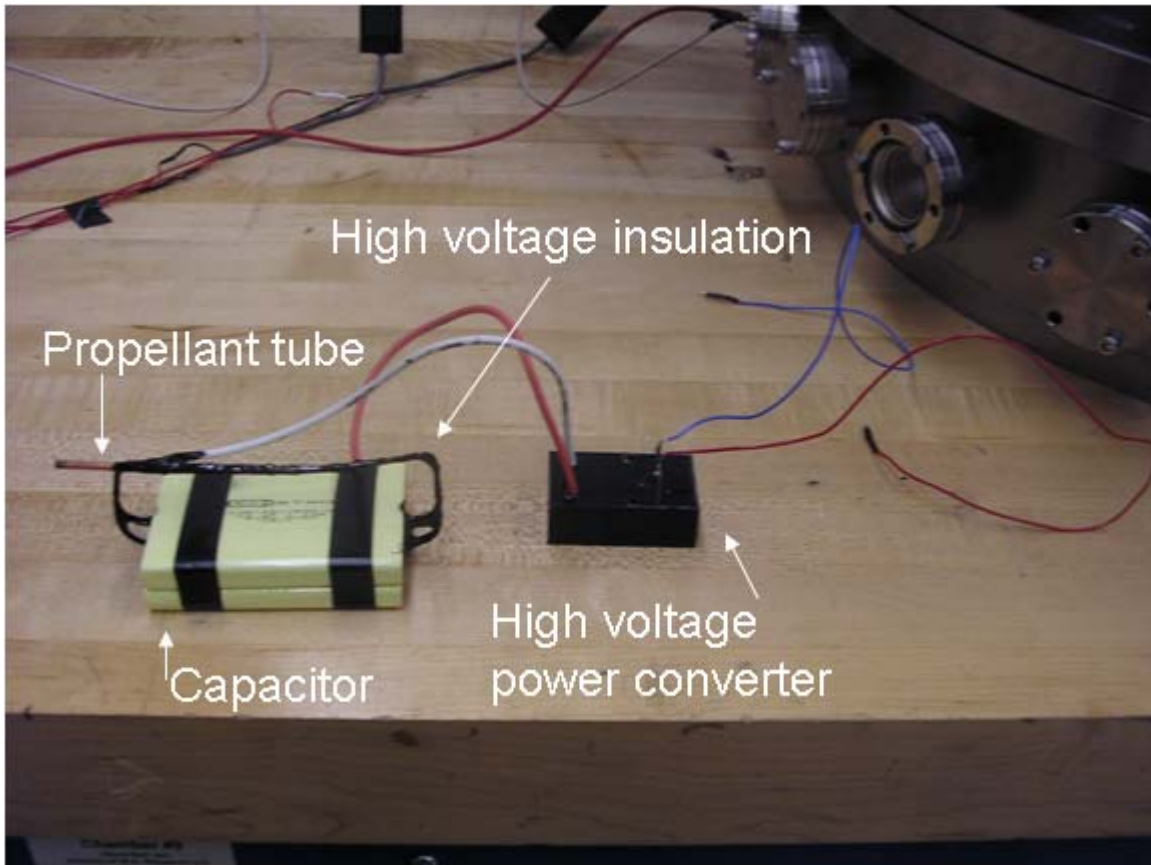
Figure 17 - Micro-PPT components

The power source supplying the initial low voltage input is fed through the walls of the vacuum chamber with pin connectors. Once inside the vacuum chamber, the low voltage inputs (the blue and red wires to the right of Figure 17) are attached to the high voltage converter. The positive lead from the high voltage converter (the red wire in the middle of Figure 17) is connected to the inner electrode of the propellant tube, along with the wire from the rear side of the capacitor. The negative lead from the high voltage converter (the white wire in Figure 17) is likewise connected to the outer electrode of the propellant tube, along with the wire from the front side of the capacitor. All of these

connections are soldered together, and all conducting materials are coated with corona dope, an insulator specifically used for high voltage devices. Corona dope is a quick drying, black lacquer insulating coating, based on cellulose resin.

One major problem that can be encountered with the micro-PPTs is arcing on places besides the tip of the propellant. The micro-PPT works correctly only when the tip of the propellant arcs at regular intervals, but any high voltage conducting surface is prone to arcing. The current is simply looking for the easiest path to pass across so an insulator must be used to keep the arc at the correct location on the thruster. Every exposed conducting surface which comes into contact with a high voltage current needs to be thoroughly insulated. Many different materials can be used to insulate the exposed surfaces, such as electrical tape, liquid electrical tape, high voltage putty, and corona dope. The ideal insulator for this application is corona dope because it can coat surfaces of unusual shapes, it is vacuum rated, and it can withstand the heating due to the high voltages.

The micro-PPT is fired for various time intervals, ranging from ten minutes to nearly two hours. Figures 18 and 19 show how the micro-PPT is aligned with the witness plates in the vacuum chamber. After each operating period, the witness plates are removed for analysis and replaced with unused plates. The scanning electron microscope (SEM) is used to count the amount of particles on each plate for each test, and the SEM images help to categorize the particles by diameter. By counting the number of particles that accumulate at a given angular location and distinguishing the size of these particles, deposition profiles, mass deposition rates, and area blockage rates can all be calculated.

34
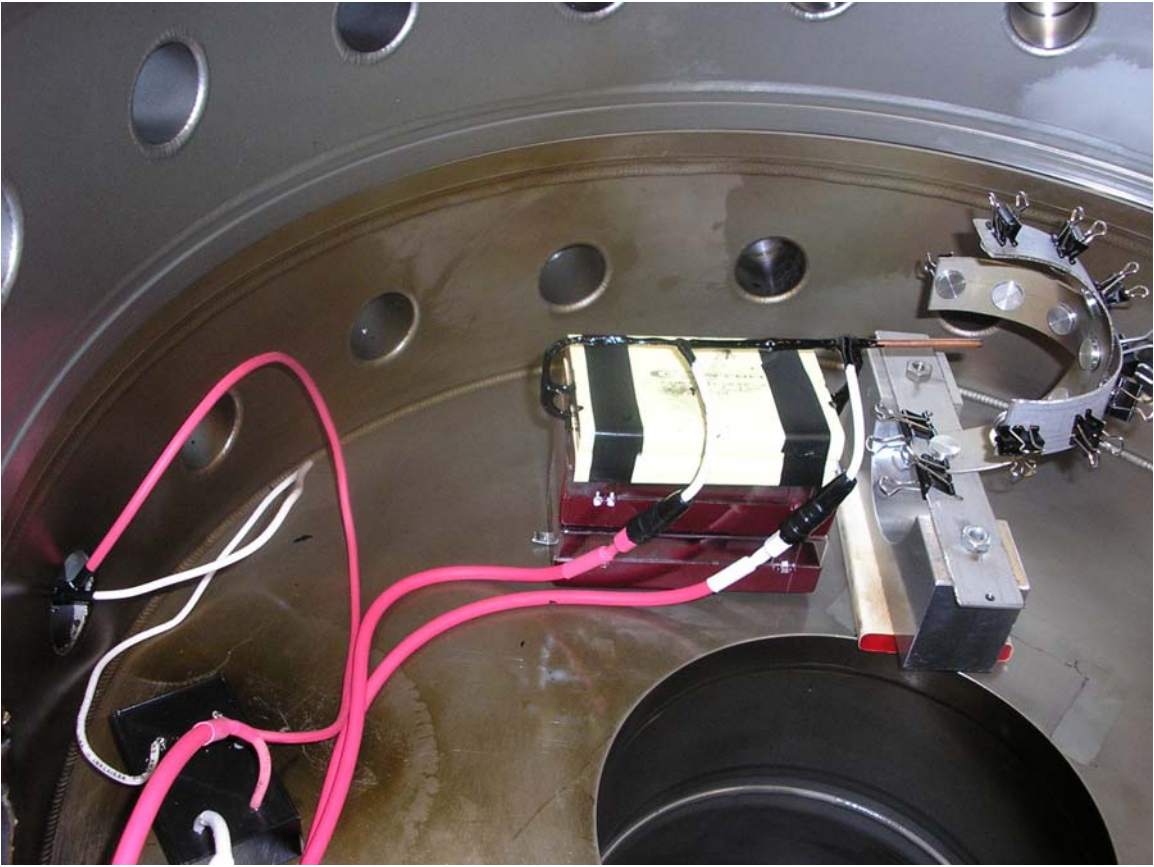
Figure 18 - Micro-PPT and test stand
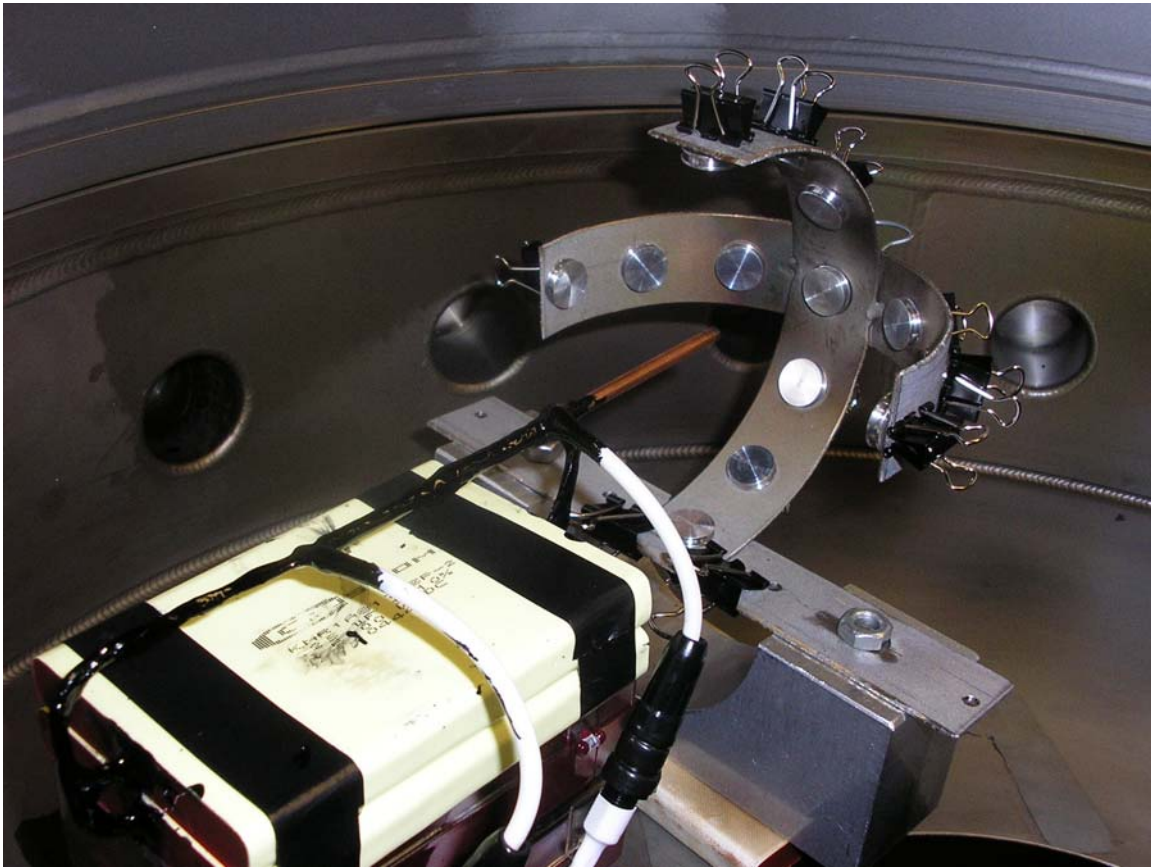
Figure 19 – Another view of the micro-PPT and test stand

Summary

Using the vacuum chamber system assembled at the AFIT laboratories, experiments with micro-PPTs and other small thrusters are possible. An array of witness plates arranged around the tip of the micro-PPT will help to understand the particle deposition profile for these thrusters.

IV. Analysis and Results

Chapter Overview

Four tests were completed with the micro-PPTs, and they each ran for different lengths of time, with different discharge rates. For each test, every witness plate was examined with a SEM at the same magnification, and the number of particles was counted. The data can be used to obtain deposition profiles and deposition rates, which are useful in understanding possible contamination issues with satellite instruments or solar panels.

Results of Test Scenarios

Before firing the thrusters and beginning the experiments, a clean sample of the aluminum targets was studied with the SEM to use as a control. Figure 20 shows the unused sample at a magnification of 100 times. At this magnification, the surface imperfections can be seen as white striations. Figures 21 and 22 show the same sample at lower and higher magnifications, respectively. Increasing the magnification gives a more detailed view of the surface grooves, while decreasing the magnification gives a more complete and broader picture of the sample's surface. The magnification of 100 times was used as the standard baseline throughout the experiment. At this magnification level, particles as small at 5 μm can be counted.

10/23/2006	WD	Mag	HV	Tilt	Spot	————500.0µm————
11:21:00 AM	10.4 mm	100x	20.0 kV	-0.1 °	3.0	
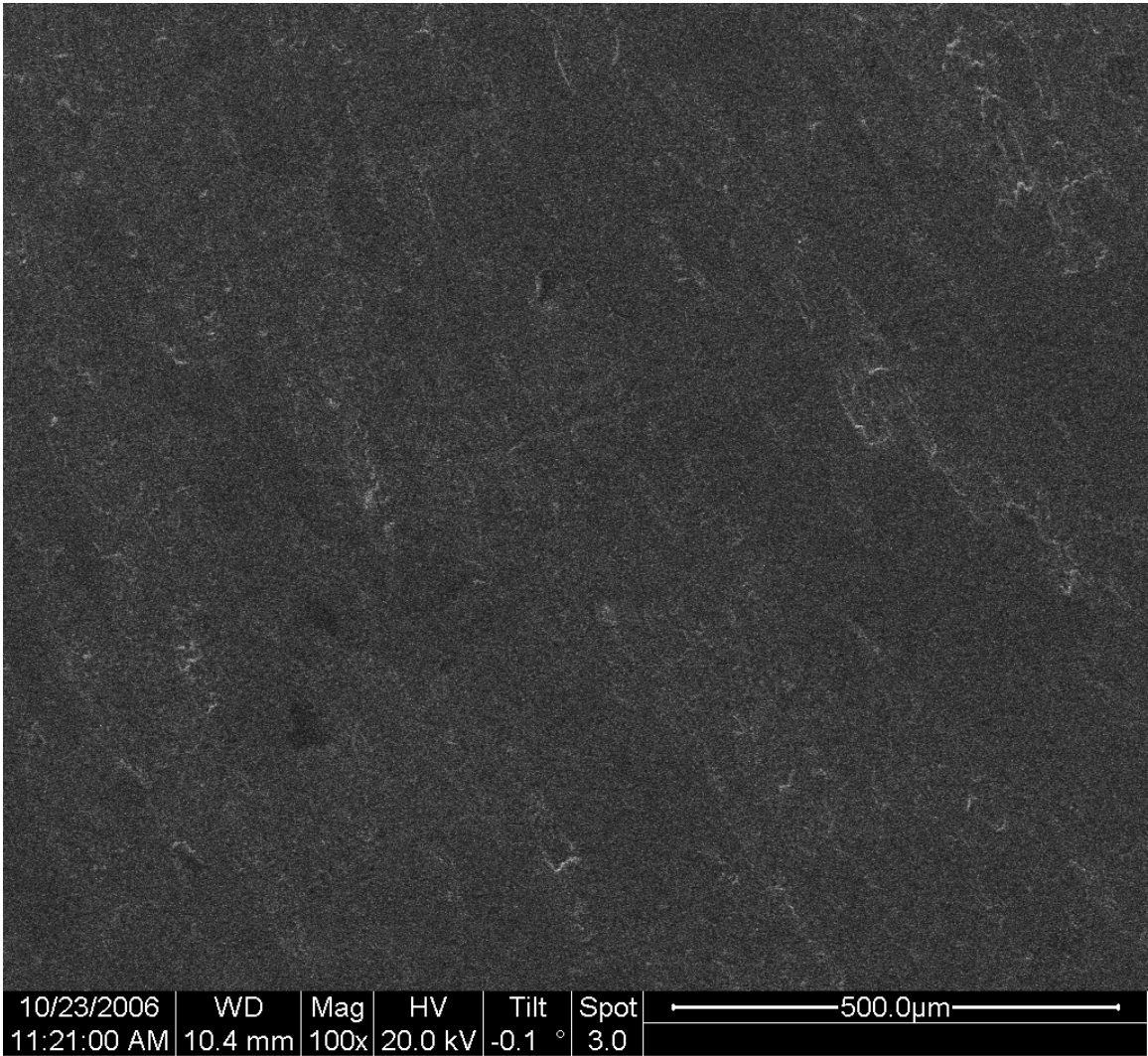
Figure 20 - Control sample - 100x magnification

| 10/23/2006 | WD | Mag | HV | Tilt | Spot | ⊢————1.0mm————⊣ |
| 11:21:47 AM | 10.4 mm | 40x | 20.0 kV | -0.1 ° | 3.0 | |
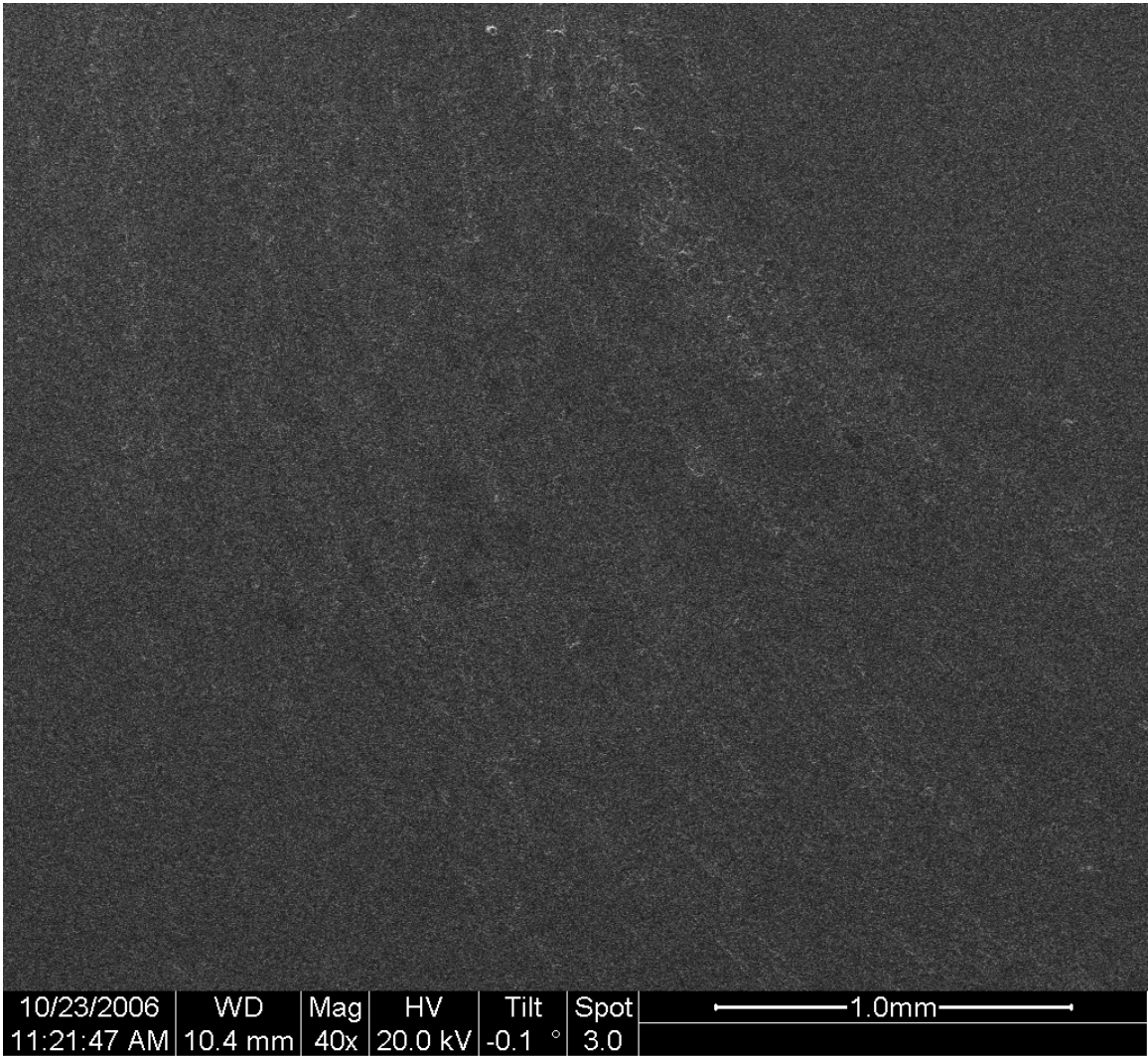
Figure 21 - Control sample - 40x magnification
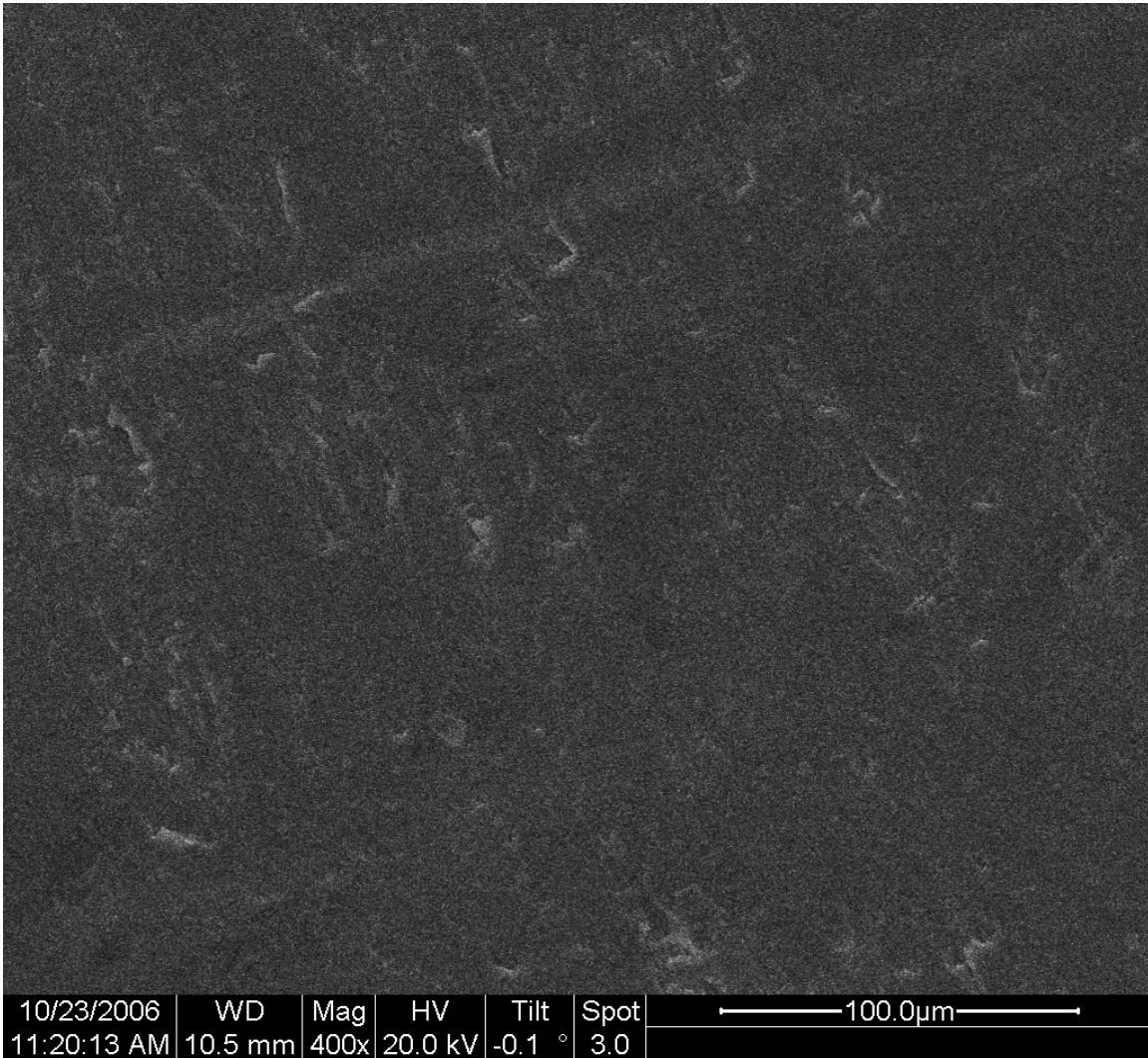
Figure 22 - Control sample - 400x magnification

The initial test with the micro-PPT only lasted ten minutes due to failure of the high voltage converter and capacitor. During this time, a distinct arc could be seen in the chamber at the tip of the propellant. The capacitor charged up then discharged, allowing the current to pass across the tip of the electrodes, similar to a spark plug. The arcing

occurred at a rate of approximately ten sparks per minute. The pressure range during the test was $5.3*10^{-3}$ pascals to $2.7*10^{-2}$ pascals ($4*10^{-5}$ torr to $2*10^{-4}$ torr).

After the test, the aluminum targets were examined with the SEM. With a preliminary review of the samples, it became apparent that counting all of the particles on each sample would be impractical. It would take over thirty photos at 100 times magnification to cover an entire sample, and the amount of particles in each photo can be numerous. To perform such extensive analysis does not add any additional value to this research effort. An alternative solution is to look at a smaller set of photos picked at random, count the particles on each photo, and take an average of these results. This still produces clear trends for deposition at varying angles. Any images at the edge of the sample are approximately 7° off-center, but the random selection of image locations mitigates this effect. The amount of particles from all ten images can be averaged to form a composite.

Figure 23 shows a typical SEM image of the central sample at 100 times magnification. The particles are easily visible, especially when compared with the control sample in Figure 20. In this photo, 27 particles of varying size can be counted.
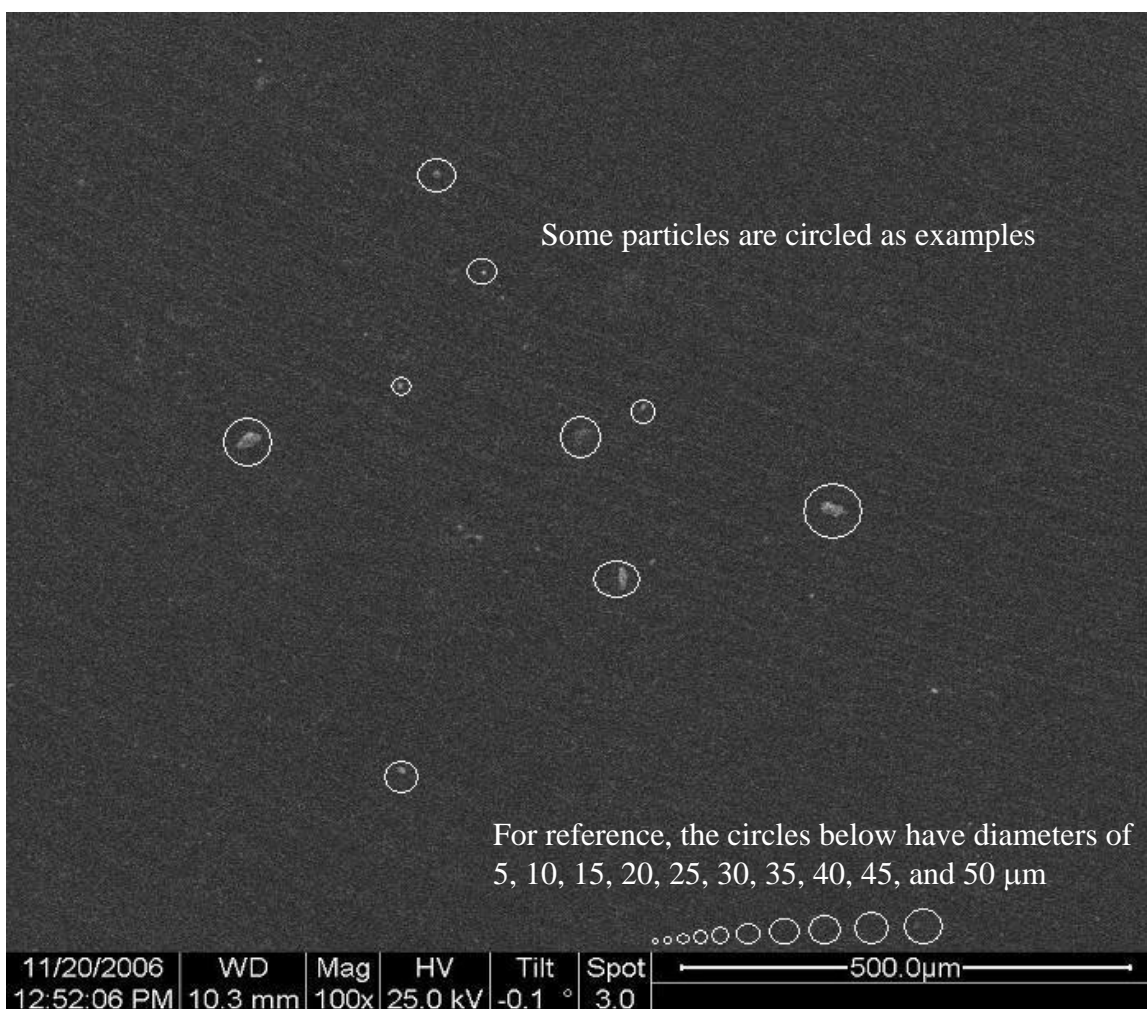
Figure 23 - SEM image of central sample – 100x magnification (Test 1)

Figure 24 shows a typical image for a target at 30°, Figure 25 shows a photo for a target at 60°, and Figure 26 shows a typical image for a target at 90°. In Figure 24 twelve particles are visible, eight particles can be seen in Figure 25, and there are four particles in Figure 26. Each of these totals is far less than the amount seen on the central target.

Reference circles with diameters
5, 10, 15, 20, 25, 30, 35, 40, 45, and 50 μm

| 11/21/2006 | WD | Mag | HV | Tilt | Spot | ⊢————————500.0μm————————⊣ |
| 10:21:50 AM | 10.4 mm | 100x | 25.0 kV | -0.1 ° | 3.0 | |
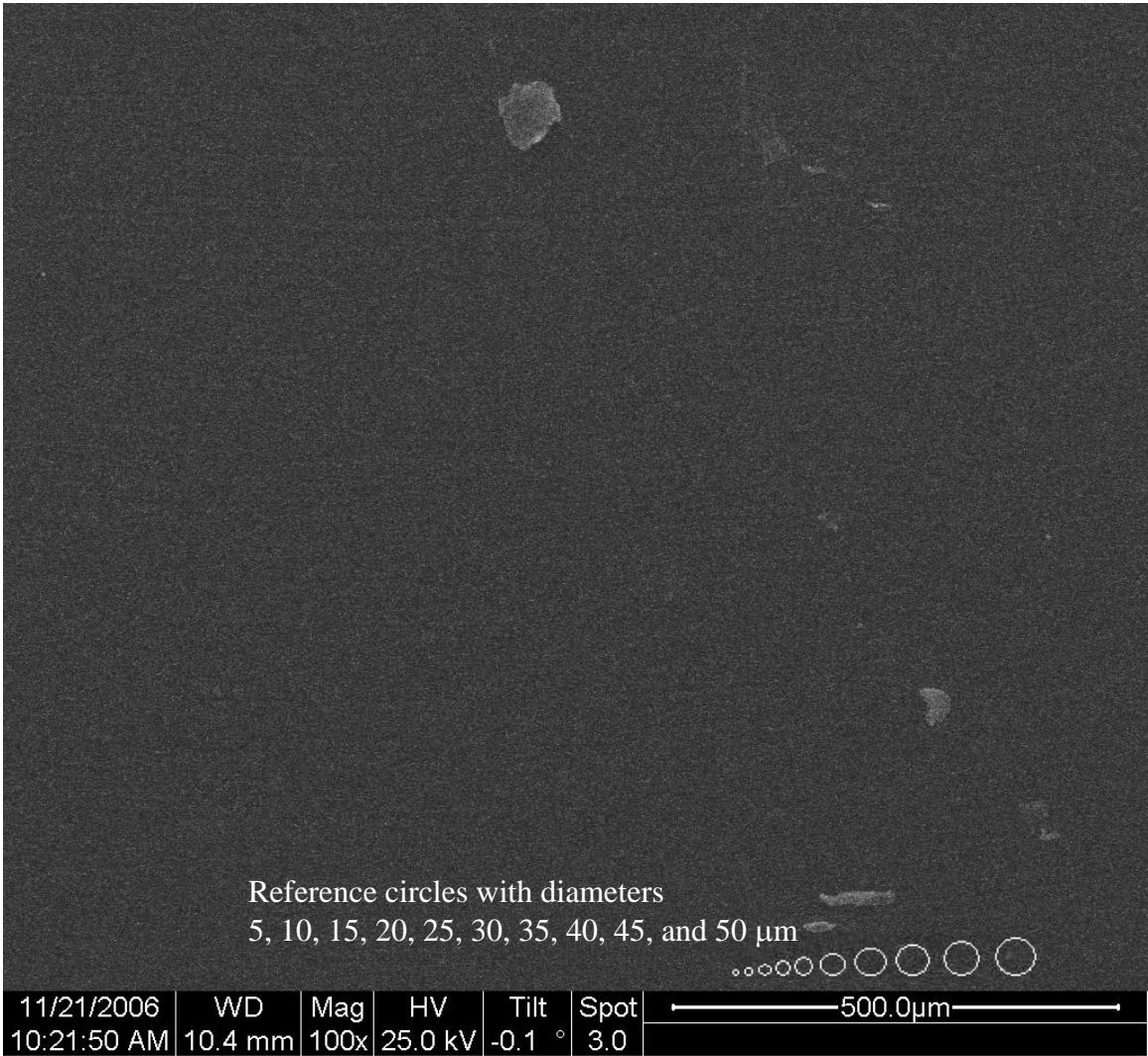
Figure 24 - SEM image of sample at 30° – 100x magnification (Test 1)

Reference circles with diameters
5, 10, 15, 20, 25, 30, 35, 40, 45, and 50 μm

11/21/2006	WD	Mag	HV	Tilt	Spot	————500.0μm————
10:35:25 AM	10.2 mm	100x	25.0 kV	-0.1 °	3.0	
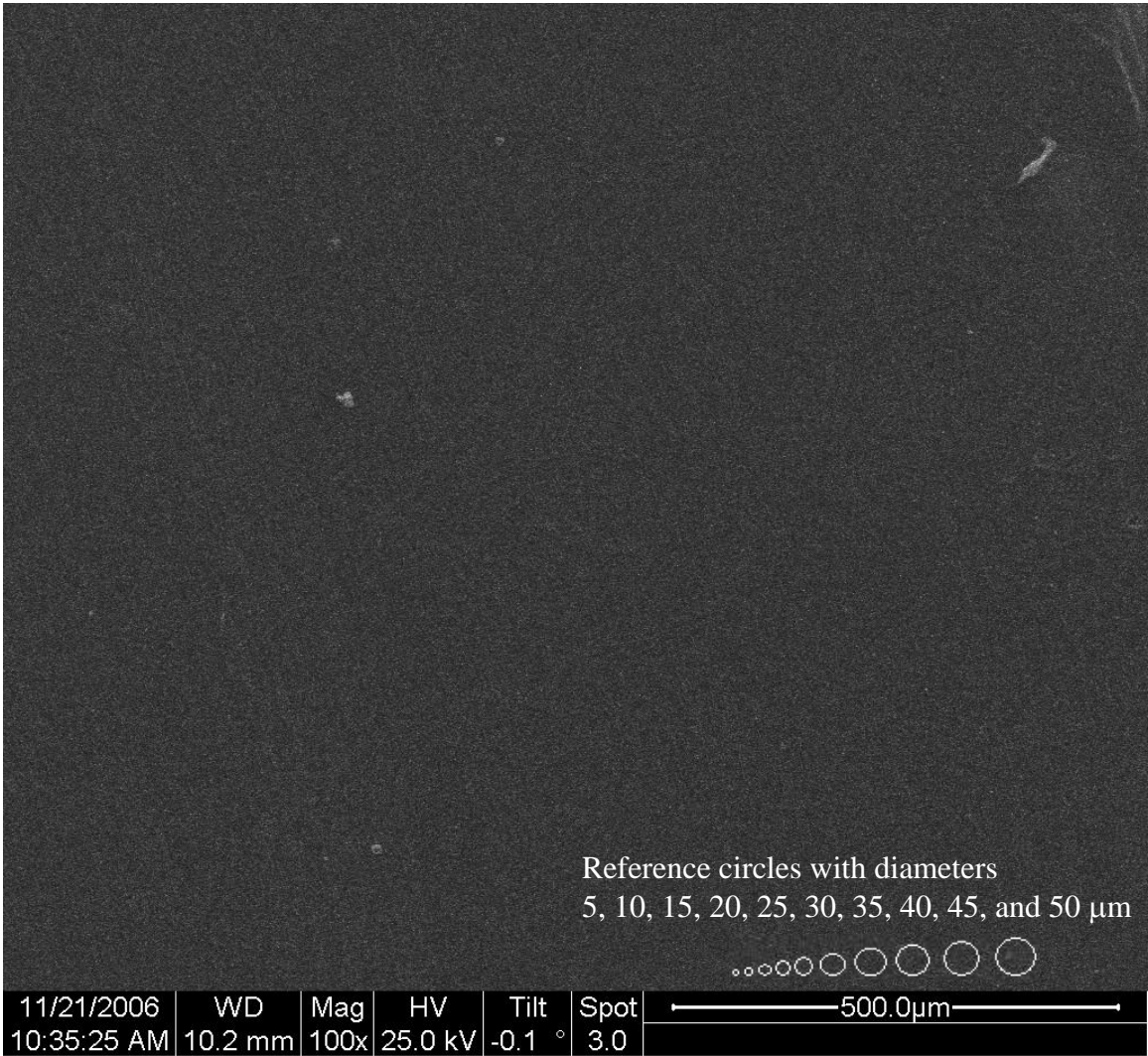
Figure 25 - SEM image of sample at 60° – 100x magnification (Test 1)

Reference circles with diameters
5, 10, 15, 20, 25, 30, 35, 40, 45, and 50 μm

11/21/2006	WD	Mag	HV	Tilt	Spot	500.0μm
9:58:27 AM	13.5 mm	100x	25.0 kV	-0.1 °	3.0	
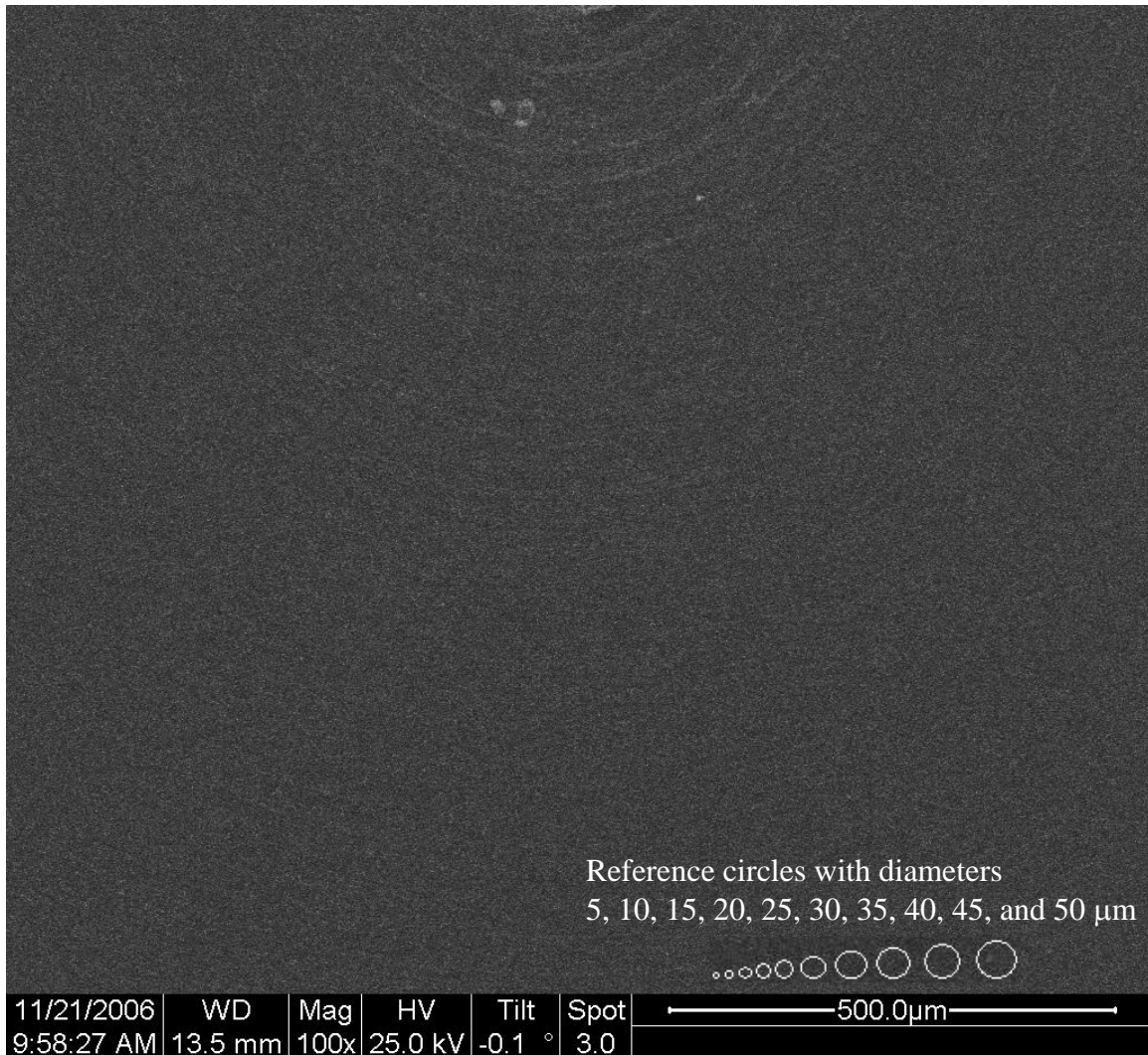
Figure 26 - SEM image of sample at 90° – 100x magnification (Test 1)

As evidenced in the above images, the central sample directly facing the propellant tip received the most particulates. A dramatic drop-off occurred from the central sample to the samples at 30°, 60°, and 90°. In order to compare the effect of angle on deposition, the average particle accumulation for each angular location is calculated (Figure 27). By applying the axisymmetric assumption, all four targets at each angular

location can be viewed as similar samples, regardless of spatial position. Data from the fourth test is presented later to support this assumption.

Test 1 - Average particle accumulation at each angular location
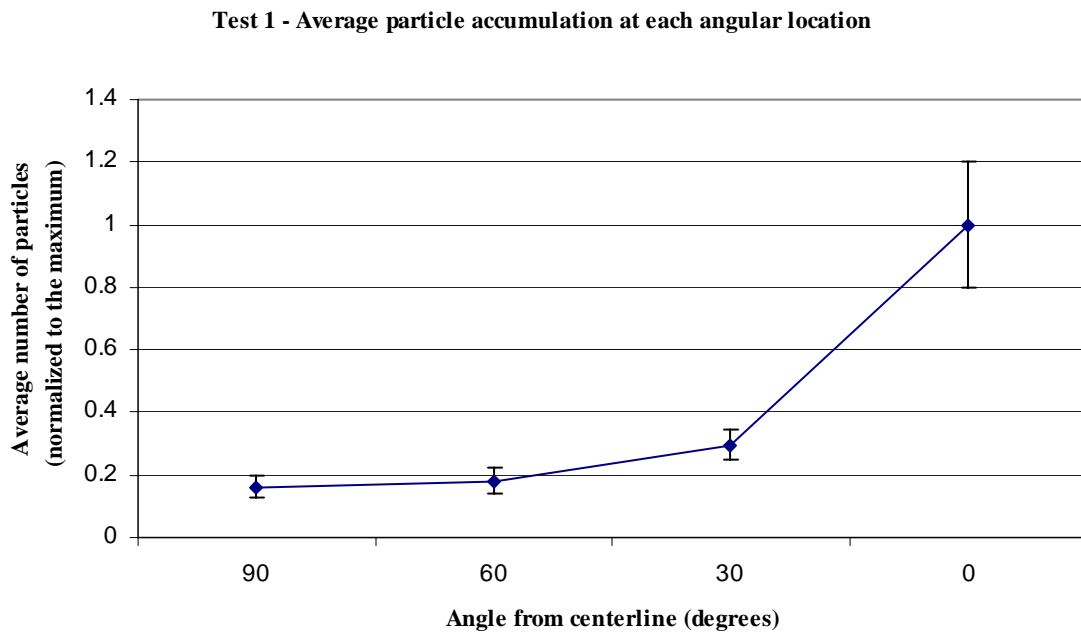
Figure 27 – Particle distribution profile (Test 1)

In Figure 27, the amount of particle deposition is normalized to the maximum value obtained from the central target. The large spike in the graph illustrates the large disparity between the amounts of particles on the central sample compared to all the other samples. The average particle accumulation of the four targets at 30° is 29.6% $\pm$ 4.75% of the maximum deposition at the central target. The average of the four targets at 60° is 18.1% $\pm$ 4.27% of the maximum, and the average of the four targets at 90° is 16.0% $\pm$ 3.53% of the maximum.

The data distribution resembles the left half of a Gaussian spread. The large disparity between the central target and 30° targets should have been bridged by an intermediate set of targets at 15° in order to give the data a more accurate shape. Unfortunately, all four tests were completed before any of the data were analyzed so the need for extra targets at 15° was not realized until after the testing was completed.

The upper and lower error limits for the data are obtained from Student's t-test. This statistical method is useful when the sample size is small, and in this study, the sample size for each target is ten samples. Equation (2) calculates the error bounds.

$$Error = A \cdot \frac{S_n}{\sqrt{n}} \tag{2}$$

where A is found from t-test table and depends on the degrees of freedom and confidence level, S_n is the square root of the variance for the data set, and n is the sample size. For each data set in this study, the value for A is fixed at 1.833, which corresponds to a confidence level of 95% for each error bound and a sample size of 10. The variance changes for each data set depending on the spread of the data. The error bars indicate that the true mean of the data lies within that range, with 90% confidence.

In addition to the statistical error present in the analysis, other sources of error need to be considered. Although some of these errors are difficult to quantify, they are still important when considering the analysis. Every step in any experimental process can be the source for new errors and uncertainty. For example, there may have been some

disparity when aligning the stands for each of the four tests. Despite great care and

attention to detail, the tip of the thruster may not have pointed in exactly the same

direction for each test. Also, using the SEM at 100 times magnification puts limits on the

minimum particle size that can be seen in the images. For these tests, particles as small

as 5 µm can be counted.

Another source of error results from the unknown percentage of particles that

strike the aluminum plates but do not stick. At the beginning of the test, one of the

assumptions stated that the Teflon™ particles traveled at a high enough velocity to stick

to the targets. Unfortunately, no data could be found discussing the percentage of high

velocity Teflon™ particles sticking to aluminum plates. However, in another PPT

particle emission test similar to this study, the researchers made the same assumption,

regarding the amount of particles that bounce off the targets as negligible [14].

By sorting the particles by size and making an assumption about particle shape,

particle mass can be calculated. Figure 28 organizes the particles by diameter, and

normalizes the data to maximum number of particles found a diameter range, creating a

particle size distribution profile. This graph shows that the particles of different sizes are

present in at each location the same proportions, regardless of the angle.

Test 1 - All particles sorted by size
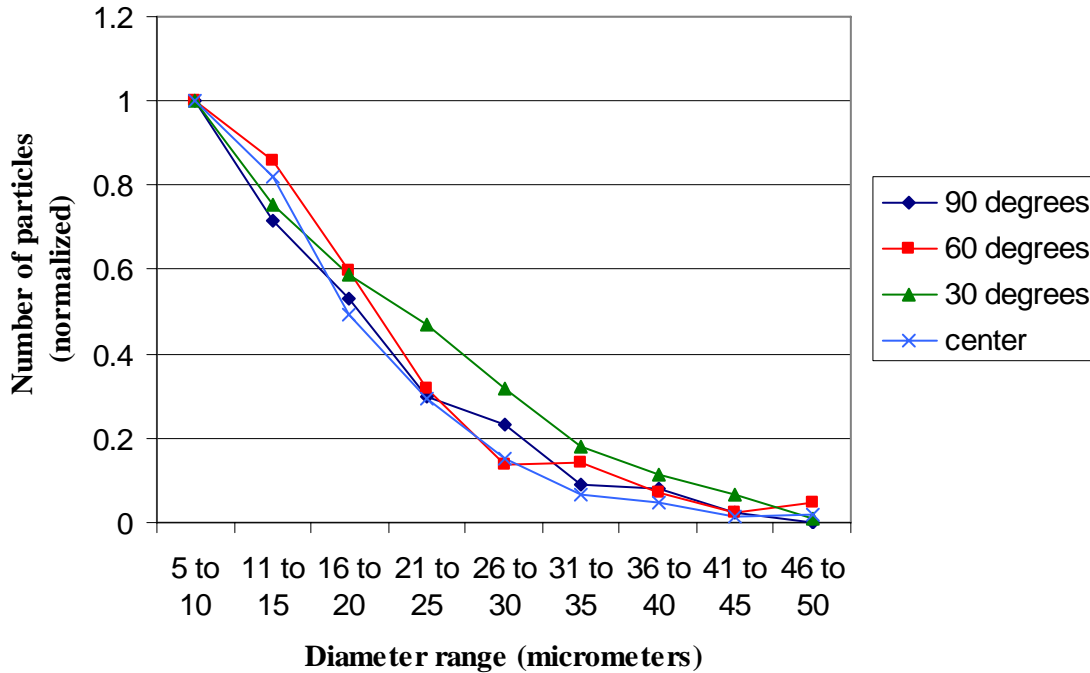
Figure 28 – Particle size distribution profile (Test 1)

If the particles are assumed to be shaped in a half-sphere, the particle volumes can be easily calculated. Although the some of the particles have irregular shapes, the great majority are half-spheres. The mass can then be found using the density of Teflon™, $2.2*10^{-3}$ nanograms per cubic micrometer. In order to remove the factors of the size of the SEM image and the radius of the test stand, the deposition is calculated in terms of steradians (Figure 29). The error bars are found using Student's t-test as before.

Test 1 - Mass deposition
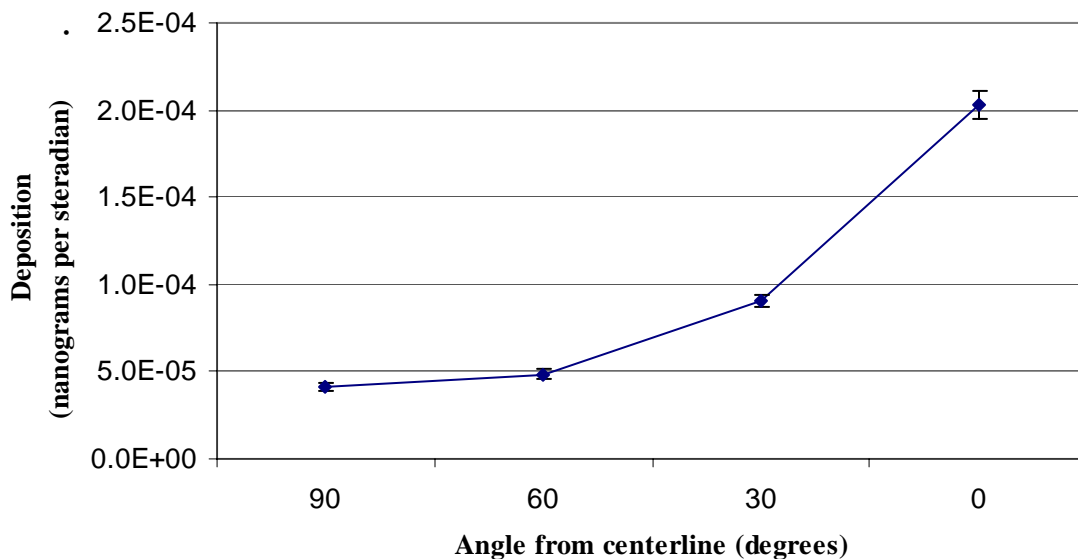
Figure 29 - Mass deposition (Test 1)

The deposition rate can be found by dividing the deposition by the runtime (the left axis of Figure 30). The deposition per spark is calculated by dividing the deposition rate by the spark rate (the right axis of Figure 30). Each of these curves has the same shape, but they are scaled differently. These values can be used to predict the amount of mass deposition for a set of arbitrary conditions if the distance from the thruster, angle from the thruster tip, surface area of the target, discharge rate, and runtime are known. For example, if another test was conducted under the same conditions as this test, except the runtime is extended to ten hours, this analysis predicts that the 396 ± 15.6 nanograms per square millimeter would deposit on the central target.

Test 1 - Mass deposition rates, scaled by runtime and spark rate

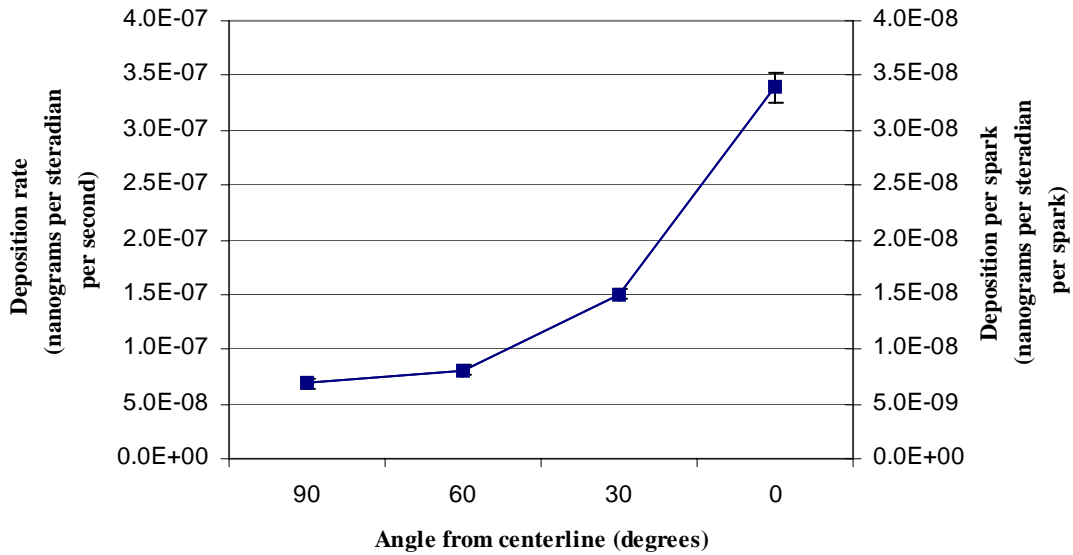**Figure 30 - Mass deposition rate (Test 2)**

The next value of interest is the amount of area that was blocked with particles during the test. This is useful to determine how solar panel performance can be degraded if the panels are in range of PPT emissions. Using the particle diameter distribution, and assuming the particles are circles, the percentage of blocked area can be calculated per steradian (Figure 31).

Test 1 - Percent of target area blocked by particles per steradian
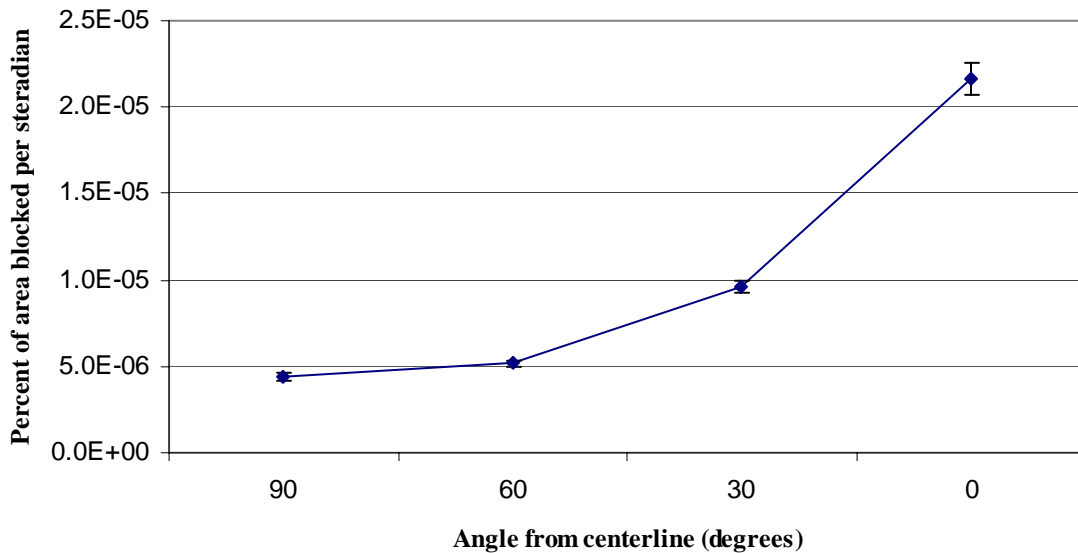
Figure 31 - Percent of area blocked by particles per steradian (Test 1)

The percent of area blocked per steradian can also be found as a rate, in terms of both runtime (the left axis of Figure 32) and spark rate (the right axis of Figure 32). Using this data in a similar manner as the mass deposition rate, the percent of area blocked by PPT particles can be calculated with this data for any set of arbitrary conditions if the distance from the thruster, angle from the thruster face, runtime, and spark rate are known. For example, if another test is conducted under these same conditions, but the runtime is extended to ten hours, this data predicts that the 27.0% ± 0.190% of the surface at the central target would be blocked with particles deposits.

Test 1 - Rate of percent of area blocked per steradian, scaled by time and spark rate
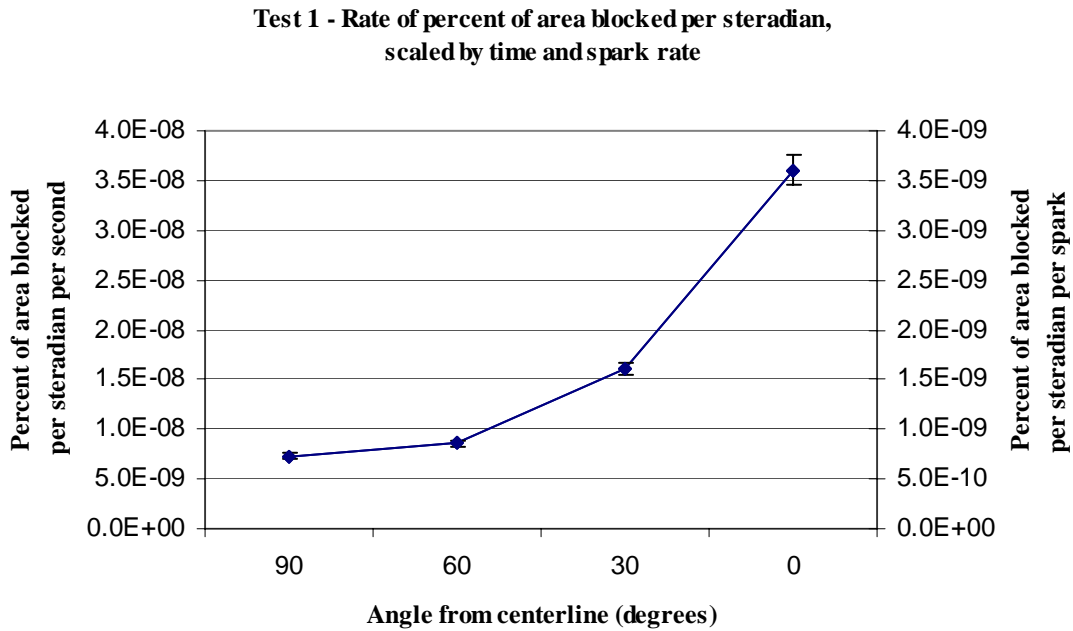
Figure 32 - Rate of percent of area blocked by particles per steradian (Test 1)

The second test lasted for 30 minutes. During this test, the thruster fired at a faster rate, approximately 30 sparks per minute. The pressure range during the test was 0.040 pascals to 0.13 pascals ($3*10^{-4}$ torr to $1*10^{-3}$ torr).

Once the test was completed, the targets were taken to the SEM for imaging. Just as in the first test, ten photo samples were taken for each target. The next four figures (Figures 33 to 36) show typical photos from target at the central location and the 30°, 60°, and 90° locations, respectively. The number of particles in each image decreases as the targets are turned away from the face of the propellant tip.
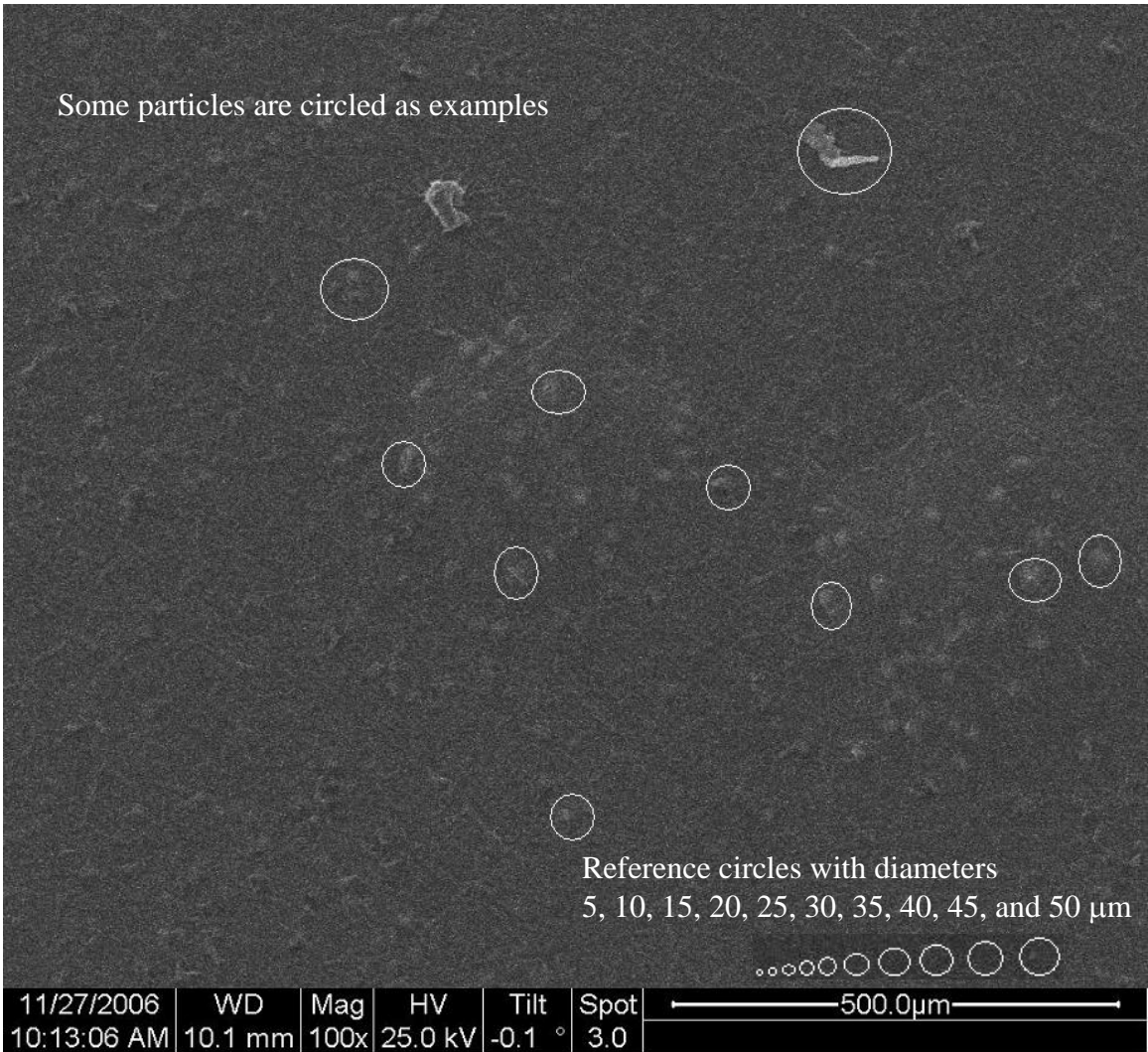
Figure 33 - SEM image of central sample – 100x magnification (Test 2)

Reference circles with diameters
5, 10, 15, 20, 25, 30, 35, 40, 45, and 50 µm

| 11/27/2006 | WD | Mag | HV | Tilt | Spot | 500.0µm |
| 10:57:02 AM | 10.1 mm | 100x | 25.0 kV | -0.1 ° | 3.0 | |
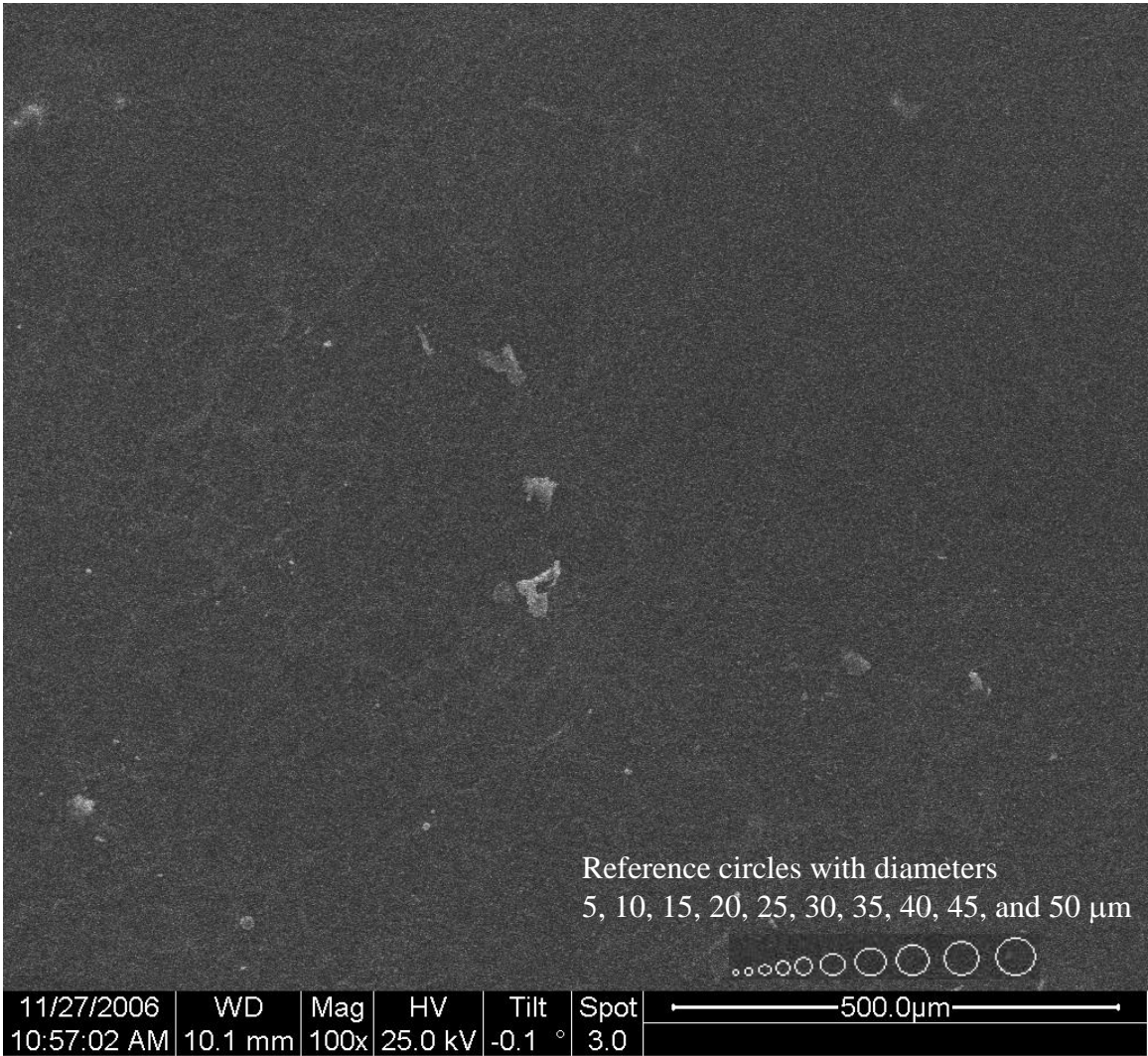
Figure 34 - SEM image of sample at 30° – 100x magnification (Test 2)

Reference circles with diameters
5, 10, 15, 20, 25, 30, 35, 40, 45, and 50 µm

11/27/2006	WD	Mag	HV	Tilt	Spot	500.0µm
9:41:24 AM	10.1 mm	100x	25.0 kV	-0.1 °	3.0	
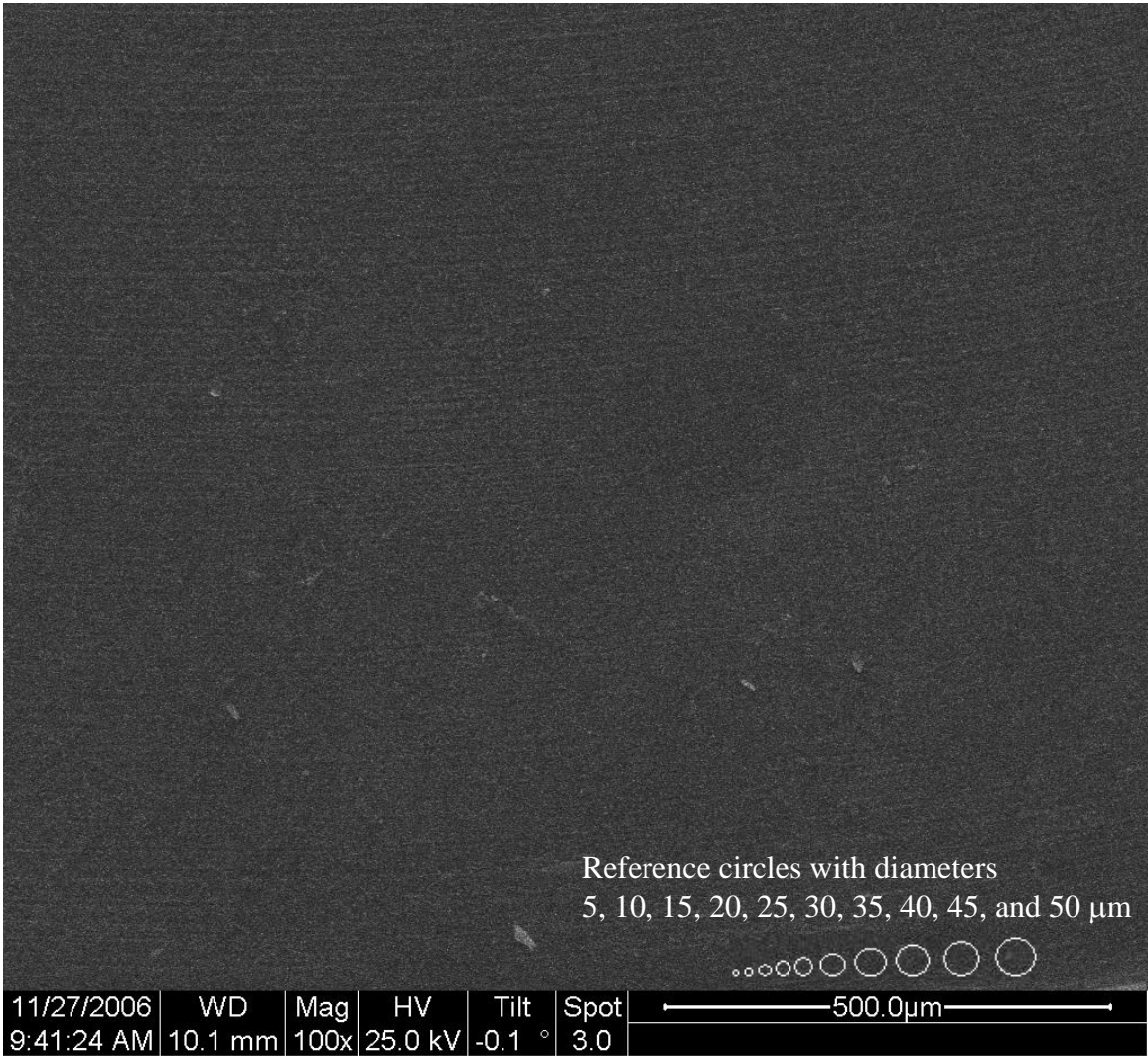
Figure 35 - SEM image of sample at 60° – 100x magnification (Test 2)

Reference circles with diameters
5, 10, 15, 20, 25, 30, 35, 40, 45, and 50 μm

11/27/2006	WD	Mag	HV	Tilt	Spot	500.0μm
10:28:02 AM	10.1 mm	100x	25.0 kV	-0.1 °	3.0	

Figure 36 - SEM image of sample at 90° – 100x magnification (Test 2)

The results for the second test yield similar trends as the first test. Because all of the data show the same behavior as the first test, the graphs are included in the Appendix instead of this section. The average number of particles on the four targets at 30° is 25.3% $\pm$ 5.77% of the amount at the center target, the average at 60° is 10.6% $\pm$ 2.14% of the maximum, and the average at 90° is 4.93% $\pm$ 1.28% of the maximum. In this test, the

57

amount of particles more than doubles for every 30° that the targets turn towards the face of the propellant tip. In a similar manner, the deposition rates and area blockage rates increase as the target angle decreases. Also, the spread of particle size is again consistent among each angular location.

The third test was completed using the same procedure as the first two tests. The thruster ran for one hour and fifteen minutes at an elevated spark rate of 75 sparks per minute. The pressure range during the test was $5.3*10^{-5}$ pascals to $2.7*10^{-4}$ pascals $(4*10^{-7}$ torr to $2*10^{-6}$ torr). The next four photos (Figures 37 to 40) are typical SEM images of the target at the central location and the 30°, 60°, and 90° locations, respectively.

Figure 37 - SEM image of central sample – 100x magnification (Test 3)

Reference circles with diameters
5, 10, 15, 20, 25, 30, 35, 40, 45, and 50 μm

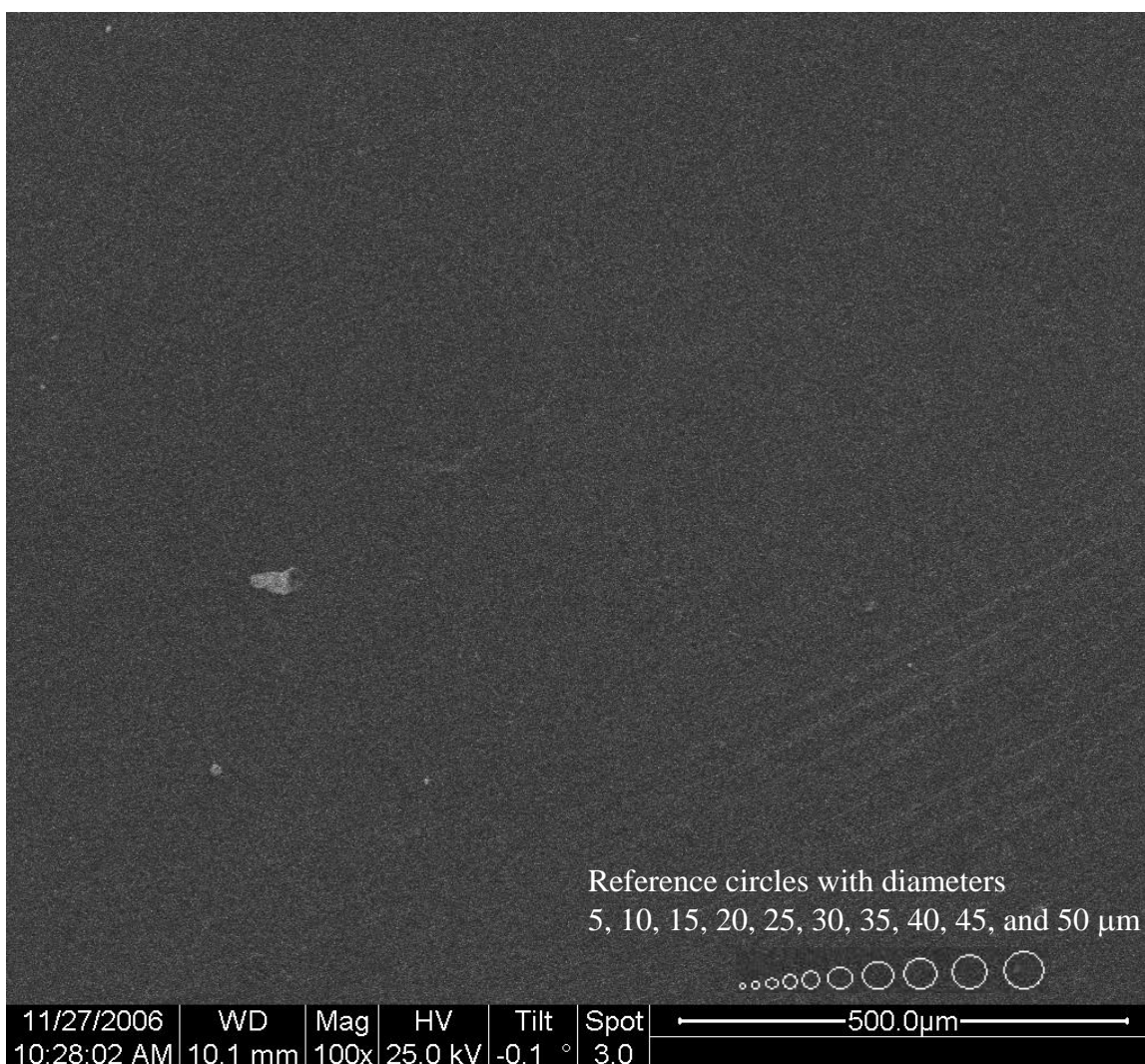| 11/27/2006 | WD | Mag | HV | Tilt | Spot | ———500.0μm——— |
| 11:34:10 AM | 10.1 mm | 100x | 25.0 kV | -0.1 ° | 3.0 | |
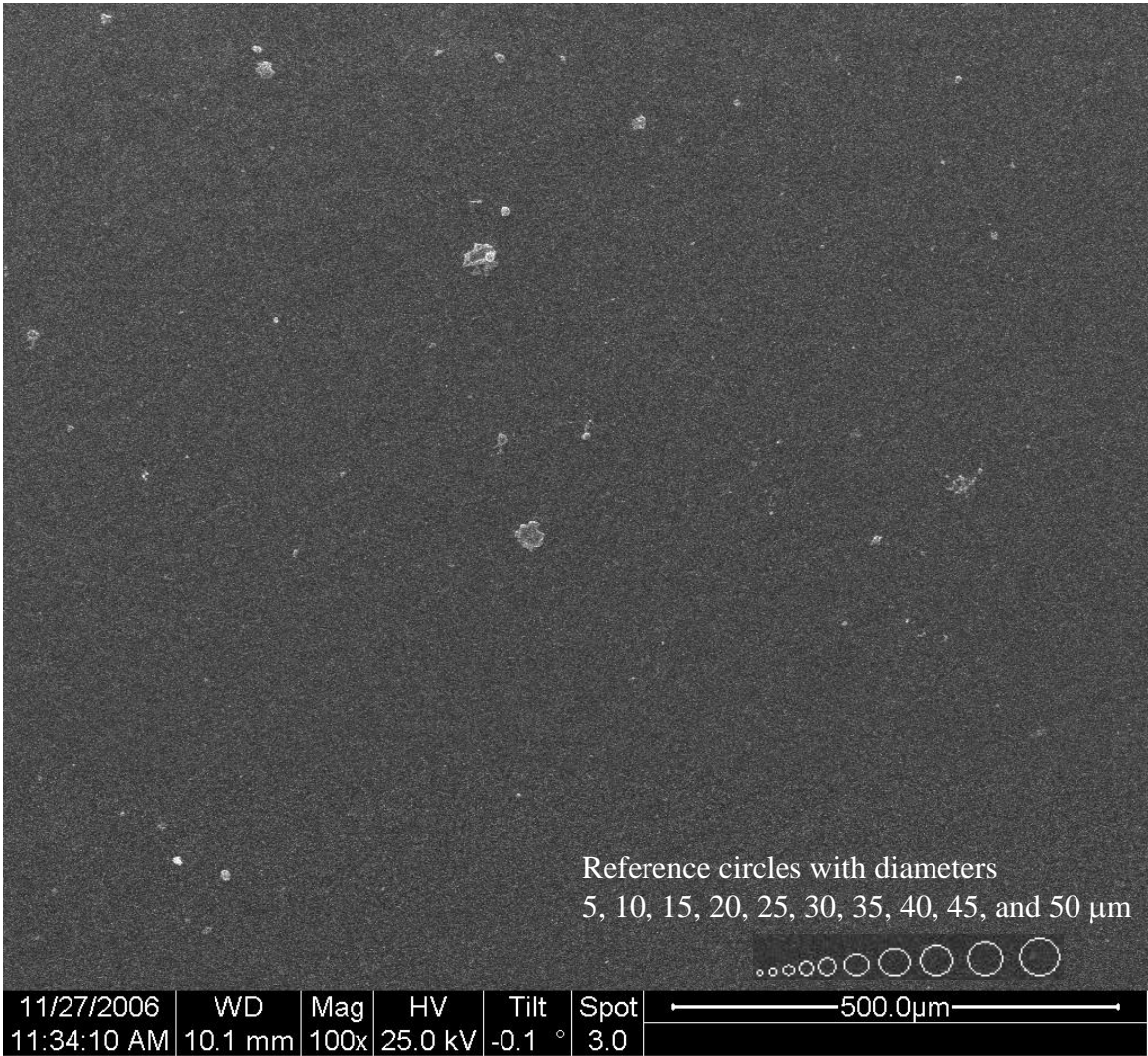
Figure 38 - SEM image of sample at 30° – 100x magnification (Test 3)

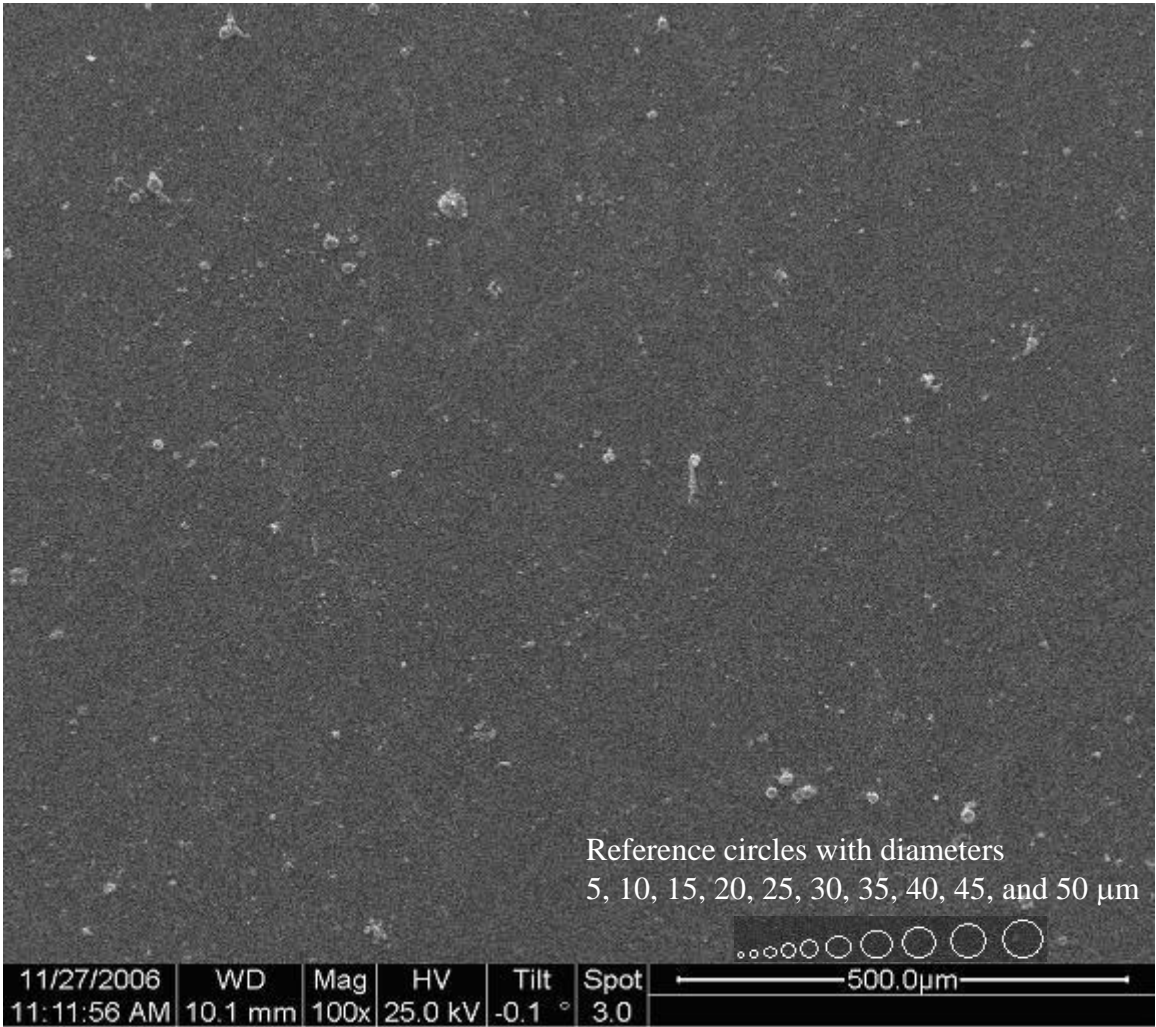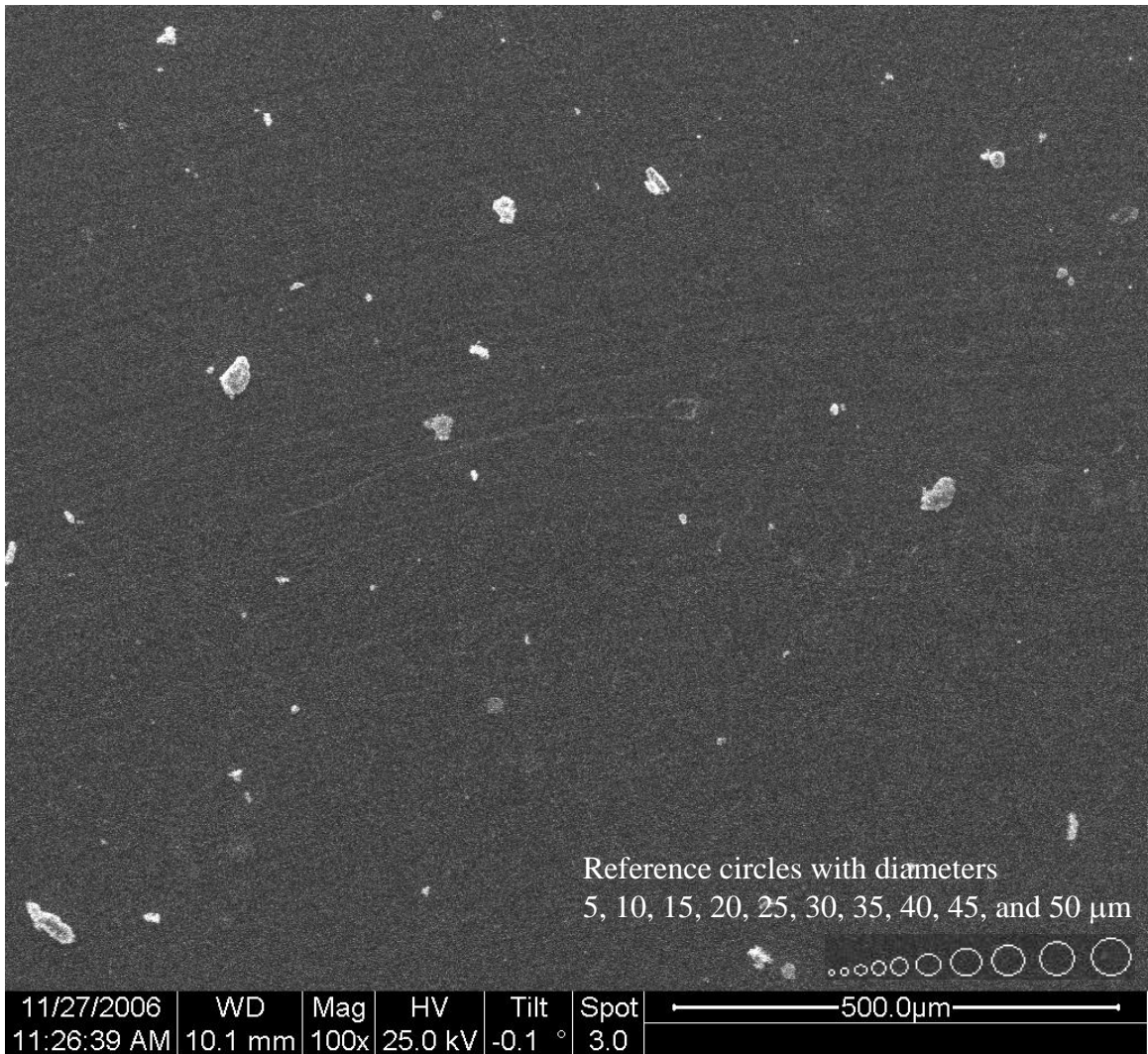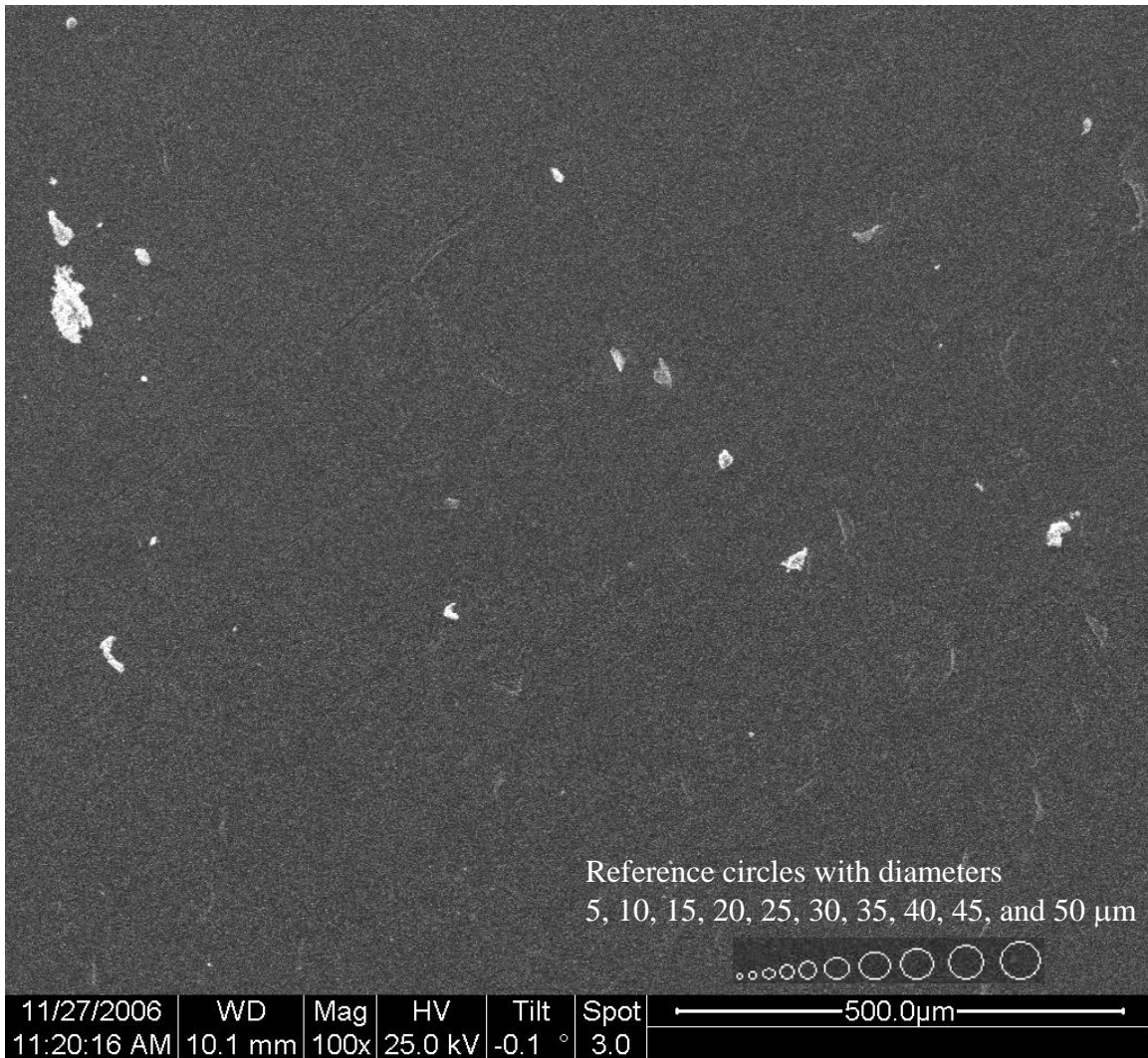**Figure 39 - SEM image of sample at 60° – 100x magnification (Test 3)**

Reference circles with diameters
5, 10, 15, 20, 25, 30, 35, 40, 45, and 50 μm

11/27/2006	WD	Mag	HV	Tilt	Spot	———500.0μm———
11:20:16 AM	10.1 mm	100x	25.0 kV	-0.1 °	3.0	

Figure 40 - SEM image of sample at 90° – 100x magnification (Test 3)

The data from the third test shows the same trends as the first two tests, so the graphs for the third test are shown in the Appendix. The central sample has by far the largest number of particles, and there are continuing drop-offs for the targets facing increased angles away from the face of the thruster tip. The four targets at 30° have an average of 11.9% ± 1.80% of the maximum amount of particles at the center target, the

62

average of the four targets at 60° is 9.55% $\pm$ 0.955% of the maximum, and the average at 90° is 3.85% $\pm$ 1.56% of the maximum.

The fourth and final test ran for the longest period of time, one hour and fifty minutes. The spark rate of 70 sparks per minute wa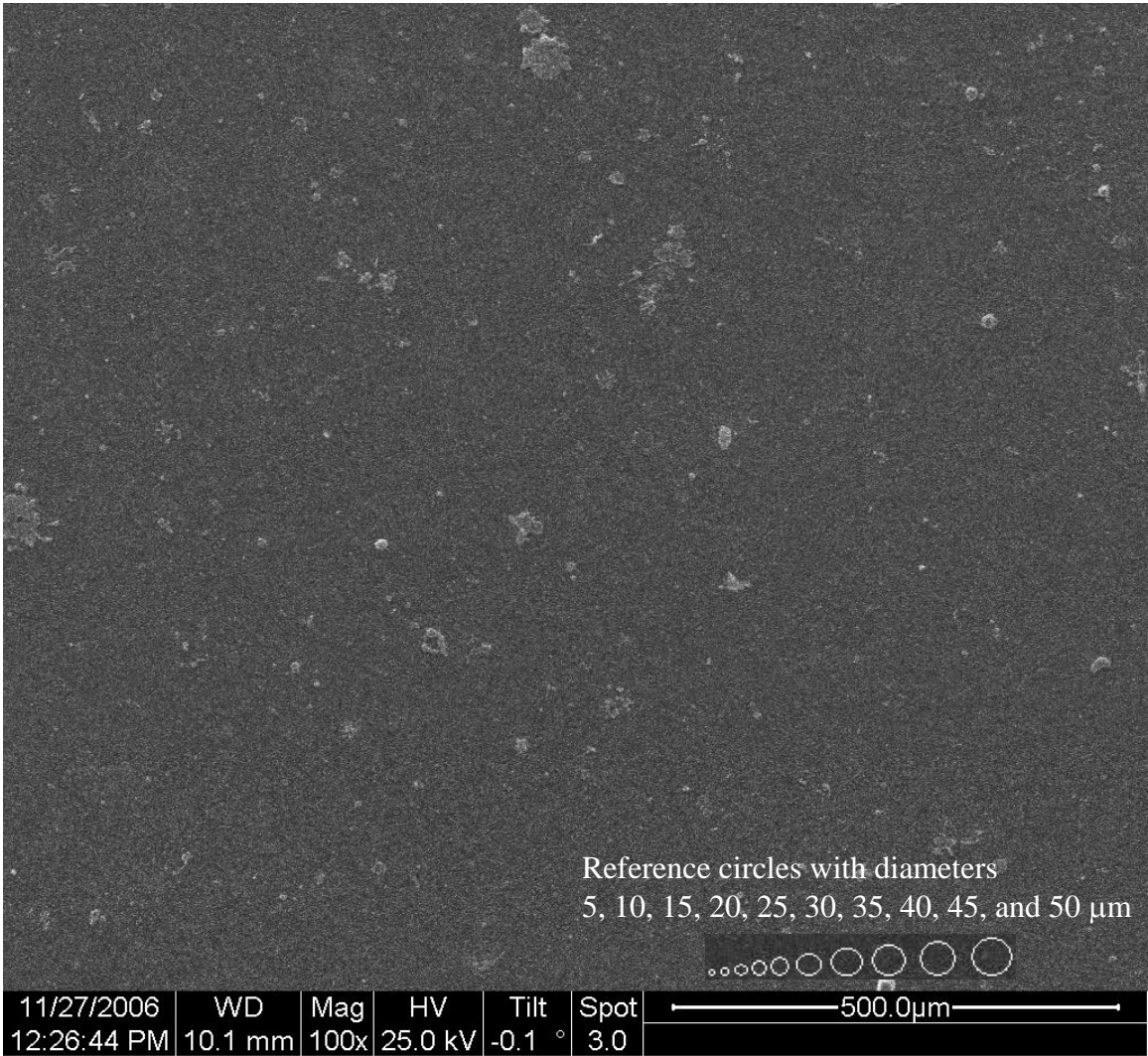s similar to the rate of 75 sparks per minute in the third test. The pressure range for this test was $8.0*10^{-5}$ pascals to $1.1*10^{-3}$ pascals ($6*10^{-7}$ torr to $8*10^{-6}$ torr). This test also produced the most particle deposits, and this can be seen visually in the following four SEM photos (Figures 41 to 44), which are typical images for each angular location.

Reference circles with diameters
5, 10, 15, 20, 25, 30, 35, 40, 45, and 50 μm

| 11/27/2006 | WD | Mag | HV | Tilt | Spot | 500.0μm |
| 11:43:17 AM | 10.1 mm | 100x | 25.0 kV | -0.1 ° | 3.0 | |
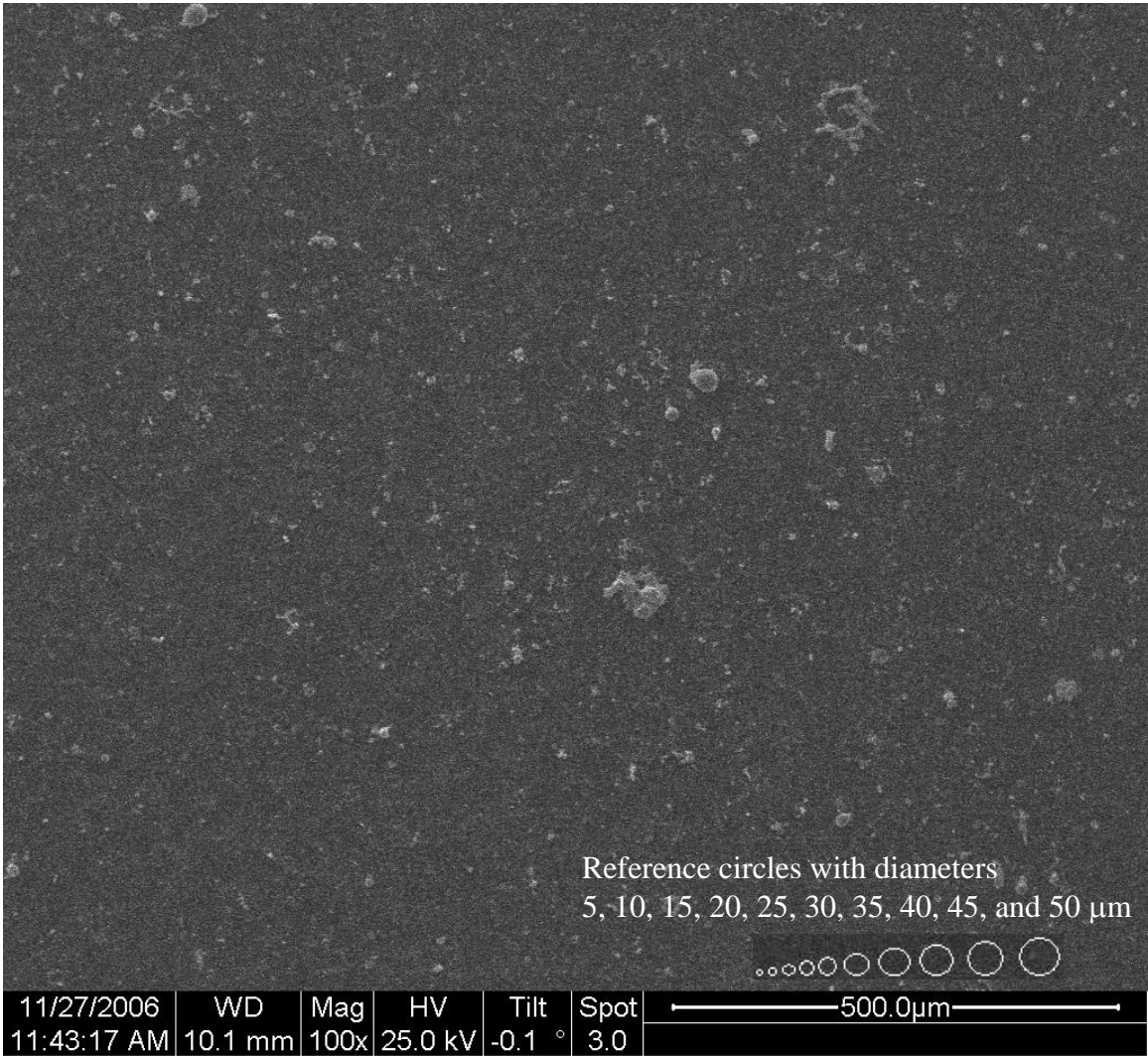
Figure 41 - SEM image of central sample – 100x magnification (Test 4)

Reference circles with diameters
5, 10, 15, 20, 25, 30, 35, 40, 45, and 50 µm

| 11/27/2006 | WD | Mag | HV | Tilt | Spot | |
| 12:26:44 PM | 10.1 mm | 100x | 25.0 kV | -0.1 ° | 3.0 | 500.0µm |

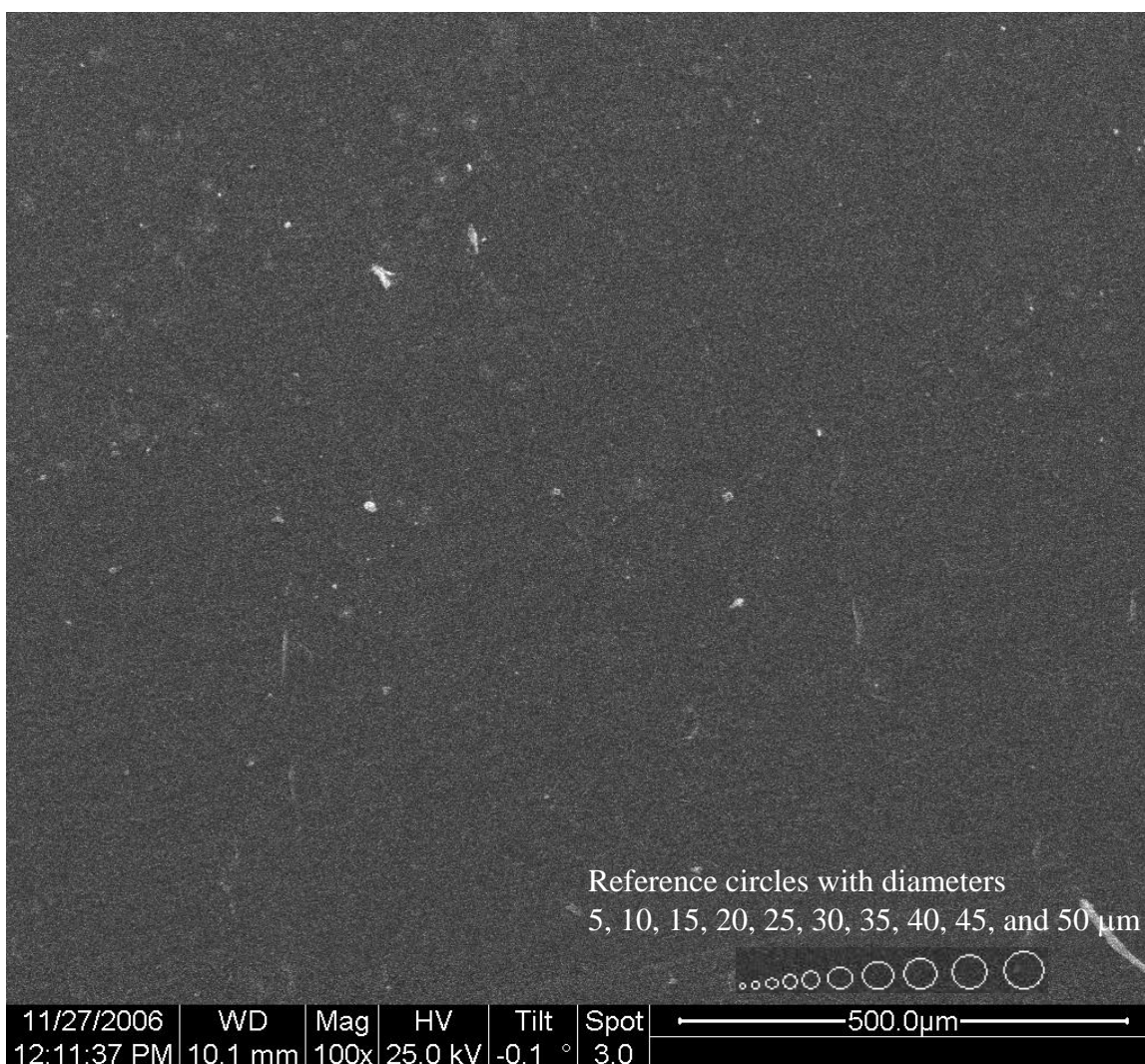**Figure 42 - SEM image of sample at 30° – 100x magnification (Test 4)**
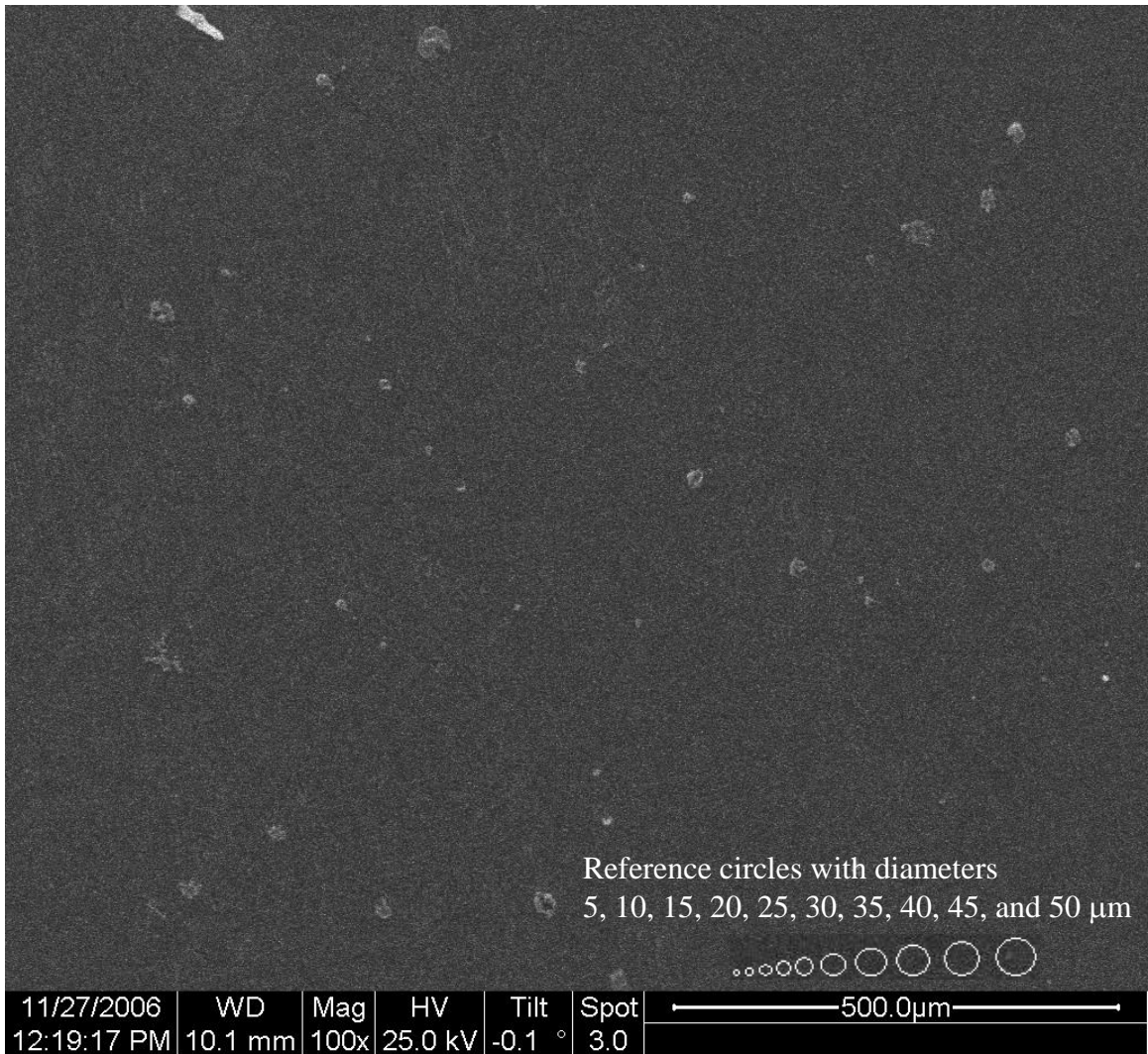
Figure 43 - SEM image of sample at 60$^{\text{o}}$ – 100x magnification (Test 4)

Figure 44 - SEM image of sample at 90$^{\text{o}}$ – 100x magnification (Test 4)

The results of the fourth test once again produced a similar trend when compared with the first three tests. In Figure 45, the amount of particles found on all thirteen targets is shown, normalized to the maximum amount from the central target. Like all previous graphs, there is a sharp spike for the central target, while the particle accumulation tapers off at a less severe rate from the 30$^{\text{o}}$ to 60$^{\text{o}}$ to 90$^{\text{o}}$ targets. The graph

shows similar values for each of the targets at each angle, as expected. Since both the vertical and horizontal directions have similar results at each angular location, the assumption of axisymmetric particle emission is justified.

Test 4 - Average number of particles on a 100x SEM image
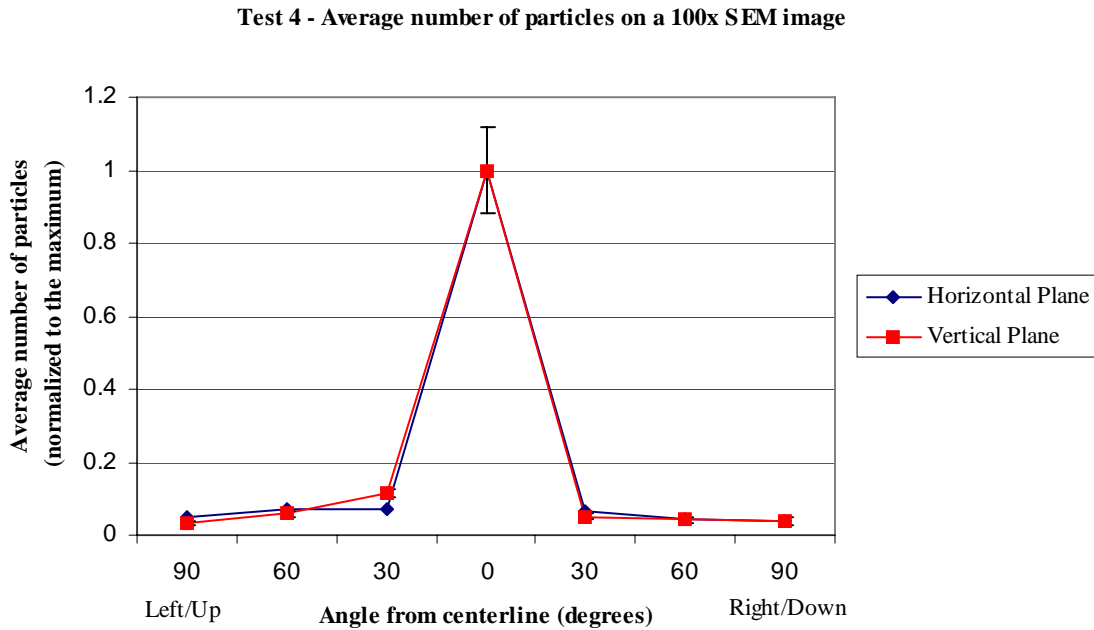
Figure 45 – Particle distribution profile for all thirteen targets (Test 4)

The rest of graphs illustrate the same trends as the first three tests, so they are presented in the Appendix. The average number of particles for the 30° targets is 7.69% ± 1.09% of the maximum at the center target, while the average for the 60° targets is 5.32% ± 0.765% of the maximum, and the average for the 90° targets is 3.84% ± 0.875% of the maximum.

Now that the basic results for each of the individual tests have been examined, it is necessary to compare these tests to look for both trends and discrepancies. First, Table 1 presents the test details for all four tests. This table can be used to try to determine what parameters caused the changes in runtime and arcing rate between each test. Each of the tests operated near the voltage rating of the capacitors. In the second test, the input voltage is slightly higher than the voltage rating. The third and fourth tests operated at lower pressure and with a different insulation than the first two tests, indicating that these conditions might have caused the changed performance levels of the last two tests. However, it is difficult to draw definitive conclusions from only four tests with varied parameters. Also, each of the tests employed a new, previously unused propellant tube.

Table 1 - Comparison of test parameters

	Runtime (minutes)	Arc rate (sparks per minute)	Input voltage (V)	Capacitor's voltage rating (V)	Pressure range (pascals)	Insulation
Test 1	10	10	2800	3000	$5.3*10^{-3}$ to $2.7*10^{-2}$	Liquid electrical tape
Test 2	30	30	3300	3000	$4.0*10^{-2}$ to $1.3*10^{-1}$	Liquid electrical tape
Test 3	75	75	5100	6000	$5.3*10^{-5}$ to $2.7*10^{-4}$	Corona dope
Test 4	110	70	5100	6000	$8.0*10^{-5}$ to $1.1*10^{-3}$	Corona dope

Using the voltage levels for each test, the specific impulse can be estimated for the micro-PPTs used in this study. First, Equation (3) can be used to calculate the exit velocity of the ionized particles [6]:

$$u_e = \sqrt{2 \cdot \frac{q}{m} \cdot V} \qquad (3)$$

where

u_e is the exit velocity (m/s)

$\frac{q}{m}$ is the charge per mass ratio (coulombs per kilogram)

and V is the voltage (volts).

Teflon™ has a charge per mass ratio of $9.62*10^5$ coulombs per kilogram, and the voltage inputs are listed in Table 1. The calculated exit velocities for each test are listed in Table 2. Only a small percentage of the particles are ionized so the average plasma velocity is significantly lower when the neutral vapor is considered. The average plasma velocity can be calculated using conservation of momentum, shown in Equation (4):

$$m_{ion} \cdot u_e = m_{ion} \cdot \overline{u} + m_{neutral} \cdot \overline{u} + m_{solid} \cdot \overline{u} \qquad (4)$$

where

m_{ion} is the percentage of mass as ionized vapor

$m_{neutral}$ is the percentage of mass as neutral vapor

70

m_{solid} is the percentage of mass as solid particles

u_e is the exit velocity of the ionized particles (m/s)

and $\bar{u}$ is the average velocity of the plasma (m/s).

The velocity of the solid particles is assumed to be negligible compared to the ionized and neutral vapors. Also, the ionized particles are assumed to comprise 10% of the plasma. The plasma velocities calculated for each test are listed in Table 2. The specific impulse can then be calculated from Equation (5):

$$I_{sp} = \frac{u_e}{g} \tag{5}$$

where I_{sp} is specific impulse in seconds and g is the gravitational acceleration (m/s^2). The specific impulses calculated for each test are listed in Table 2. All of these values are within range of published values for a micro-PPT's specific impulse.

Table 2 - Calculated vapor velocities and specific impulses

|	Ionized vapor velocity (m/s)	Plasma velocity (m/s)	Specific impulse (seconds)
Test 1	73,400	7,340	748
Test 2	79,700	7,970	812
Test 3	99,000	9,900	1,010
Test 4	99,000	9,900	1,010

Figure 46 compares the average particle size distribution profile for each test. Each data set is normalized separately to the maximum value obtained from each respective test. Just as the size distribution profile does not vary with angular location, the profile does not change with increased runtime.

Comparison of average particle size distribution profiles
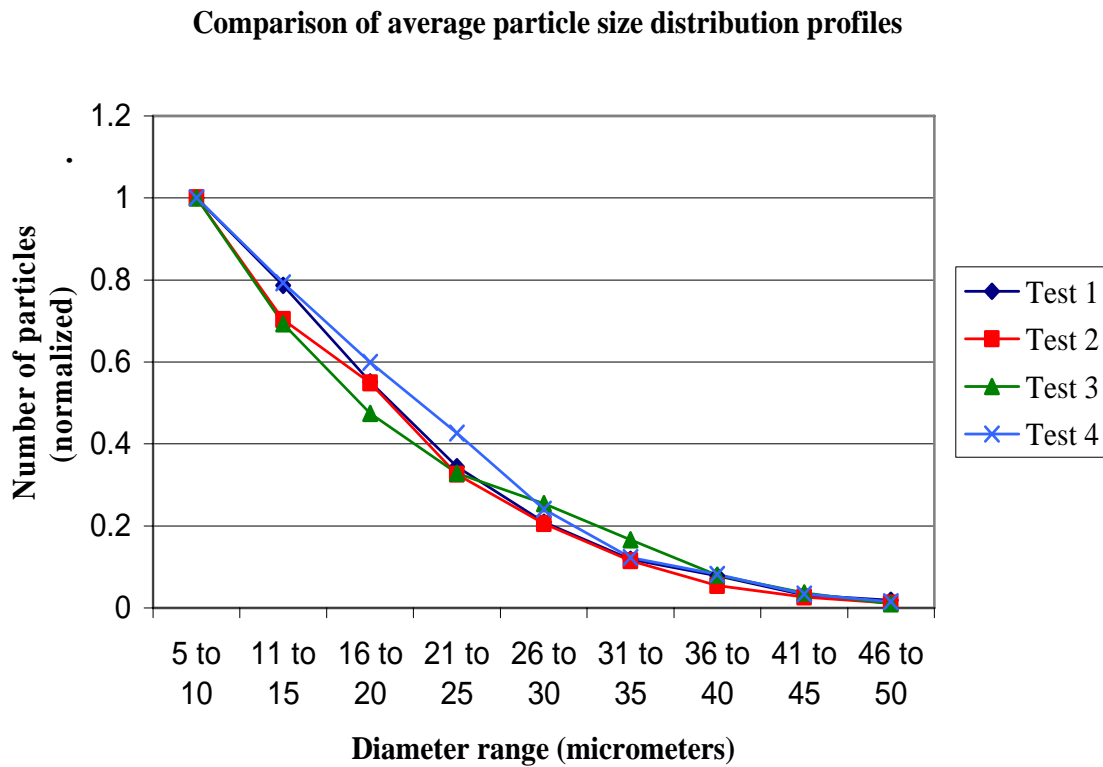
Figure 46 - Comparison of particle size distribution profiles

By combining some of the previous graphs, the increase in particle deposition for each successive test can be readily seen (Figure 47). In this graph, the values were

normalized to the maximum amount of particles, obtained at the center target in the

fourth test. The error bars were removed from this graph and the subsequent graphs for

readability. The amount of error stays at the same percentages previously calculated

because the next graphs simply combine the prior figures and plot them in terms of

runtime.

Comparison of particle accumulation
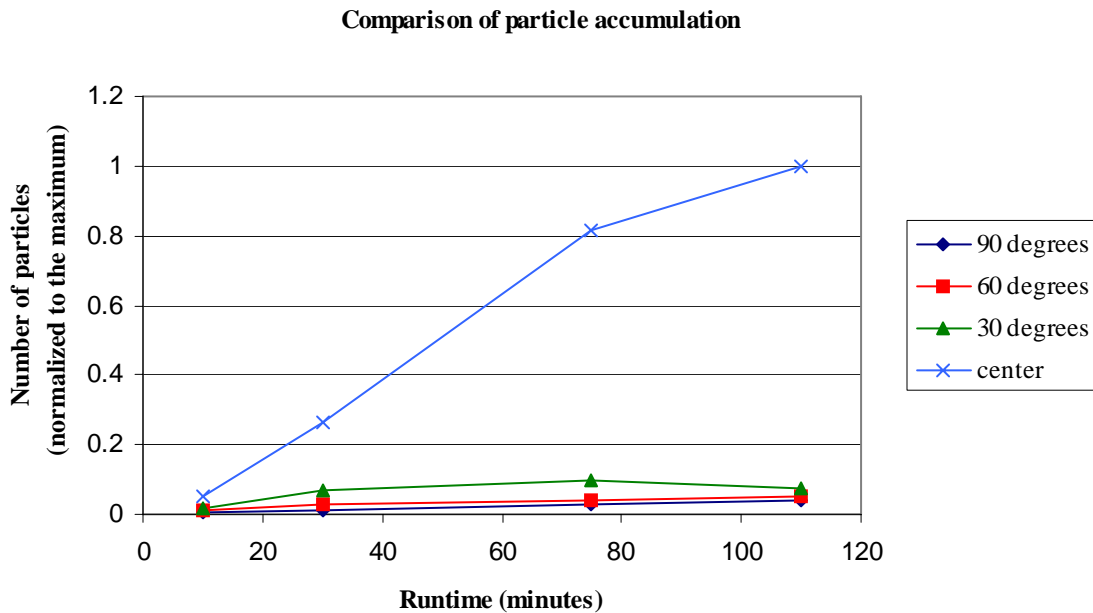
Figure 47 – Comparison of particle deposition from each test

This graph shows how the particle deposition greatly increases between tests, as

the runtime and spark rate increases. The difference between the third and fourth tests is

less pronounced, because only the runtime increased, while the spark rate decreased. The

large increase in particles on the central target is much more distinct than the increase in

the surrounding targets. However, the central target data also skews the data for the adjacent targets. Figure 48 shows the same data as Figure 47, except the data for the central target is excluded.

**Comparison of particle accumulation (excludes central target)**
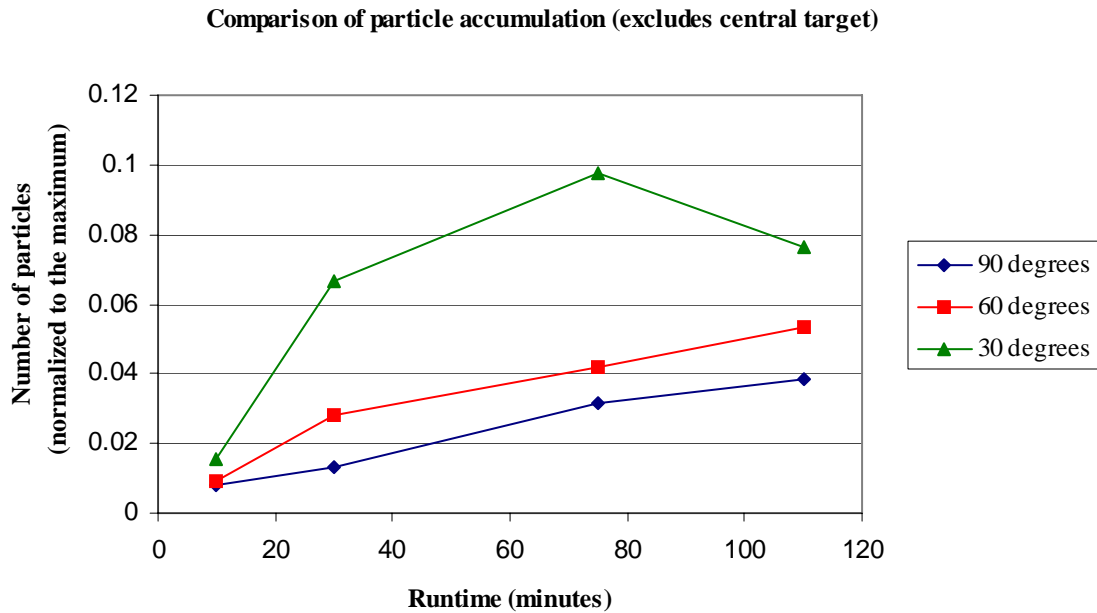
Figure 48 - Comparison of average particle deposition at each angular location (excluding the central target)

Figure 48 shows that the amount of particles in every test increases for the 60° and 90° targets, but in one instance for the 30° targets, the amount of particles decreases between the third and fourth tests. This disparity could be the result of the lower spark rate in the fourth test.

The simple explanation for the increase in deposition for each test is the increased runtime. In addition, the different arcing rates for each test could cause increases in particle deposition. As stated previously, the first test had an arcing rate of only 10 sparks per minute, the second test had a rate of 30 sparks per minute, the rate of the third test was 75 sparks per minute, and the fourth test arced at a rate of 70 sparks per minute. Further analysis needs to be performed in order to understand the effect of the varied spark rates on the particle depositions.

All of these results agree with expectations. With increased runtimes and increased arcing rates, more particles should emit from the thruster. These are the next factors that need to be considered. Even though each test has different values for average number of particles on each target, the tests should have similar values for mass deposition rate, once the test runtime and arcing rate are taken into account. This value should be consistent when comparing each target for each test. Figure 49, however, illustrates how this deposition rate is not a constant, but rather changes for each test.

Comparison of mass deposition rates
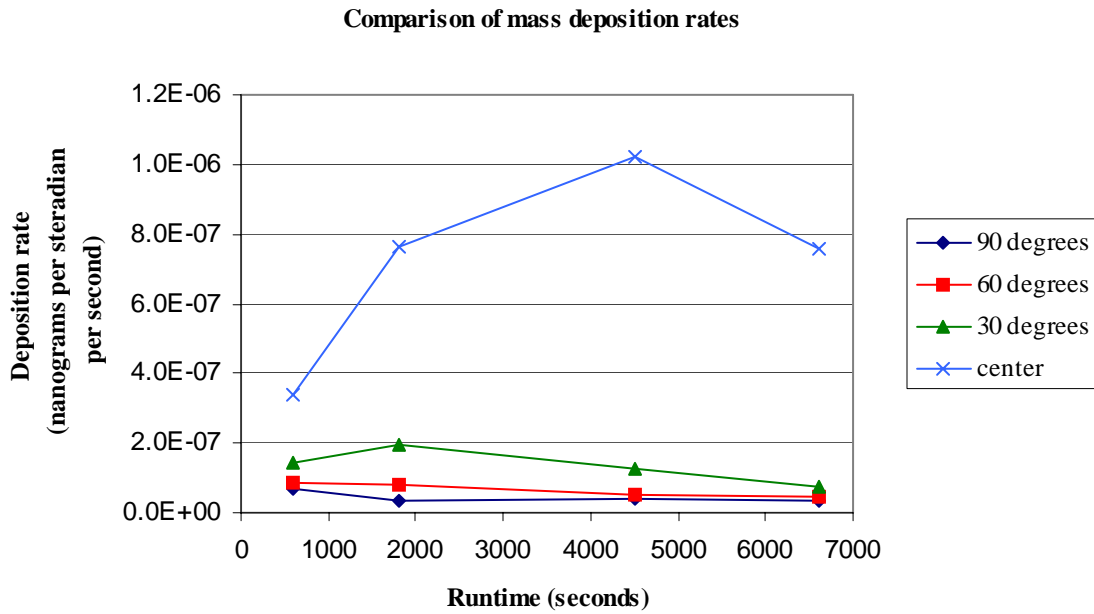
Figure 49 – Comparison of particle deposition rate

The variations in mass deposition rates between tests can be attributed to the different spark rates among the tests. Figure 50 examines the mass deposition per spark for each test.
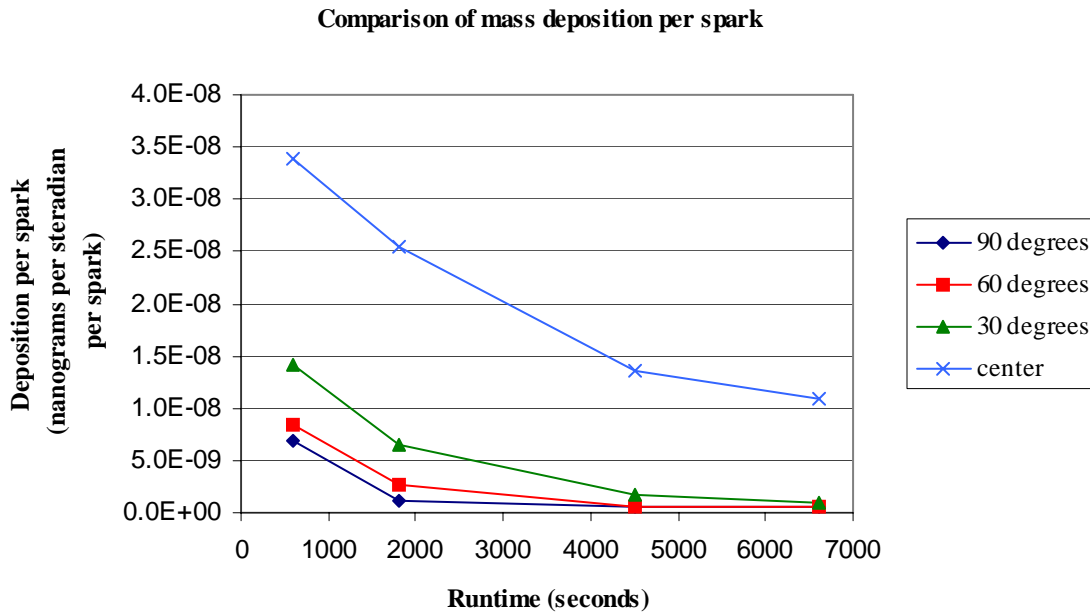
Figure 50 - Comparison of mass deposition per spark for each test

If all other aspects of the thrusters are equal besides the runtime and arcing rate, then a similar amount of particles should be emitted in a similar pattern with each spark. Figure 50 indicates that even though the latter tests had a larger total number of particles, the first test has a significantly higher deposition rate than the other three tests, and the second test has a significantly higher deposition rate than the third and fourth tests, which have similar deposition rates. The average drop in deposition rates between the first test and the second test is 61%, while the average drop in rates between the second test and third test is 66%. The average decrease in deposition rates between the third and fourth test is a lower value of 18%. These curves are important because they suggest that the

total operating time, with respect to lifetime of the thruster, may be a significant factor in particle deposition.

One explanation for this behavior is that the PPTs emit more particles during the first few minutes of firing. A larger amount of particles may ablate from the tip of the propellant tube until the tip's surface smoothes out after multiple arcing events. If the initial arcs do ablate more material than an arc that occurs later in the test, then the effect would be more pronounced on shorter tests and less noticeable as runtimes increase. This is exactly the behavior observed during the four tests of this study. The first test only ran for ten minutes, with an arc rate of only ten sparks per minute, yet the deposition rate is by far the highest during this test. The second test runs for 30 minutes, with an arc rate of 30 sparks per minute, and it has a significantly lower deposition rate than the first test. The third and fourth tests run for over an hour and almost two hours, with arc rates of 75 and 70 sparks per minute, respectively, but these tests recorded the lowest deposition rates. These results suggest a tapering effect in particle deposition rate, where the deposition rate is highest during the first few minutes, and then decreases as the test runs for a longer time. If the first two tests ran for longer times, then the effect of the higher amount of initial ablation may have been less noticeable, and the deposition rates would have more closely matched the values for the third and fourth tests.

A study at AFRL supports this theory by describing a micro-PPT experiment in which the thruster was discharged over 100,000 times before beginning their experiment. This allowed for any surface shaping and smoothing to occur before the experiments began, and the tests could be run at the steady state deposition levels. The study

describes how the propellant tip surface erodes from a flat face to a slightly concave shape [14].

This same behavior occurred during the four tests of this study. As an example, Figures 51 and 52 show the tip of an unused propellant tube and the tip of the propellant tube after the fourth test, respectively. The tip of the new tube is clearly flat, while the tip of the tube after testing has a distinct concave shape. This behavior suggests that the PPT should be operated on the ground until the steady state concave shape is obtained in order to pass through the portion of the life cycle with increased deposition. By pre-firing the thruster in such a manner, the operational usage of the PPT would contaminate the sensors or solar panels to a lesser degree.
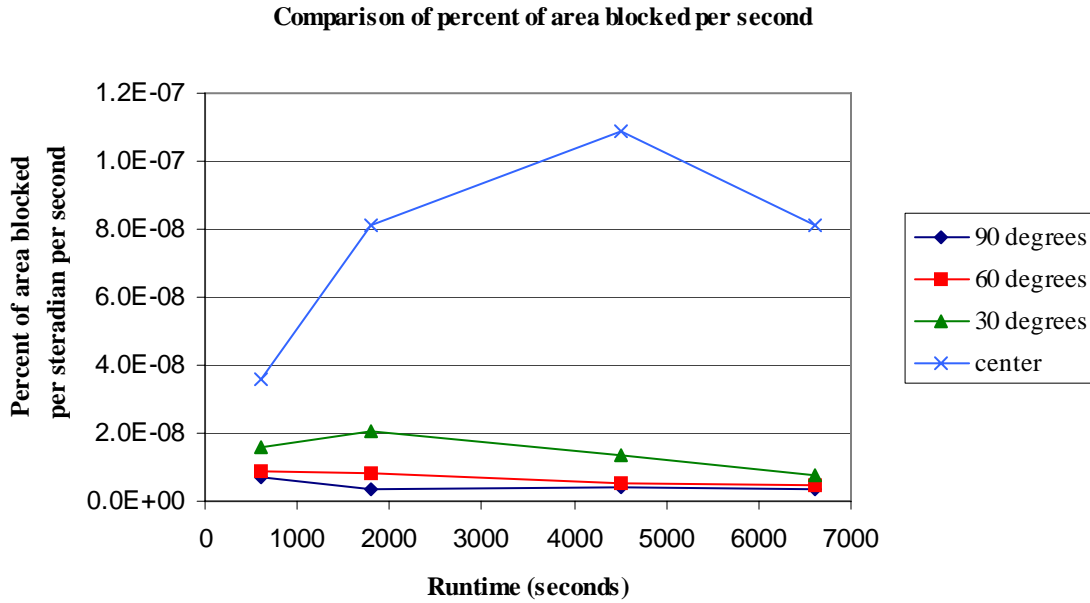
Figure 51 - Flat tip of an unused propellant tube
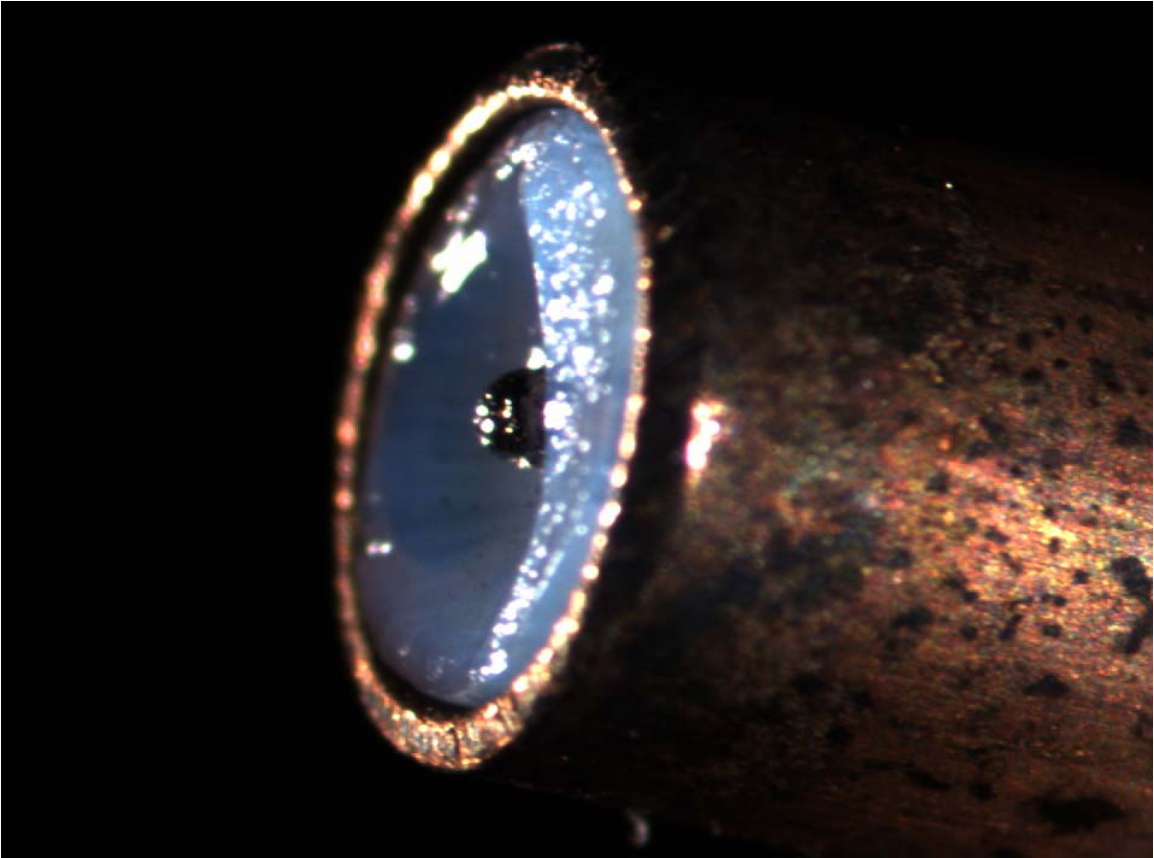
Figure 52 – Concave ablated tip of the propellant tube after the fourth test

Similar to the comparisons between mass deposition rates for each test, the area blockage rates can be examined as a function of runtime (Figure 53) and spark rate (Figure 54).

Comparison of percent of area blocked per second

**Figure 53 - Comparison of percent of area blocked by particles per second**

Comparison of percent of area blocked per spark
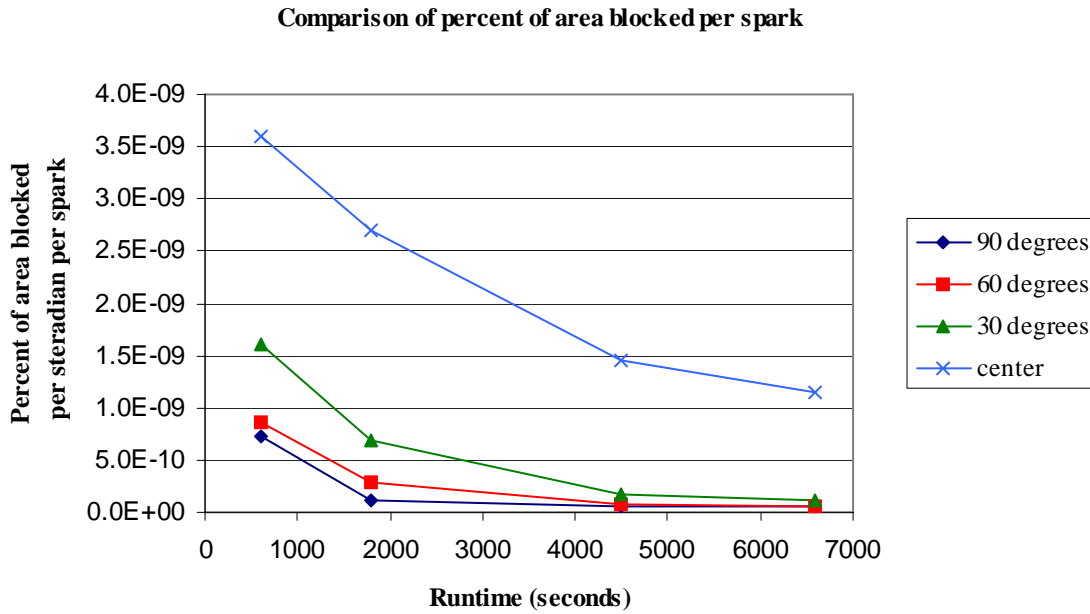
Figure 54 - Comparison of percent of area blocked by particles per spark

These graphs show the same trends as the graphs comparing the mass deposition rates. They are still important, however, because they present nondimensionalized values relating to area blockage, which is one of the main concerns motivating this study. The values obtained here can be applied directly to any similarly rated micro-PPT. If the distance from the thruster, angle to the face of the propellant tip, the spark rate, and runtime are known, then a simple calculation using the rates from the above graphs will output a predicted percent of the area that the particles will block. Likewise, the mass deposition rates can be used for any arbitrary distance, angle, runtime, and spark rate.

83

Comparisons to Previous Research

The results from this study can be compared to a previous study by AFRL where witness plates were used to estimate propellant losses due to particulate emission for a standard PPT [14]. Although the AFRL uses a standard PPT rather than a micro-PPT, the basic behavior of the particle emissions shows a similar pattern to the deposition profiles calculated in this study. Figure 55 illustrates the particle size distribution on the central witness plate after 1,000 discharges. The pattern is very similar to size distribution in this study. The AFRL study did not count particles smaller than 25 micrometers because they were too numerous on the witness plates. The standard PPT produces significantly larger particles than the micro-PPT. In the AFRL study, particles as large as 200 micrometers were counted, as opposed to a maximum of 50 micrometers from the micro-PPT in this study.
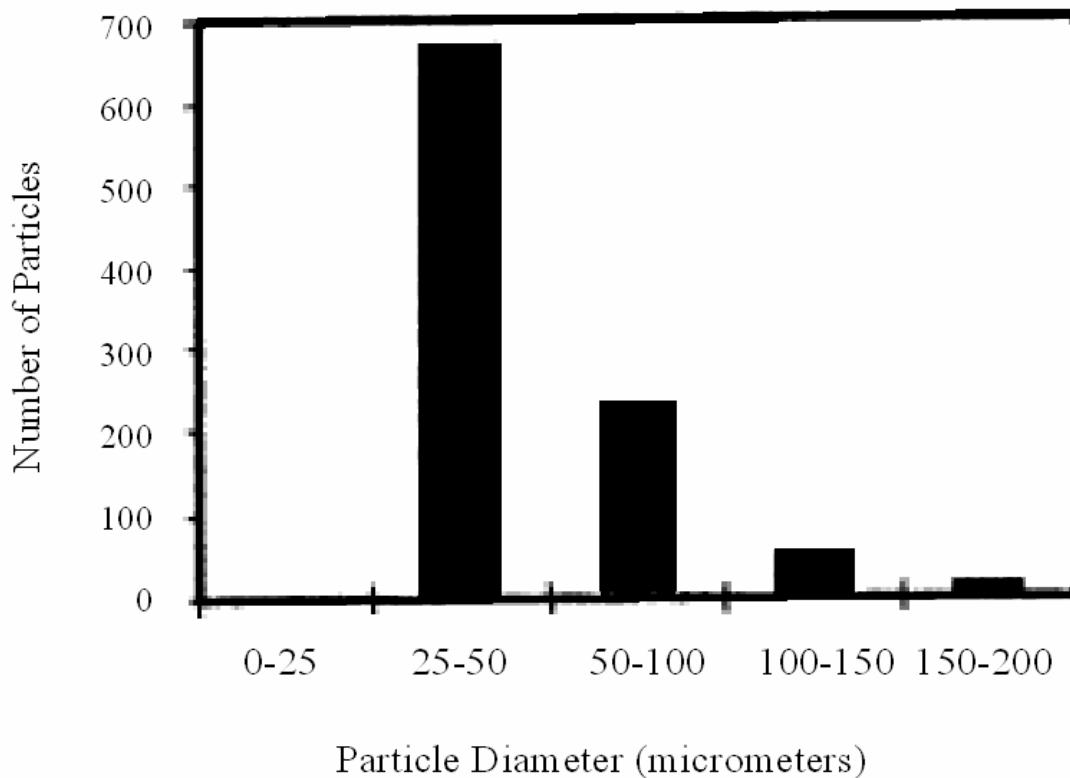
Figure 55 - Histogram of particle distribution on the central plate [14].

The estimated mass density distribution is shown in Figure 56. The data spread has a similar shape to the mass deposition profiles calculated for each of the four tests in this study. The main difference between the AFRL study and the findings of this study is the significant gap in particle mass density between the two targets at 30°. This indicates that a symmetric assumption could not be applied in the AFRL study. Figures 55 and 56 combine to show that the data spreads obtained for the micro-PPT are consistent with previous research on standard PPTs.
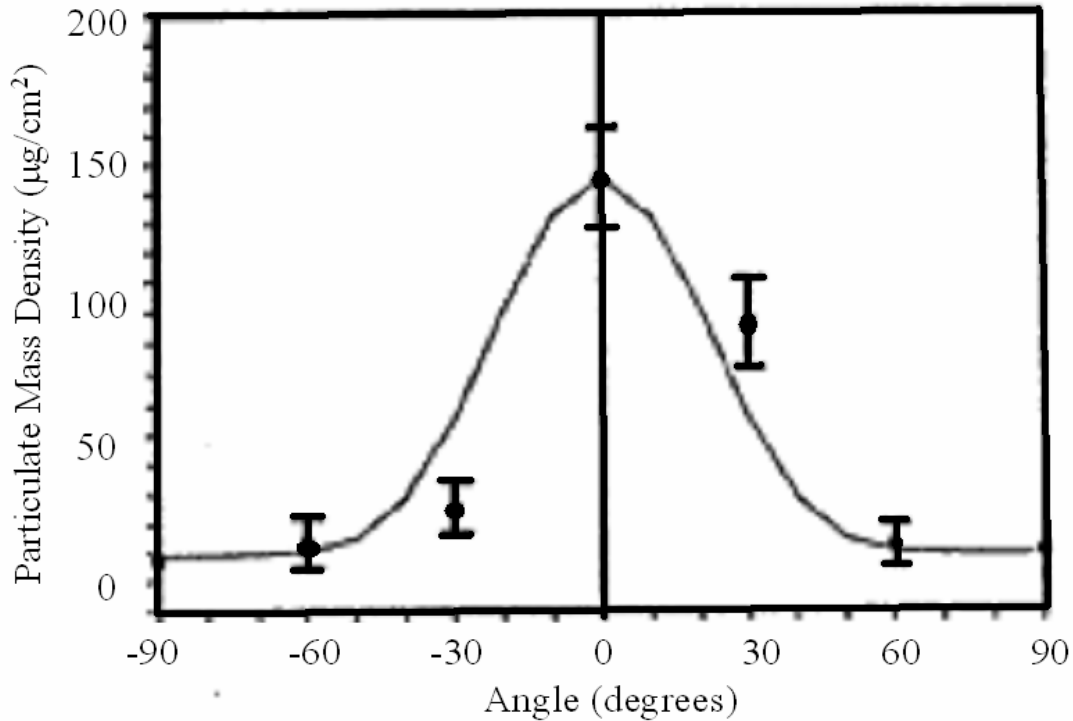
Figure 56 – Spatial distribution of the particulate mass on the witness plates, shown with a cos$^2\theta$ fit [14].

Part of the numerical studies done at the University of Michigan included modeling ablation rates [13]. Figure 57 shows the distance the propellant recedes after a single pulse. This numerical data can be used to predict the ablation profile of the propellant tube for a given runtime and discharge rate. The profile in Figure 57 agrees with the tip shaping behavior seen in this study, where the propellant tip changed from a flat surface to concave.
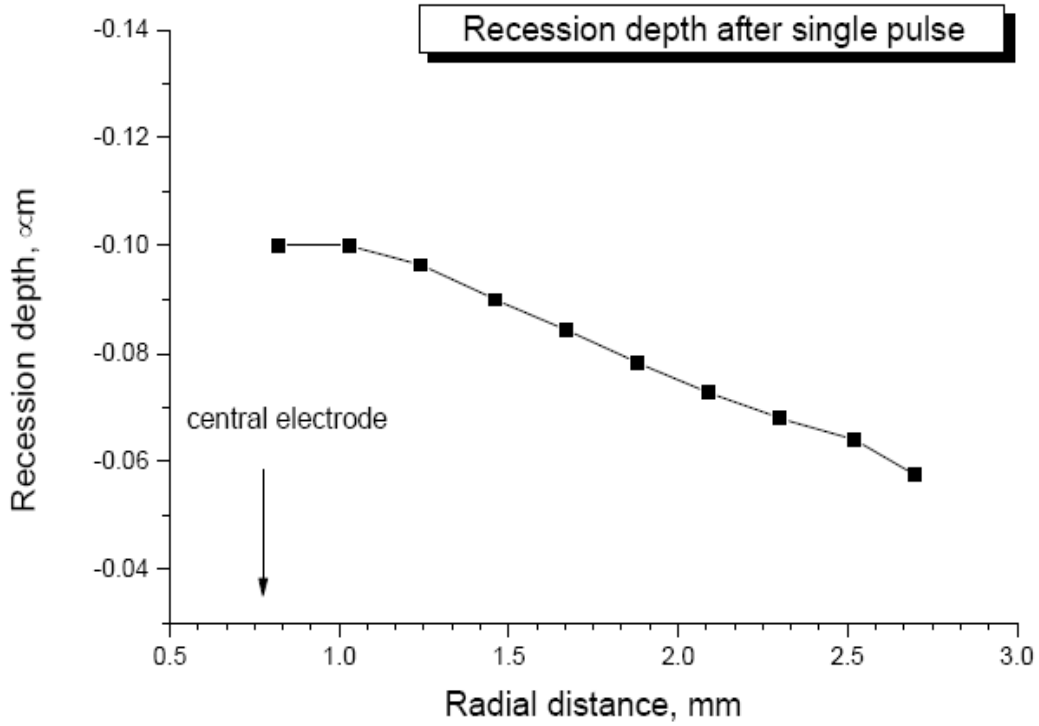
Figure 57 – Model prediction of ablation depth after a single pulse [13].

Investigative Questions Answered

The four tests of this study give a clear and consistent deposition profile for a micro-PPT. Any material directly facing the tip of the propellant will receive a significantly larger amount of emission particles compared with locations facing the tip of the propellant at skewed angles. In addition, mass deposition rates and area blockage

rates were calculated, giving multiple tools to satellite designers who may be concerned about the effects of micro-PPT emissions on surrounding instruments or solar panels.

Summary

The main objective of this study was to gain a more complete understanding of the deposition profile of a micro-PPT, and how the deposition behavior changes with axis angle. This profile was obtained from four separate tests, and they combined to form a picture of the deposition behavior for the lifetime of the thruster. The differing runtimes and discharge rages were used to calculate the deposition could be calculated per spark so that the date from each test could be compared with a common basis. When the micro-PPT initially fires, more propellant is ablated as the tip changes from a flat to concave surface. Once the propellant reaches a steady state shape, the deposition rate decreases to a steady state level.

V. Conclusions and Recommendations

Chapter Overview

In this chapter, final conclusions, recommendations for future study, and lessons learned throughout the experimental process will be presented. Although the tests gave reasonable data, it would have been useful if the micro-PPTs worked more consistently. A larger number of tests, where the runtime and discharge rate could be controlled, would help corroborate the conclusions made in this study.

Conclusions of Research

This study has shown that particulate emission from a micro-PPT can reach every direction, even surfaces that are turned 90° away from the face of the propellant tip. By far the largest amount of particulate deposition occurred on the surfaces that directly faced the tip of the propellant. Sensitive instruments or solar panels should not be within range of these particles, or their performance can potentially deteriorate over time. The area directly facing the tip of the propellant should particularly be avoided, due to the significantly higher deposition rate. If possible, propellant tips from a micro-PPT should extend beyond any satellite surface to prevent accumulation of particles from the thruster. If the location of such components on a satellite cannot be altered, then this data will help calculate the deposition buildup and give designers an opportunity to plan for the particulate accumulation. Finally, the micro-PPT should be operated before installation until the steady state concave shape is formed at the propellant tip in order to avoid the increased initial deposition.

Significance of Research

The research performed in this study helps in understanding the behavior of particle emissions from a micro-PPT. As with other studies performed using micro-PPTs, deposition behavior is an important aspect to understand before these thrusters are used extensively in flight programs. Using the data from this project, satellite designers can have more knowledge of potential problems that can occur due to particulate deposition on essential satellite components.

Lessons Learned

In addition to further tests, the runtime and arcing rate should be able to be controlled. During this study, the PPTs operated flawlessly for a given period of time, but they would stop working due to a component failure, rather than a user defined condition. The tests ended when the capacitor failed, the high-voltage converter overheated, or the electrodes burnt out. None of the studies lasted long enough to come close to using the entire tube of propellant. Also, the arcing rate was not adjusted due to reluctance to change any parameters on a PPT that was working correctly. If the PPTs operated correctly on every attempt, then the thruster could be turned off at any desired time, and power levels could be adjusted in an attempt to alter the arcing rate.

As stated previously, additional targets should have been placed at the 15° locations. The large difference in particles deposition from the central target to the 30°

targets should have been bridged by an intermediate set of targets. These additional

targets at 15° would have given the data distribution a more accurate figure.

Recommendations for Future Research

The main drawback of this study was the inconsistent performance of the micro-

PPTs. Only four tests were completed because the thruster only operated for an extended

period of time on those four occasions. Countless other attempts were made to perform

more tests, but these were all unsuccessful. Many other research projects have been

completed with micro-PPTs that were able to run more tests and operate for much longer

periods. Although four tests gave enough data to support the results and conclusions,

more tests would be useful in order to form a more complete picture of the entire lifetime

of the thruster. As stated above, these future studies should also examine methods to

control the runtime and arcing rate, and more witness plates should be incorporated,

specifically at the 15° location.

A further study should examine the percentage of Teflon™ that strikes the

aluminum targets but does not stick to the surface. This study assumed all of the particles

carried enough momentum to stick to the plates. However, the possibility exists that a

significant percentage of the particles reflect off the surface instead. The percentage of

reflecting particles could also change with angle, most likely increasing as the angle

between the target surface and propellant tip increases.

Another useful study would look at performance degradation of solar panels when

they are exposed to PPT emissions. Such an experiment would give more precise

information about how particle accumulation affects the performance level of an actual satellite component.

This study focused on particles that ejected forward out of the propellant tube. An assumption was made that none of the particles traveled backwards. Placing witness plates completely around the tip of the propellant, in order to see if any particles traveled backwards, could test this assumption. If this occurred on an actual satellite, the particles would be heading back towards the satellite instead of out into space, causing potential problems.

Summary

This study shows that particles from a micro-PPT will accumulate on surfaces that face the propellant tube. The surface that directly faced the propellant tube accumulated more particles at a greater rate than any of the surrounding locations. To help determine whether the amount of particle deposition is great enough to affect the performance of satellite instruments or solar panels, the mass deposition rates and area blockage rages were calculated for each test. The four tests of this study give useful information about the deposition profile and deposition rates, but if the PPTs worked more consistently, a greater body of data could have been used to support these conclusions as well.

Appendix

Test 2 - Average particle accumulation at each angular location
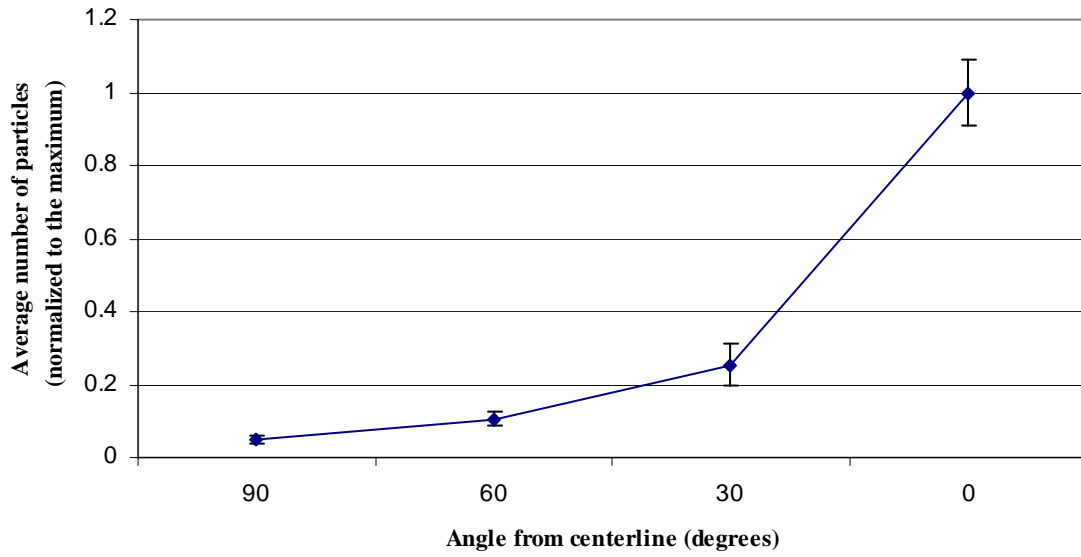
Figure 58 - Particle distribution profile (Test 2)

Test 2 - All particles sorted by size
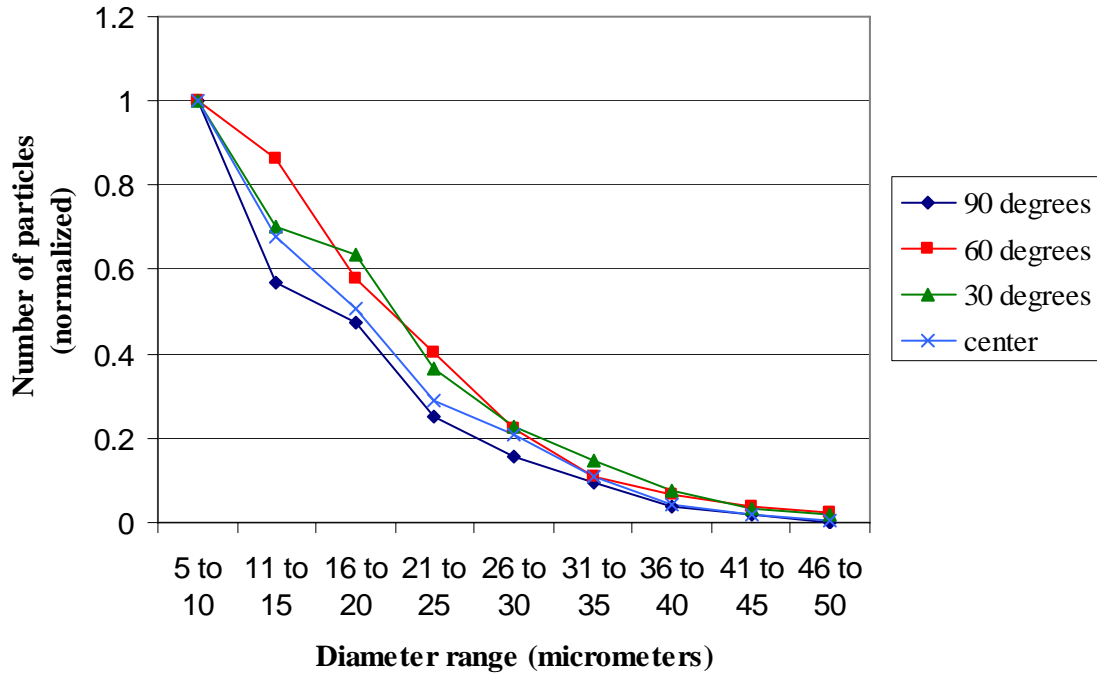
Figure 59 – Particle size distribution profile (Test 2)

Test 2 - Mass deposition
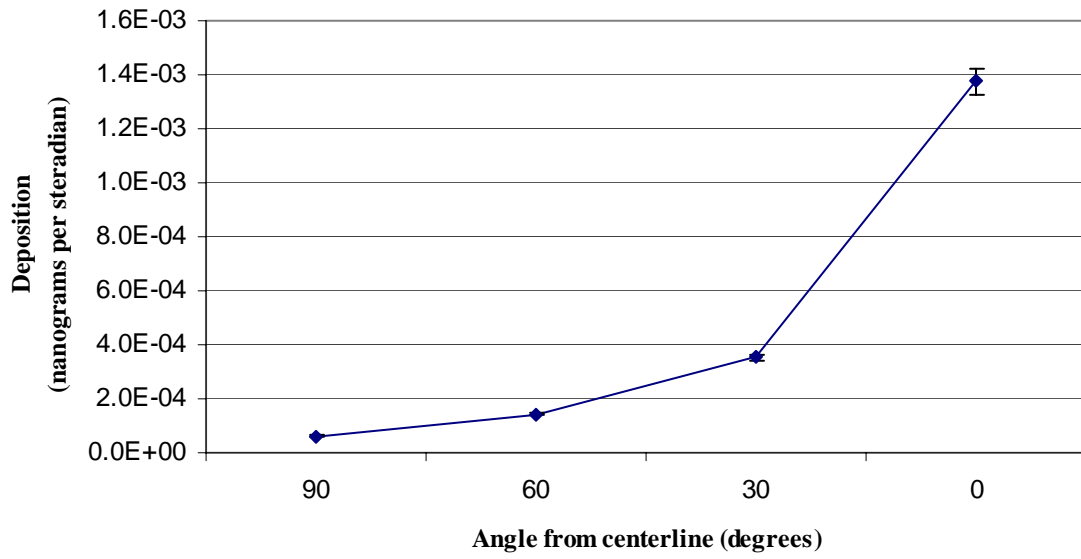
Figure 60 - Mass deposition (Test 2)

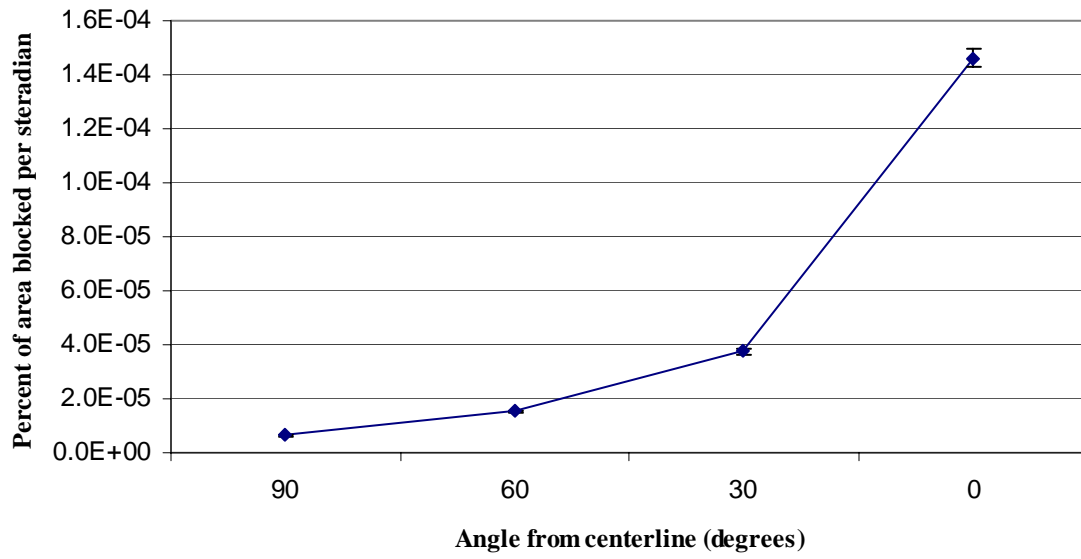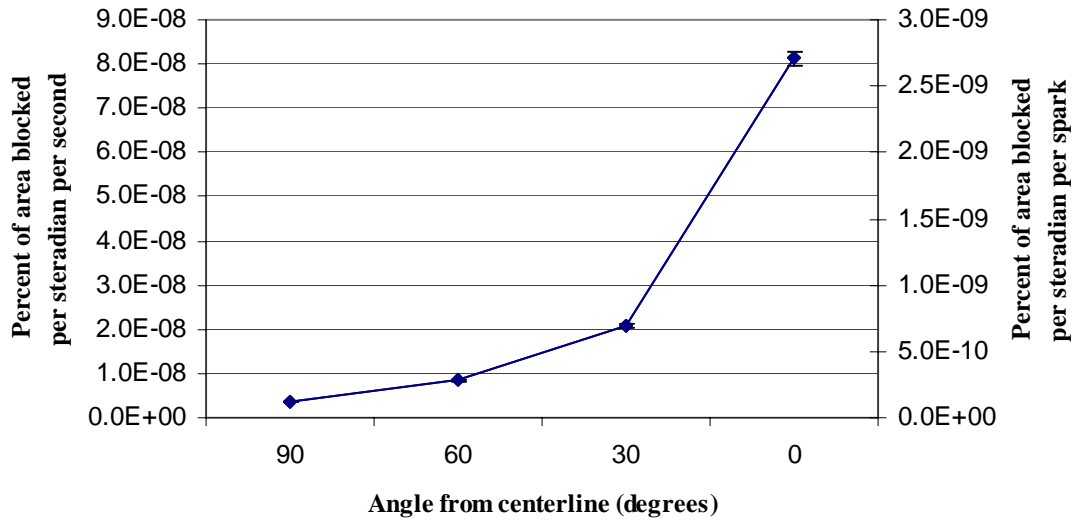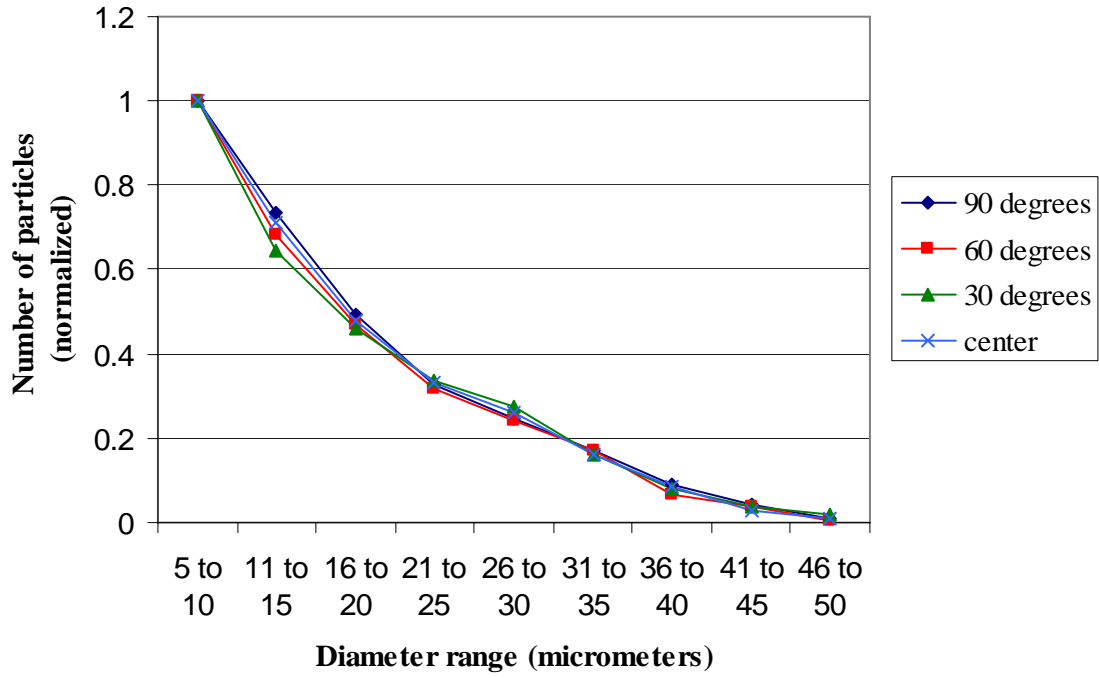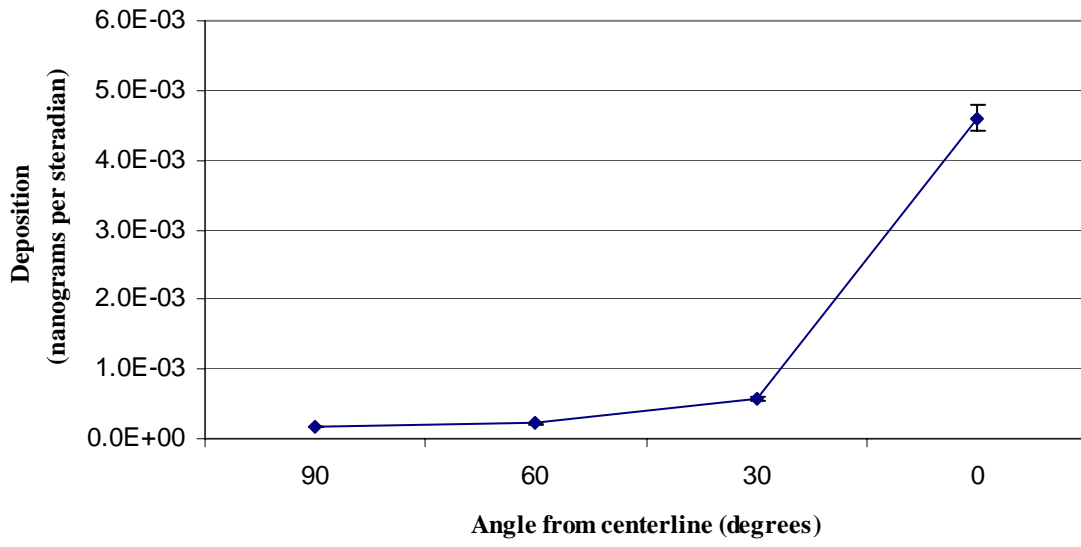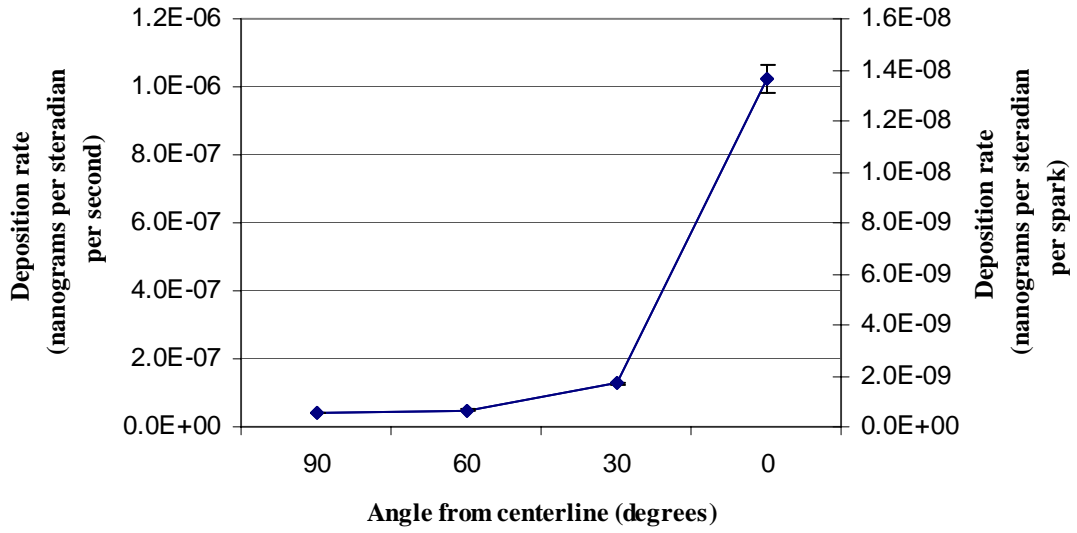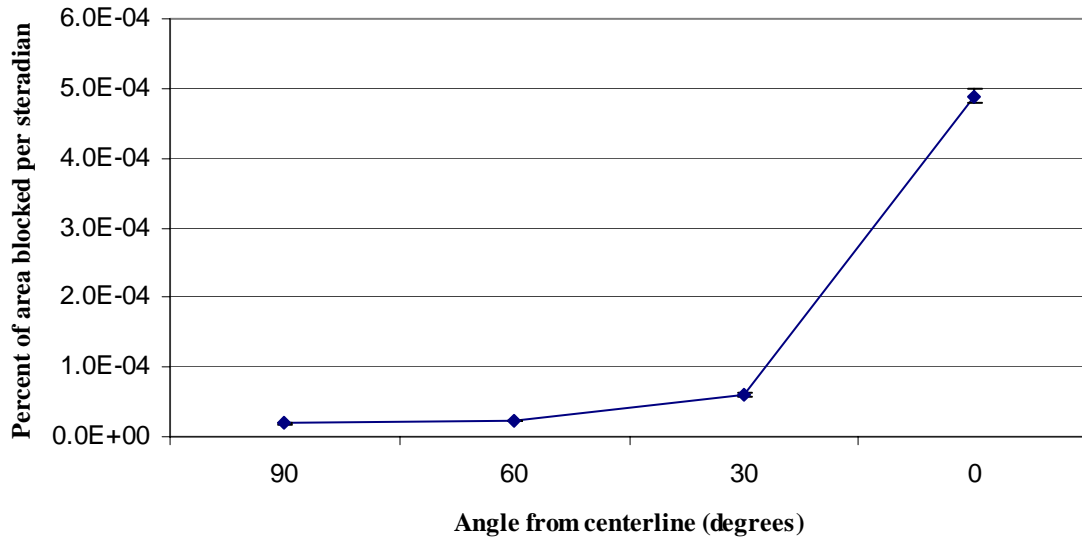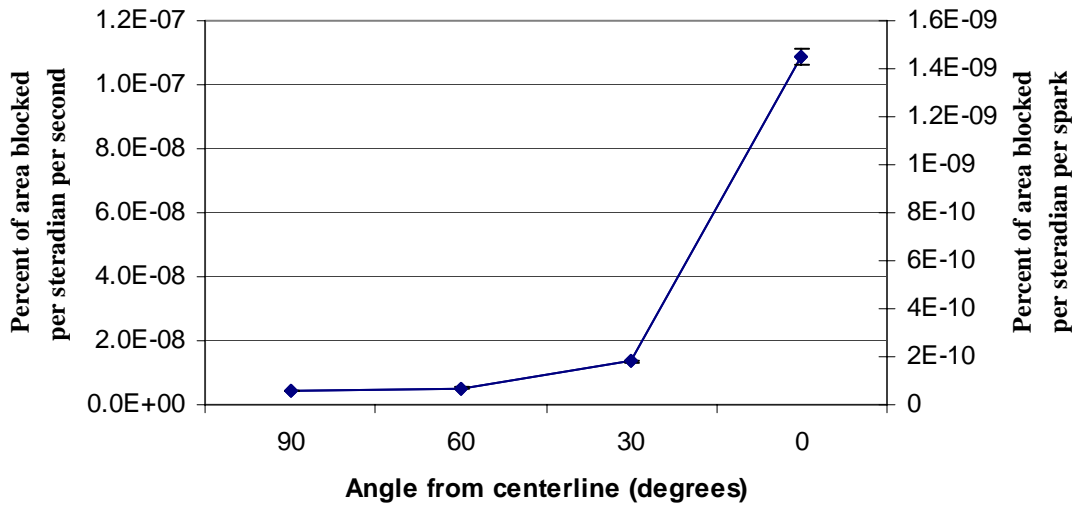**Test 2 - Mass deposition rate, scaled by runtime and spark rate**
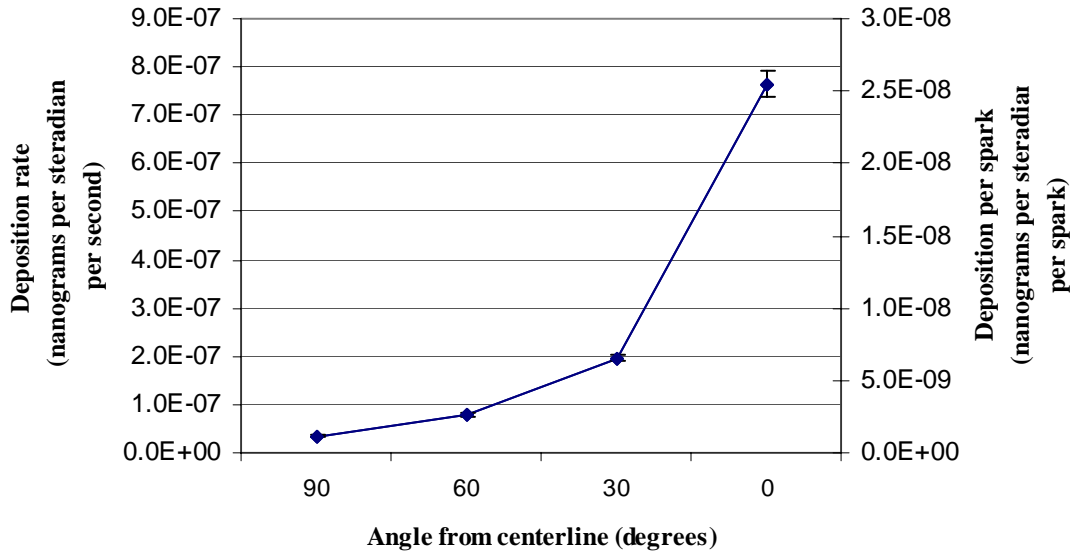
Figure 61 - Mass deposition rate (Test 2)

Test 2 - Percent of area blocked by particles, per steradian

Figure 62 - Percent of area blocked by particles per steradian (Test 2)

Test 2 - Rate of percent of area blocked per steradian, scaled by runtime and spark rate

Figure 63 – Rate of percent of area blocked by particles per steradian (Test 2)

Test 3 - Average particle accumulation at each angular location
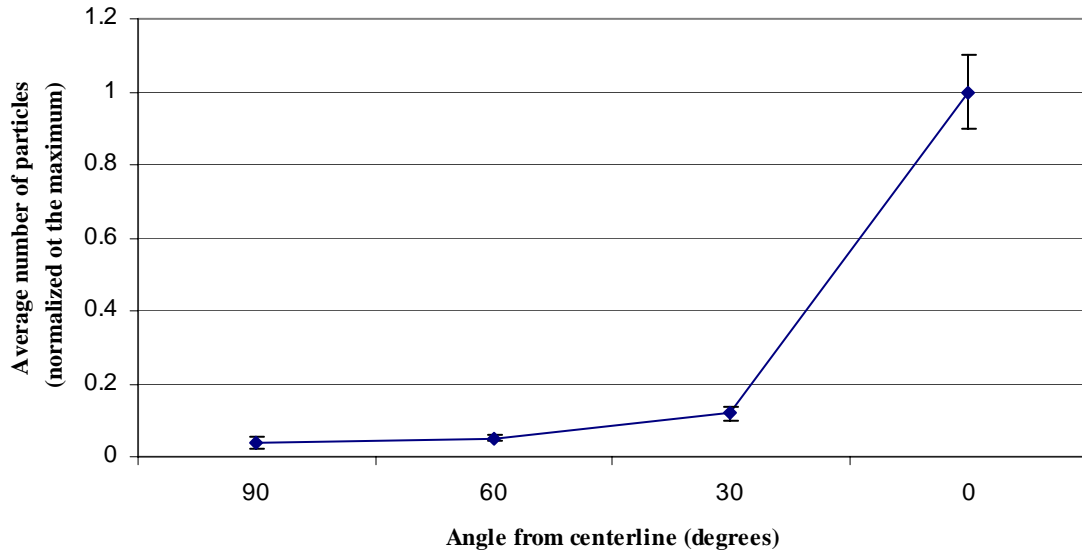
Figure 64 - Particle distribution profile (Test 3)

Test 3 - All particles sorted by size

Figure 65 - Particle size distribution profile (Test 3)

Test 3 - Mass deposition

Figure 66 - Mass deposition (Test 3)

Test 3 - Mass deposition rate, scaled by runtime and spark rate

Figure 67 - Mass deposition rate (Test 3)

Test 3 - Percent of area blocked by particles per steradian

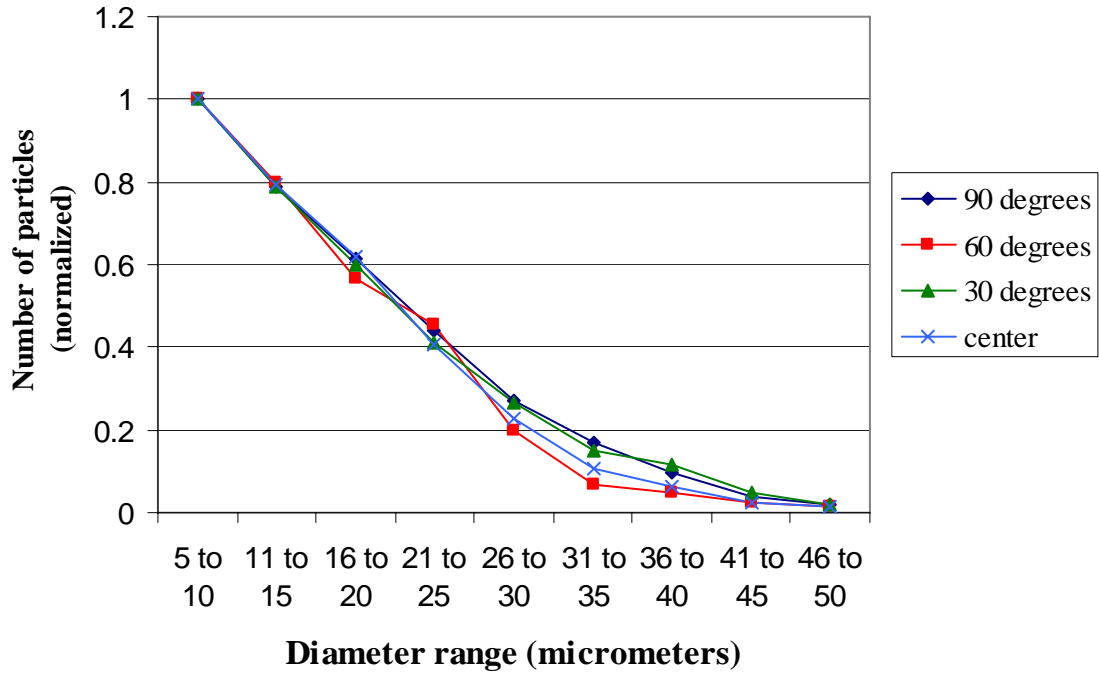**Figure 68 - Percent of area blocked per steradian (Test 3)**

Figure 69 - Rate of percent of area blocked per steradian (Test 3)

Test 4 - Average particle accumulation at each angular location
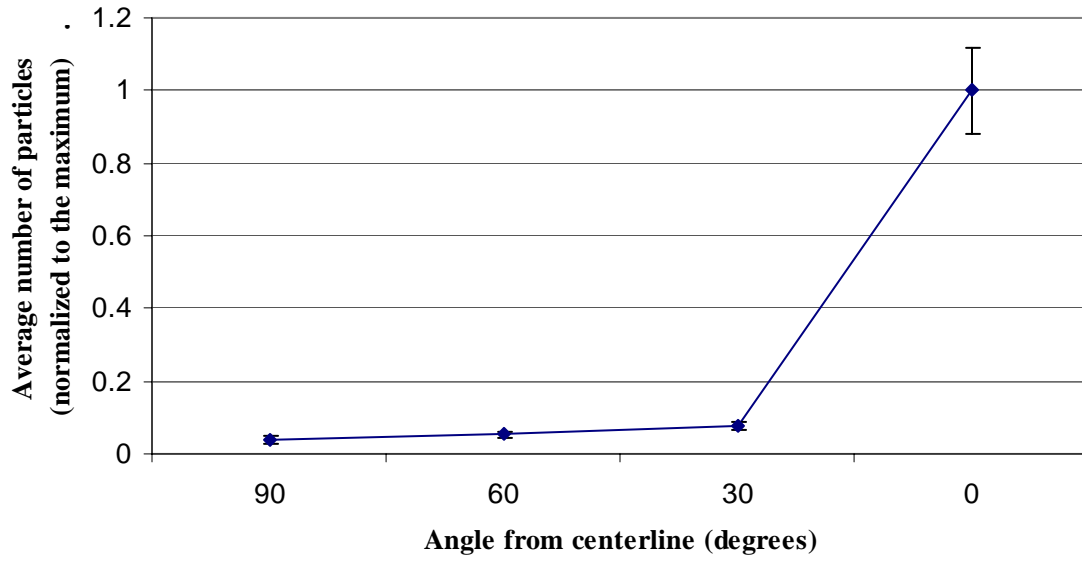
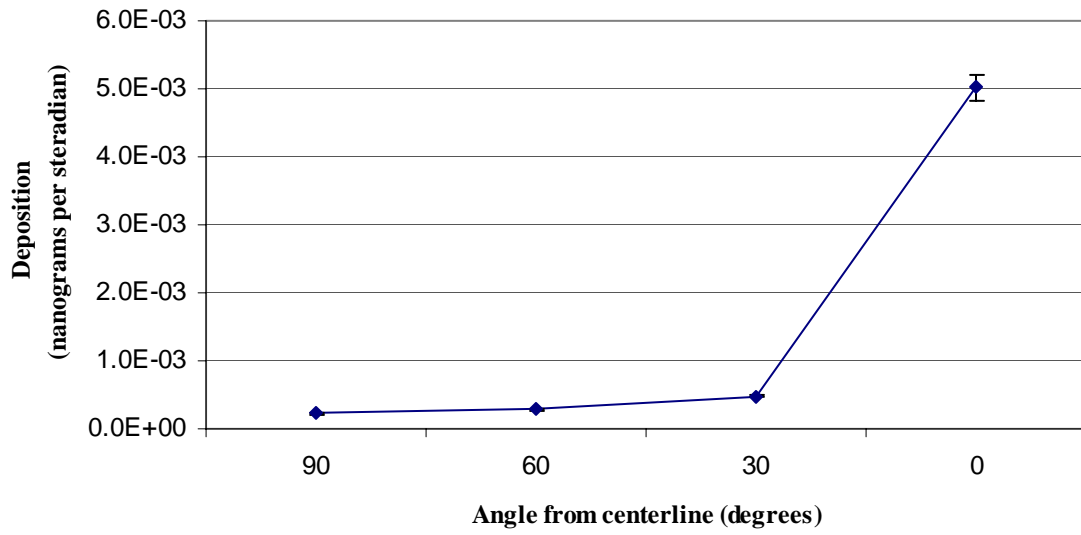**Figure 70 - Particle distribution profile (Test 4)**

Test 4 - All particles sorted by size

Figure 71 – Particle breakdown by size (Test 4)

Figure 72 - Mass deposition (Test 4)

Test 4 - Mass deposition rate, scaled by runtime and spark rate
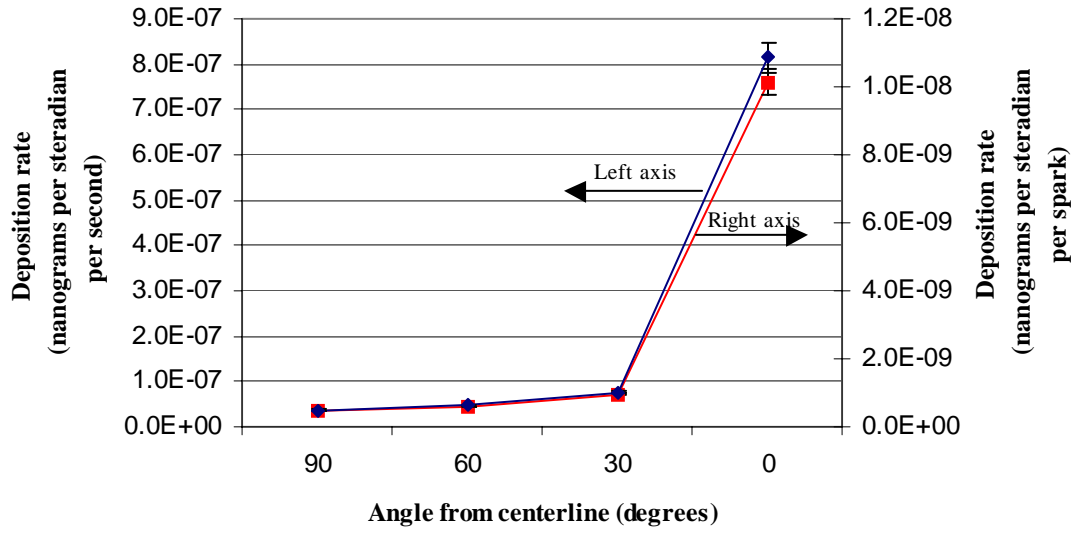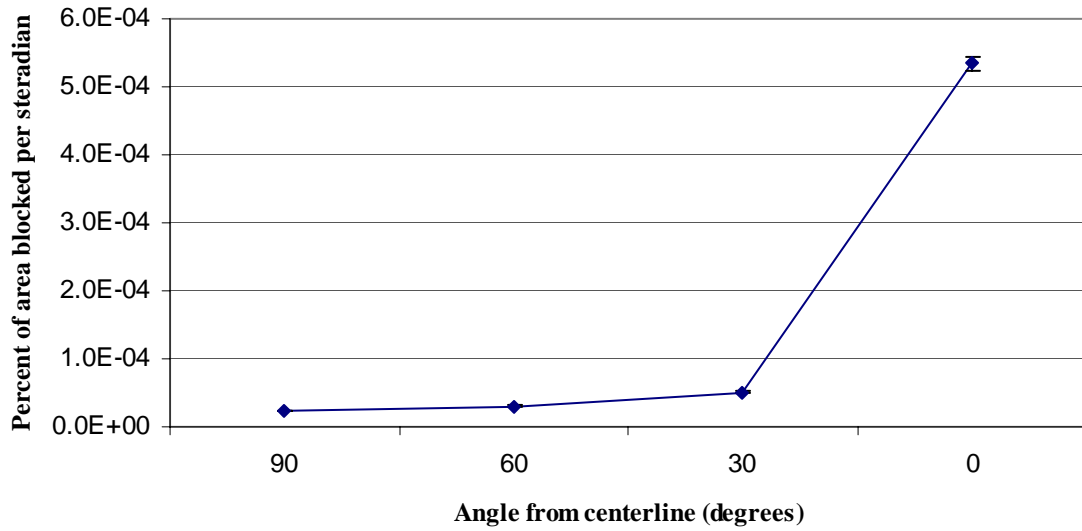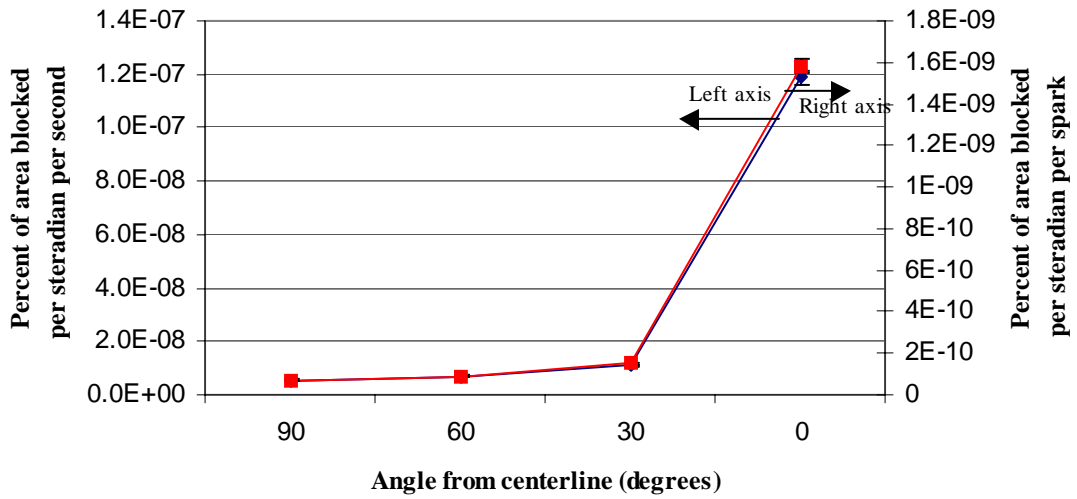

Figure 73 - Mass deposition rate (Test 4)

Test 4 - Percent of area blocked by particles per steradian

Figure 74 - Percent of area blocked per steradian (Test 4)

Test 4 - Rate of percent of area blocked, scaled by runtime and spark rate

Figure 75 - Rate of percent of area blocked per steradian (Test 4)

Bibliography

1. *Basic Vacuum Practice*. Lexington, MA: Varian Associates, Inc., 1992.

2. Hablanian, M. and K. Caldwell. "The Overload Conditions in High-Vacuum Pumps." *Proceedings of the 34th Annual Technical Conference of the Society of Vacuum Coaters.* SVC Publications. (1991). 10 August 2006 http://www.svc.org/EP/EP_FeatureGuide.html

3. NASA Glenn Research Center. "Pulsed Plasma Thruster Fact Sheet." 5 September 2006 http://www.nasa.gov/centers/glenn/about/fs23grc.html

4. NASA Glenn Research Center. "Pulsed Plasma Thruster Technology Development and Flight Demonstration Program." 5 September 2006 http://www.grc.nasa.gov/WWW/RT1997/6000/6910curran.htm

5. Spanjers, Gregory G., John H. Schilling, Scott Engelmann, and Robert A. Spores. "The Micro Pulsed Plasma Thruster." *Technical Report*. AD-A407730. Air Force Research Laboratory, Space and Missile Propulsion Div. (May 1999). 5 September 2006 http://stinet.dtic.mil/cgi-bin/GetTRDoc?AD=ADA407730&Location= U2&doc= GetTRDoc.pdf

6. Jahn, Robert G. *Physics of Electric Propulsion*. New York: McGraw-Hill Book Company, 1968.

7. Benson, Scott W., Lynn A. Arrington, W. Andrew Hoskins, and Nicole J. Meckel. "Development of a PPT for the EO-1 Spacecraft." *Proceedings of the 35th AIAA/ASME/SAE/ASEE Joint Propulsion Conference and Exhibit.* (July 1999). 8 December 2006 http://ntrs.nasa.gov/archive/nasa/casi.ntrs.nasa.gov/ 20000121223_2000175841.pdf

8. Gulczinski, Frank S., III and Gregory G. Spanjers. "Micropropulsion Research at AFRL." *Technical Report.* AD-A407732. Air Force Research Laboratory, Space and Missile Propulsion Div. (May 2000). 10 September 2006 http://stinet.dtic.mil/cgi-bin/GetTRDoc?AD=A407732&Location=U2&doc= GetTRDoc.pdf

9. Pobst, J. A., G. G. Spanjers, I. J. Wysong, and J. B. Malak. "Basic Research in Electric Propulsion. Part I: Pulsed Plasma Thruster Propellant Efficiency and Contamination. Part II: Arcjet Remote Plume Measurement and Hydrogen Density." *Technical Report*. AD-A408488. Air Force Research Laboratory, Space and Missile Propulsion Div. (Feb 2002). 10 September 2006 http://stinet.dtic.mil/cgi-bin/GetTRDoc?AD=A408488 &Location=U2&doc=GetTRDoc.pdf

10. Spanjers, Gregory G., Jamie B. Malak, Robert J. Leiweke, and Ronald A. Spores. "Effect of Propellant Temperature on Efficiency in the Pulsed Plasma Thruster." *Journal of Propulsion and Power.* Vol. 14 No. 4. (July 1998).

11. Keider, Michael, Iain D. Boyd, and Isak I. Beilis. "Model of Particulate Interaction with Plasma in a Teflon Pulsed Plasma Thruster." *Journal of Propulsion and Power.* Vol. 17 No. 1. (January 2001).

12. Keider, Michael and Boyd, Iain D. "Electromagnetic Effects in the Near Field Plume Exhaust of a Pulsed Plasma Thruster." *Proceedings of the 37th AIAA/ASME/SAE/ ASEE Joint Propulsion Conference and Exhibit.* AIAA-2001-3638. (July 2001). 15 September 2006 http://hpcc.engin.umich.edu/CFD/research/NGPD/Publications/aiaa-01-3638.pdf

13. Keider, Michael and Iain D. Boyd. "Progress in Development of Modeling Capabilities for a Micro-Pulsed Plasma Thruster." *Proceedings of the 39th AIAA/ASME/SAE/ASEE Joint Propulsion Conference & Exhibit.* AIAA-2003-5166. (July 2003). 16 September 2006 http://hpcc.engin.umich.edu/CFD/research/NGPD/Publications/aiaa-03-5166.pdf

14. Spanjers, Gregory G., Jason S. Lotspeich, Keith A. McFall, and Ronald A. Spores. "Propellant Losses Because of Particulate Emission in a Pulsed Plasma Thruster." *Journal of Propulsion and Power.* Vol. 14 No. 4. (July 1998).

Vita

       Lieutenant Jacob H. Debevec graduated from Cardinal O'Hara High School in Springfield, Pennsylvania. He entered undergraduate studies at the University of Notre Dame in Notre Dame, Indiana where he graduated with a Bachelor of Science degree in Aerospace Engineering in May 2005. He was commissioned through the Detachment 225 AFROTC at the University of Notre Dame. In August 2005, he entered the Graduate School of Engineering and Management, Air Force Institute of Technology. Upon graduation, he will be assigned to the Aerospace Vehicles Technology Assessment and Simulation Branch of the Air Force Research Laboratory, Air Vehicles Directorate at Wright Patterson Air Force Base, Ohio.

REPORT DOCUMENTATION PAGE

1. REPORT DATE *(DD-MM-YYYY)*	2. REPORT TYPE	3. DATES COVERED *(From – To)*
13 December 2006	Master's Thesis	March 2006-December 2006

4. TITLE AND SUBTITLE	5a. CONTRACT NUMBER
VACUUM CHAMBER CONSTRUCTION AND CONTAMINATION STUDY OF A MICRO PULSED PLASMA THRUSTER	5b. GRANT NUMBER
	5c. PROGRAM ELEMENT NUMBER
6. AUTHOR(S)	5d. PROJECT NUMBER
Debevec, Jacob H., 2d Lt, USAF	5e. TASK NUMBER
	5f. WORK UNIT NUMBER

7. PERFORMING ORGANIZATION NAMES(S) AND ADDRESS(S)	8. PERFORMING ORGANIZATION REPORT NUMBER
Air Force Institute of Technology Graduate School of Engineering and Management (AFIT/EN) 2950 Hobson Way, Building 640 WPAFB OH 45433-8865	AFIT/GAE/ENY/07-D01

9. SPONSORING/MONITORING AGENCY NAME(S) AND ADDRESS(ES)	10. SPONSOR/MONITOR'S ACRONYM(S)
Dr. William A. Hargus, Jr. AFRL/PRSS 1 Ara Road Edwards AFB, CA 93524 DSN: 525-6799	11. SPONSOR/MONITOR'S REPORT NUMBER(S)

12. DISTRIBUTION/AVAILABILITY STATEMENT

APPROVED FOR PUBLIC RELEASE; DISTRIBUTION UNLIMITED.

13. SUPPLEMENTARY NOTES

14. ABSTRACT

The micro pulsed plasma thruster (micro-PPT) is a simple and versatile electric thruster capable of performing multiple missions, from precise attitude control on standard satellites to primary propulsion for nanosatellites. In order to fill this role as both industry and government move toward utilizing smaller satellites, micro-PPTs first need to be thoroughly tested on the ground. This study examines the deposition profile and rate of particle emission from the thruster so that satellite designers understand any potential contamination issues with sensitive instruments and solar panels. Employing a newly assembled vacuum chamber system, four tests were completed with the micro-PPTs, and the results showed that particles discharge in all directions, with the surfaces directly facing the propellant tube collecting exponentially more particle deposition than surfaces at wider angles.

15. SUBJECT TERMS

Micro pulsed plasma thruster, deposition, deposition profile, witness plates, vacuum chamber, diffusion pump

16. SECURITY CLASSIFICATION OF:			17. LIMITATION OF ABSTRACT	18. NUMBER OF PAGES	19a. NAME OF RESPONSIBLE PERSON
a. REPORT	b. ABSTRACT	c. THIS PAGE	UU	128	Richard Branam, Maj, USAF
U	U	U			19b. TELEPHONE NUMBER *(Include area code)* (937) 255-6565, ext 7485 (Richard.branam@afit.edu)